Effect of non-Newtonian slurries on the hydraulic characteristics of centrifugal pumps

Arnoud Dom

Delft University of Technology
Section of Dredging Engineering

version 4.2 November 3, 2017

Effect of non-Newtonian slurries on the hydraulic characteristics of centrifugal pumps

Author:

Arnoud Dom 4159519

Thesis Committee:

Dr. ir. A.M. Talmon	Delft University of Technology
Dr. ir. S.A. Miedema	Delft University of Technology
Dr. ir. H.J. de Koning Gans	Delft University of Technology
ir. M. Van den Broeck	DEME - Dredging International NV
ir. S. Claessens	DEME - Dredging International NV

DEME
Dredging, Environmental & Marine Engineering

TU Delft

In collaboration with DEME - Dredging International NV and Delft University of Technology

This page is intentionally left blank

Abstract

In the dredging industry, centrifugal pumps are most commonly used and selected based on their operational capacities and expected slurry characteristics. The handling capacity of a centrifugal pump is however supplied for handling water and cannot be applied to other slurry conditions without an applicable correction. For handling Newtonian fluids there exist a well established de-rating method by Hydraulic Institute (1983) and further improved until most recently ANSI (2015) was obtained. For non-Newtonian fluids however, no such generally accepted method exist, especially not for large centrifugal pumps as encountered in the dredging industry. In order to obtain a de-rating prediction for non-Newtonian fluids, researchers have tried to predict pump de-rating by applying the Hydraulic Institute (1983) method. This is only possible if all fluid characteristics of a non-Newtonian fluid are summarized into a single value as used to characterise a Newtonian fluid. Several approaches are suggested by Walker and Goulas (1982), Graham et al. (2009) and others. Dependant on which non-Newtonian parameter was found to be governing, apparent viscosities, Bingham plastic viscosity, and limiting viscosity were used in time.

Because all methods developed until today are based on small centrifugal pumps handling a mixture with a constant rheological behaviour, validity on centrifugal pumps with larger impellers and additional features as cover flushing cannot be guaranteed. Therefore the aim of this thesis research is to obtain a valid input parameter for a Newtonian de-rating method to predict the pump performance when handling a non-Newtonian fluid and determine the validity for large centrifugal pumps. To achieve this research goal, a measurement campaign on board the Trailing Suction Hopper Dredger 'Pallieter' of DEME - Dredging International NV, working in a viscous environment was carried out. Measurement data for pump head, power and efficiency were obtained by installing a torque measurement device. Additional a device was installed to measure the dissolved gas volume fraction in order to separate effects caused by increased viscosity from multi-phase flow problems. After measurement data is obtained, available de-rating methods are compared and conclusions are drawn with respect to applicability.

Dissolved air in the mixture is of significant influence on the complete pumping process. After filtering the data to remain with performance data only influenced by the higher viscosity, de-rating models are analysed. Head showed very little to none de-rating when a viscous mixture was handled. At lower viscosities the de-rating method showed little deviation from the theoretical pump head, only at higher viscosities a significant de-rating was predicted but measurements didn't confirmed this. The same effects as for head yields for power. Significant de-rating was expected at high viscosities but measurements contradict this phenomenon. Although the Bingham plastic viscosity is the most conservative characterisation of a non-Newtonian viscosity, over-prediction still exist at high viscosities. This is most probable caused by the absence of viscous material in the axial gap between impeller and casing which in turn result in much less disk friction losses as would be expected.

This page is intentionally left blank

Preface

This dissertation is submitted for the degree of Master of Science in Offshore Engineering at the Technical University of Delft, the Netherlands. The research as described herein was supervised by Dr. A.M. Talmon and ir. S. Claessens. I have given full-time commitment for this research in the period between 1 October 2016 until 16 November 2017.

My technical background and strong practical interest have substantiated the choice of conducting a measurement campaign on a working dredging vessel. When I was given the possibility of researching the performance of a working centrifugal pump, I was enthusiastic and honoured for receiving this opportunity. The research was partly undertaken at the head office of DEME - Dredging International NV in Zwijndrecht and partly on-board TSHD ''Pallieter' while dredging on the river Scheldt in Antwerp. Many challenges arose but for each a solution was found with the help of a specialist within DEME and my daily supervisor. My technical background was particular useful during the design and installation of the torque measurement system which was ultimately installed and exploited on board a vessel under continuous operation. Also during gathering of the sediment samples, inventiveness was necessary to obtain good results.

After an intensive literature study, two sources affective pump performance were identified which are inseparably connected. Knowledge about the relation between both is however almost nonexistent to date but nevertheless existing during each dredging operation and affecting pump performance to a large extend. For this reason, I decided to research both the effect of non-Newtonian mixtures in combination with multiphase flow handling capability of the pump and quantify the losses to be expected. Further I wanted to provide recommendations to reduce the negative effects and valuable continuation research topics.

This research aims to extend the field of knowledge in non-Newtonian centrifugal pump performance to particular large centrifugal dredge pumps. By researching this effect, I hope more detailed knowledge is available to researchers in this field and dredging contractors working in a similar environment. Future dredging works could be estimated more accurately and similar negative effects can be assigned and mitigated due to this research.

Arnoud Dom
Antwerp,
November 3, 2017

This page is intentionally left blank

Acknowledgements

Without the help, motivation and support of everyone direct or indirect involved with this research, the work as presented here would not have obtained the same result. Therefore I want to thank everyone involved for their help and dedication.

I would like to express my gratitude to everyone at DEME who offered their time and effort during my research. First of all Marc van den Broeck and Stijn Claessens who believed in my abilities and provided the research topic and facilities to bring it to a good end. Further everyone of the project team, crew, captain and electrician of TSHD Pallieter who welcomed and helped me whenever needed. In particular Ben who assisted me with several electronic device installations and provided constructive feedback. Also Ortwin van Thillo, Bart van den Broeck, Jorne Beyen and Koen Van Den Maegdenbergh from the Technical Department Automation for their time, persuasion and knowledge during the installation and operation of the torque measurement devices which proved to encompass more challenges as expected in advance. Further the crew of the Multraship responder and Iso Audenaert from the DEME soil laboratory, who provided me with equipment and advice, were indispensable for the gathering and processing of samples from the river Scheldt.

I am also very grateful to everyone of my thesis committee, especially Arno Talmon for providing constructive feedback, indispensable information and offering multiple weekends to read and complement draft versions of this research. Also Cees van Rhee and H.J. de Koning Gans for teaching me all the knowledge as gained during the courses and afterwards at the TU Delft.

At last, but certainly not least, I would like to express my gratitude to my family, girlfriend and friends who supported me wherever possible at any given time. First of all my girlfriend, Karen Borms, who supported me during long nights of processing data and writing the final report. Also my parents who assisted in every possible way and did make sure everything necessary was forehand to complete this graduation research. My friends with in particular Lode van Cauwenberg and Arnaud Verschelde who made being at the head office so much more interactive.

During this research I lost my precious and sincere friend Bob Kerssens. I had the privilege of knowing Bob during our mutual study time at the TU Delft. It was during this time that Bob taught me so many new things including what real friendship looks like. Therefore I would like to dedicate this work to Bob and his Family and fornicate all the great memories we had the opportunity to share together.
(Bob, 14 August 2017)

Arnoud Dom
Antwerpen,
November 3, 2017

This page is intentionally left blank

Contents

Chapter 1

Introduction

1.1 Background to the problem

Dredging is a method of gathering sediments from a river or seabed for different purposes. It could be for removing accumulated sediment in order to keep a waterway navigable, beach nourishment, harvesting materials, contaminant re-mediation or gathering material in order to construct new artificial land. When conducting the first mentioned type of projects, a vast majority of the projects will incorporate soils with small sand fractions and clays as both are most subjected to erosion and sedimentation. The most convenient and suitable vessel for this maintenance purpose is a Trailing Suction Hopper Dredge (TSHD). A exception is made for maintenance in small harbours and difficult to reach places where a TSHD is unable to manoeuvre.

A TSHD is based on the principle of trailing its suction pipe alongside the vessel over the seabed. On one end of the suction pipe, a dredge drag head is fitted to the pipe which loosens and mixes the soil with water by a combination of cutting tooth and/or jets, depending on the soil-type. This mixture of water and solids can be handled by the rest of the equipment. The other end of the suction pipe is connected to the inboard centrifugal pump which performs both a suction force, to transport slurry from the drag head to the pump and a driving force to pump the slurry into the 'hopper'. Sometimes, when the disposal area is close to the reclamation site, a pipeline can be connected to the vessel in order to pump the slurry directly to the final destination.

Figure 1.1: The Trailing Suction Hopper dredger 'Pallieter'.

1.2 Problem Statement

In the dredging industry, mainly centrifugal pumps are used because of their handling capabilities of the dredged medium. A centrifugal pump consist of an impeller rotating in its housing. This rotating impeller adds mechanical energy to the fluid flow, resulting in a pressure increase over the pump. The increase in pressure from inlet to outlet is also called the energy head or 'head' (Gulich (2008))(Matoušek (2004)). This characteristic, and all others (Power versus flow rate and Efficiency versus flow rate) are provided by the manufacturer in the form of a curve. A combination of flow rate and head gives the performance characteristic of the pump, which is measured by the manufacturer for the specific pump in water. Pumping a different medium than water results in a different behaviour and characteristics of the centrifugal pump.

When pumping fluids with a viscosity much higher than cold water, additional hydraulic losses will affect the performance of the pump. For this reason, pump characteristics given by the manufacturer cannot be applied in a viscous environment without an applicable correction-factor, as encountered in high concentration clay dredging for example. To predict the de-rating of a centrifugal pump, handling Newtonian fluids (i.e. fluids characterized by only one parameter = 'dynamic viscosity'), the method of Hydraulic Institute (1983) is well established within the range of validity. For non-Newtonian fluids however, no such method exist and most researchers have fallen back on Hydraulic Institute (1983). In order to be able to use this method, all characteristics of a non-Newtonian fluid have to be summarized into one parameter. For this purpose, no general accepted method exist and several approaches are available.

Additional, although the method for calculating Newtonian pump de-rating is well established within it's range of validity, this range is limited to pumps with a maximum impeller diameter of 620 mm. Extrapolating this method to larger pumps as encountered here encompasses large uncertainty.

Another negative effect on pump performance can be expected when the dredged material contains gas. Gas can be present in different phases and compositions but is nevertheless manifest for good pump performance. This influence was discussed by Florjancic (1970) but at a much smaller pump and under different pumping conditions.

1.3 Aim and objective

As both the influence of viscosity on pump performance and gas influence are not researched at either a impeller size of 2.25 meter or during operation with negative inlet pressures, both effects are to date unknown at these conditions and should be researched for more detailed understanding. Only after researching both effects separately, validating existing de-rating models becomes possible.

The aim of this research is to identify which Newtonian de-rating method is most applicable to large centrifugal pumps and which fluid characterisation of a non-Newtonian fluid should be used as input for this method. The approach of Walker and Goulas (1982) and Graham et al. (2009) will both be evaluated in this respect.

Also the influence of dissolved gas in the mixture will be analysed and used for interpretation of the measurement data set. Measurements on board will be compared to research in the past, i.e. Florjancic (1970), to quantify head and power de-rating based on volumetric gas percentage.

1.4 Problem Approach

Both these effects are encountered in different industries as for example mining or oil processing. The research therefore started by thorough literature research on both effects and conclusions from this existing knowledge served as a starting point for the field measurements.

In order to obtain deeper understanding about pump performance characteristics on a large pump scale, it was chosen to initiate a measurement campaign on a working TSHD. Already many parameters are

measured and logged on board with respect to head but no data was available for power and consequently efficiency. Constructing a complete data set is essential for full understanding of the problem. Obtaining the power and efficiency characteristics required a torque measurement on the pump input shaft in combination with flow rate measurements.

A second measurement on board was installed, namely the Sonartrac, which measured the dissolved GVF of the mixture after the dredge pump. Only by the combination of head, power and GVF measurements, it became possible to separate the effects from each other. When it was possible to eliminate the data where the influence of gas was noticeable, de-rating models for viscous influence on centrifugal pumps could be validated with measurement data from a TSHD working in a viscous environment.

1.5 Report Outline

The report follows a consequent problem approach, starting with the working principle of a Trailing Suction Hopper dredger and the function of the centrifugal pump in the system. More essential information about the centrifugal pump is than elaborated on in chapter 3 where all information is provided necessary for understanding the performance characteristics dealt with later.

As the influence on pump performance is dependent on the rheological parameters of the mixture, samples are researched to obtain complete insight. One of the rheological parameters needed as input to the de-rating methods is a flow curve. All facets encountered during the construction of such curve are discussed in chapter 4. Other parameters for full characterisation are also discussed. Next in chapter 5, all effects when pumping a viscous fluid will be discussed in combination with the present available models and their application range.

The field and rheological experiments will be discussed and interpreted accordingly in chapter 6. This chapter is followed by the results of the concerned field and rheological measurements and interpretation of the data. Lastly the measurements are compared with the present models and literature findings to conclude the applicability of present models. Also a comparison is made between air de-ratings as encountered in literature and measured on board of TSHD 'Pallieter'.

Figure 1.2: TSHD Pallieter trailing on the river Scheldt in Antwerp.

Chapter 2

Trailing Suction Hopper Dredger

2.1 Working Principle

A Trailing Suction Hopper Dredger (TSHD) is a vessel used in the dredging industry with full sailing capacity because of it's shape and is mainly used for maintenance, deepening and land reclamation purposes. This is done by means of large and powerful centrifugal pumps. Practical examples of DEME - TSHD projects are the widening and deepening of the Panama canal, maintenance of the river Scheldt, construction of new artificial harbours, airfield, islands and many more projects.

The principle of a TSHD is straight forward. The vessel is equipped with 1 or 2 suction tubes which are located on the sides of the vessel. The suction tube consist of a dredge drag head on one end (figure 2.1) and a centrifugal pump on the other end. The drag head is equipped with high pressure water jets and cutting teeth to loosen the soil and mix it with water to make it pump-able, see Figure 2.1. The placement of the centrifugal pump is depending on the characteristics of the pump and depth to which the vessel needs to dredge. By placing a second centrifugal pump on the suction tube under the water line, the vacuum limit is increased as the pump is operational in a higher static pressure environment. This configuration is not the case on board Pallieter and only a single dredge pump is powering the dredging process.

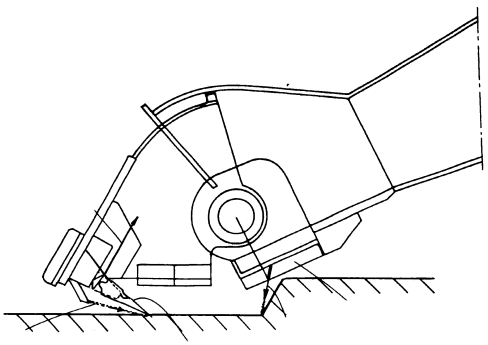

Figure 2.1: Schematic drawing of a draghead.

2.2 Loading

As mentioned before, the hopper is equipped with one or two suction tubes. In the case of 'Pallieter' the vessel only has one suction tube. After the draghead has loosened the soil and mixed with water, the formed mixture is pump-able and will be first transported through the suction tube due to the generated under pressure. The under pressure is limited by the vacuum limit at which vapour bubbles start to form.

After travelling through the suction tube and dredge pump respectively, the mixture is loaded into the cargo space 'hopper' of the vessel for further transportation. For Pallieter two possible loading options exist depending on the type of mixture (settling on non-settling) and are illustrated in figure 2.2. Two diffusers are installed which can be operated with the use of distribution valves. The overflow is located at the front of the basin (circular shape) and the diffusers at the middle and on the rear. In the case of dredging clay, only the rear diffuser is used. Loading will stop when the discharge level is reached or continues to further fill the hopper with overflow depending on the soil type and sailing regime. For the particular case of Pallieter on the river Scheldt, dredging will stop before overflow due to contractual agreements on spillage in the harbour area.

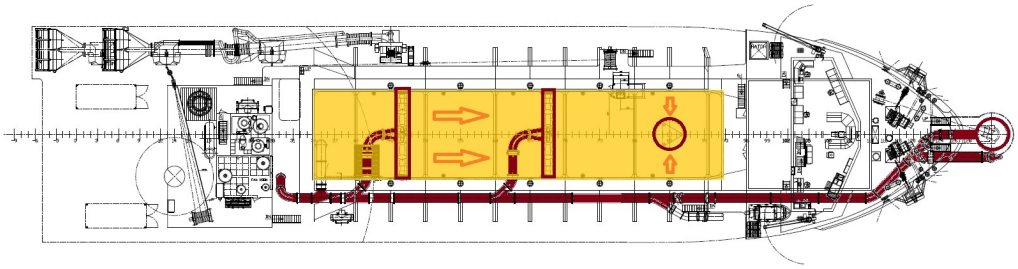

Figure 2.2: Overview TSHD 'Pallieter' with highlighted loading and discharge piping.

The loading capacity is dependant on the loading method, specific weight of the dredged material or volumetric capacity of the ship. At DEME a large variety of hoppers are available ranging from 2000 m^3 upto 30,000 m^3 hopper capacity for the vessel Congo River. Pallieter can carry up to 5230 m^3 if loaded until maximum overflow.

2.3 Discharging

A Trailing Suction Hopper dredger is capable of discharging the mixture in various ways. Depending on the destination of the mixture and governing circumstances, one of the following options can be chosen on Pallieter:

1. Rainbowing: If the mixture needs to be placed at a certain location in the sea or beach, a fast and accurate way is discharging through the rainbow jet ahead of the vessel. The mixture is loosened and liquefied with the use of jets in the hopper and pumped to the bow of the ship. Projects where rainbowing is used are for example: construction of artificial islands or beach supplementations.

2. Pumping to shore: Another method forehand is connecting a floating pipe to the vessel through the bow coupling. The end of the floating pipe is picked up by the ship and hoisted in the bow-coupling. Further the same process occurs as when rainbowing. Now the mixture is transported to shore in liquid form and will there be separated to obtain dry solids.

   Note: For the two options above, a high initial pressure is necessary to transport the mixture over certain distance because pipeline pressure losses are present and increase with length. To do so, one of the ship's propulsion engines (not in use at the time of discharging) is used to parallelize with the MID engine, enabling a higher pump rotation speed, higher power input and consequently a higher discharge pressure.

3. Dumping: The last discharge option is dumping the mixture at a certain location through the bottom doors of the vessel. This is the method used by Pallieter at the Scheldt river for discharging. Again dependant on the mixture, settled or still in suspension, opening the bottom doors will initiate the mixture to flow out or water jets are deployed to liquefy the soil again. After all material has left the hopper space, the dredge crew starts the dredge pump again (without the suction pipe connected to the side of the vessel) to flush the space through the diffusers with fresh water. This fact will later be used to interpret the registered data points for pumping 'water'.

2.4 Centrifugal Pump

The most essential part of the dredging process is the centrifugal pump, driving the complete system. Centrifugal pumps are used in the dredging industry for transporting liquids by raising a specified flow of volume to a pressure level defined by the Q-H characteristic. A centrifugal pump is composed of an impeller, housed in a casing and driven by a pump shaft. The liquid to be pumped flows through the suction nozzle to the impeller eye. From the eye of the impeller, the liquid is displaced outwards due to centrifugal forces. The energy transfer in this hydrodynamic process is proportional to the square of the rotational speed of the impeller. When the energy added by the centrifugal pump is sufficient to overcome the friction force in the pipe and any changes in elevation, the fluids will start to flow. Criteria for minimum flow velocity are given by particle settling characteristics governing in the pipe.

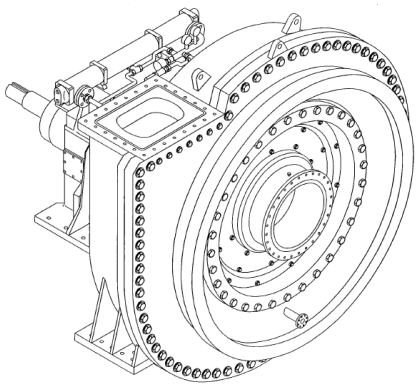

Figure 2.3: Double walled IHC dredge pump from TSHD Congo River.

The centrifugal pump encountered in a TSHD is a compromise between constructional requirements on wear/solids handling and hydraulic requirements. High concentration mixtures also need to be pumped although excessive wear can be the result. To mitigate dangers associated with wear, doubled walled pumps (figure 2.3) can be deployed in dredging vessels. Here the inner casing can be made from very hard and brittle material which is more resistive to wear but is secured by an outer casing built from welded or cast steel plates. The inner casing can than, so to speak wear completely down without damage. An important aspect of double walled pumps is the equal pressure between the impeller space and void water between the casings. On board Pallieter a single walled pump is used as cost effective alternative.

When the centrifugal pump is handling fluids other than water, various effect exist dependant on the mixture characteristics. If the fluid is characterised as settling and the particle size distribution is forehand, the solids effect on Head-Flowrate, Power-Flowrate and consequently Efficiency-Flowrate can be predicted with the use of solids effect laws (for example Stepanoff (1965) or Miedema (1999)). In many cases, the pumped slurries may be more viscous than water, which significantly affects the pump performance. Viscous fluids cause greater hydraulic losses in the pump so at higher viscosity liquids the head and efficiency decrease while required input power increases. Further theoretical elaboration on centrifugal pumps and performance characteristics can be read in the following chapters.

Chapter 3

Centrifugal Pumps

In this chapter all theoretical facets concerning centrifugal pumps will be discussed based on their relevance on the subject of measuring and modelling centrifugal characteristics in a viscous environment. First the theoretical pump characteristics will be explained as this will form the basis to compare measurement results with performance specifications as prescribed by the manufacturer. Hereafter scaling of performance data based on varying rotational speed will be discussed as measurements are conducted in a constant changing set-up. Lastly a brief introduction will be given about viscous effects on centrifugal pump performance as opening for the consecutive chapters dedicated to viscous effects.

3.1 Theoretical pump characteristics

3.1.1 Euler

Theoretically it is possible to calculate the pump characteristics based on the equation of Euler and apply corrections for practical implications. The head curve obtained by the theoretical Euler model is a straight declining line and represents in essence the change in angular momentum of water between suction and discharge. In practice, the model has only proven to be reliable around the design point. For lower flow rates and overcapacity's the reliability decreases significantly. It is better to use the measured pump characteristic data provided by the manufacturer. From this characteristic the most efficient working range can be derived van den Berg and Stam (2013). Losses which should be taken into account are the following:

1. Correction for incongruity of impeller blades and flow, the finite number of blades, the blade thickness and the internal friction encountered by the fluid. This incident loss can best be illustrated by the difference in flow and blade angle. This blade direction crosses the flow direction leading to impingement and recirculation losses. This effect will grow when operating further away from BEP.

2. Correction for losses from frictional contact with the walls and deflection and diversion in the pump. This loss increases quadratically with the velocity as can be seen in the figure.

3. Correction for inlet and impact losses. Also recirculation occurs at this specific flow condition leading to tremendous energy dissipation in these stall areas.

All of the above effects are visualised in figure 3.1 below. Important for the research are the losses encountered at part-load and over-load moments during a dredging operation.

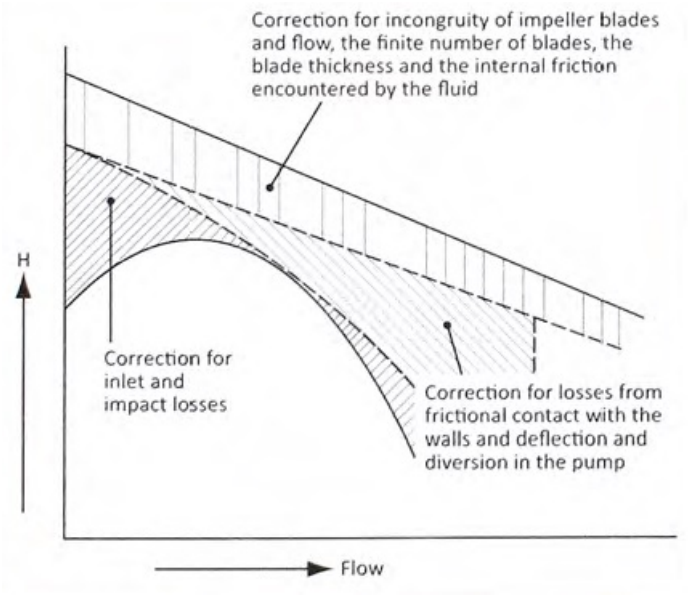

Figure 3.1: Correction factors applied to Eulers' equation to include practical implications. [van den Berg and Stam (2013)]

3.1.2 Head - Flowrate

The pump head, as will be discussed further in this research, is defined as the difference in total pressure between the discharge and suction side of the centrifugal pump and is represented by the Bernoulli equation. Depending on the application, this pressure can be expressed in three different measures namely: pressure as 'kPa', 'meter water column' or 'meter slurry column'. Further in the report, principally for the de-rating methods, the measure of meter slurry column will be used.

$$\Delta P \ or \ P_{man} = \frac{\rho_m \ (V_2^2 - V_1^2)}{2} + P_2 - P_1 + \rho_m \ g \ (\Delta h) \qquad \text{[Pa]} \quad (3.1)$$

Head follows from tree different forms of energy, summarized by the Bernoulli equation above (3.1). In eq 3.1 the first part is the kinetic energy of the fluid, also called the velocity head. This part is depending on the local speed of the fluid as pressure is speed dependant. A difference in inlet and outlet diameter can result in flow speed difference and thus a pressure difference. Second is the static pressure contribution as can be read from the pressure gauges installed before and after the pump. The final term represents the static head. The physical height difference between the center of the inlet and outlet relative to a reference level. This contribution is of great importance on-board of dredging vessels as difference in height between pressure sensors can be up to a few meters.

The following representation of Bernoulli's equation expressing Head (H) or Total Dynamic Head (TDH) in meter. Depending on which value is substituted for density (water density of slurry density) the units represent consequently meter water column (mwc) or meter slurry column (msc).

$$H = TDH = \frac{\Delta P}{\rho \ g} \qquad \text{[m]} \quad (3.2)$$

The reason why specifically the head is discussed into detail originate from the many different forms of notation in the corresponding literature. To clarify these different forms, a small overview will be presented.

1. **Meter water column** - On the y axis, the head is expressed in meter water column. A increase in liquid density will result in upward shift of the H-Q curve with a factor equal to the ratio of the densities.

2. **Meter slurry column** - The H-Q curve will not shift in y direction as with increasing density, the curve will remain equal to the theoretical water head. Only a effect of solids reducing the head can be seen as a small shift downwards. This curve should be read with care.

3. **Pressure in kPa** - Head can also be expressed in manometric pressure expressed in kPa. When head is expressed in kPa, use is made of the water density.

Dimensionless Head

The last option of representing a curve describing the relation between pressure and flow rate is with the use of dimensionless parameters. The H-Q curve can be approximated by a polynomial equation with two degrees of freedom or also known as the dimensionless pumpcurve Ψ in function of Φ . From this dimensionless quantity, easy conversion calculations can be made for other pumping conditions (for example: different rotational speed, impeller diameter or discharge flow rate), with the use of affinity laws. Further depending on which parameter is known, the dimensionless power and/or efficiency can be calculated. In the case of the DEME vessel Pallieter, the pump dimensionless head as well as dimensionless power (Π) factors ($\alpha_0 - \alpha_2$ and $\beta_0 - \beta_3$) are provided by the manufacturer (IHC). The values are obtained during the pump acceptance tests and thus rely on actual measurement points. During this test no other fluid is used than water.

Dimensionless Head:

$$\Psi = \alpha_0 + \alpha_1 \Phi + \alpha_2 \Phi^2 \quad [-] \tag{3.3}$$

where Φ is the dimensionless discharge parameter [-].

3.1.3 Power - Flowrate

In order to obtain the head characteristics as stated above, power will be consumed by the pump relative to the required rate of flow. This power is transferred from a driving source to the impeller by a pump shaft. Consequently power characteristics are obtained by measuring the mechanical power consumed by the pump. The amount of power needed depends on required head, flowrate, mixture density and pump design efficiency. As the power is transferred by means of a steel shaft, subsequent torque can function as alternative measure for power.

$$P = \frac{\rho \; g \; Q \; H}{\eta} \tag{3.4}$$

This input power is directly related to the measured torque by the following relationship:

$$P_{in} = \frac{2\pi}{60} \; n \; T \tag{3.5}$$

The power output of the pump is represented by the required power of the hydraulic system which follows from:

$$P_{hy} = Q \; p_{man} \tag{3.6}$$

The ratio between the subsequent shaft input power and hydraulic output power gives the efficiency of the centrifugal pump by the following relation:

$$\eta = \frac{P_{hy}}{P_{in}} = \frac{Q \; p_{man}}{\frac{2\pi}{60} \; n \; T} \tag{3.7}$$

Dimensionless Power and Efficiency

Again, as with dimensionless head, also power characteristics can be approximated by a polynomial equation. The difference between head and power lies in the number degrees of freedom. The dimensionless power parameters given by IHC describe a polynomial equation with three degrees of freedom as can be seen below in equation 3.8. In acceptance test, measuring the torque on the input shaft while throttling the discharge of the pump results in head and power characteristics. From these two quantities, the pump efficiency can be calculated by the relation presented in equation 3.9.

Dimensionless Power:

$$\Pi = \beta_0 + \beta_1\Phi + \beta_2\Phi^2 + \beta_3\Phi^3 \quad [-] \quad (3.8)$$

Efficiency can be calculated on its turn by the following formula, given the dimensionless parameters for head and power, Ψ and Π consequently.

$$\eta = \frac{\Psi\Phi}{\Pi} \quad [-] \quad (3.9)$$

Note: The parameters provided by IHC are scaled to 1 Hz (60 RPM) and need further processing with affinity laws as explained above. For this case, a reference circumferential speed of 180 RPM will be used for further data processing. The characteristic curves for the dredge pump of Pallieter, obtained with the dimensionless parameters, can be seen in the figure below. The red dot marks the location of Best Efficiency Point (see section 3.3)

3.1.4 NPSH - Flowrate

Last parameter related to flow rate is the Net Positive Suction Head (NPSH). Vlasbom (2004) described the NPSH as total (energy) head available to the pump above the vapour pressure in front of the pump.

A distinction is made between NPSH Available and NPSH Required. With NPSHa, which is the available NPSH related to the available system conditions at the pump inlet. NPSHr is the 'required' suction head required to keep the medium in liquid state and prevent cavitation from occurring. If the NPSHa is lower than NPSHr, cavitation will inevitably happen affecting performance and pump life. Contrariwise, if the NSPHa is greather than NPSHr, no cavitation will occur and the difference is called NPSH Margin. The decreasing NPSH margin in function of flow rate is illustrated in figure 3.2.

The Required NPSH is also determined during the acceptance tests of the centrifugal pump. By increasing the vacuum at the suction side of the pump, gradually cavitation is initiated. Dependant on the pump application, an allowed drop in head is specified. For most dredging application, a 5 % drop in head is used to determine the NPSHR.

In this particular research it is of great importance to monitor NPSH with care. As high gas fractions already occur due to dissolved gas in the dredged material, effects due to cavitation would deteriorate the problem even more and could result in the termination of the dredging cycle.

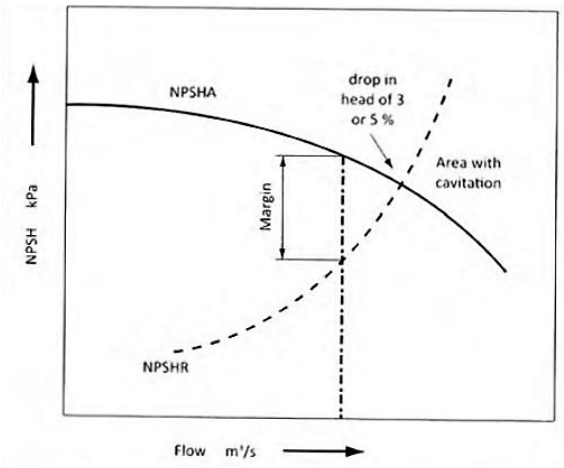

Figure 3.2: NPSH - Flowrate curve : NPSHA vs NPSHR

3.1.5 Specific speed

Selection of a pump is based on a combination of all characteristics as mentioned before. Depending on the application, a suitable pump is chosen based on the value for Q_{opt}, H_{opt} and rotational speed 'n'. A value combining all these parameters is given by "specific speed". The interpretation of specific speed varies between countries but is used in some de-rating models. A brief overview is presented below in Table 3.1.

Further in this research the first representation of specific speed in EU units will be used.

Specific Speed		
EU customary units	US customary units	Dimensionless
$n_q = n\frac{\sqrt{Q_{opt}/f_q}}{H_{opt}^{0.75}}$	$N_s = n\frac{\sqrt{Q_{opt}/f_q}}{H_{opt}^{0.75}} = 51.6\ n_q$	$\omega_s = \frac{\omega\sqrt{Q_{opt}/f_q}}{(g\ H_{opt},)^{0.75}} = \frac{n_q}{52.9}$
n in [rpm] Q in $[m^3/s]$ H in [m]	n in [rpm] Q in [gpm] H in [ft]	ω in [1/s] Q in $[m^3/s]$ H in [m]

Table 3.1: Overview of specific speed definitions.

3.2 Affinity Laws

Varying pump parameters as rotational speed, impeller diameter or the number of impeller blades all have their influence on the pump characteristics. In the following paragraph the effect of these individual parameters on the characteristics will be discussed. As explained before, first the dimensionless parameters by IHC need to be scaled from 60 RPM to 180 RPM. Second the measured data points other than 180 RPM during operation need to be scaled to 180 RPM. The affinity laws are only valid when considering the following similarities during both operations:

1. There is similarity of flow in a pump in case the ratio between fluid velocity c and tangential velocity of the impeller u is constant.

2. Full similarity can only be maintained in case the width / radius ratio is constant. Van Rhee (2009)

These considerations can be summarized by the assumption that the coefficient of hydraulic losses in the flow through the impeller is independent of the rate of flow resulting in $\eta_1 = \eta_2$. When the similarity considerations are satisfied, the affinity rules can be applied.

Effect of impeller rotational speed (ω)

$$\frac{Q_1}{\omega_1} = \frac{Q_2}{\omega_2} \rightarrow \frac{Q_2}{Q_1} = \frac{\omega_2}{\omega_1} \tag{3.10}$$

$$\frac{p_1}{\omega_1^2} = \frac{p_2}{\omega_2^2} \rightarrow \frac{p_2}{p_1} = \left(\frac{\omega_2}{\omega_1}\right)^2 \tag{3.11}$$

Effect of impeller diameter ($D_{impeller}$)

$$\frac{p_1}{D_1^2} = \frac{p_2}{D_2^2} \rightarrow \frac{p_2}{p_1} = \left(\frac{D_2}{D_1}\right)^2 \tag{3.12}$$

$$\frac{Q_1}{D_1^2} = \frac{Q_2}{D_2^2} \rightarrow \frac{Q_2}{Q_1} = \left(\frac{D_2}{D_1}\right)^2 \tag{3.13}$$

3.3 Best Efficiency Point - BEP

A centrifugal pump is unable to convert all kinetic energy into pressure energy over its full working range. Some of the energy is lost due to internal and external losses. The internal losses are mainly governed by hydraulic and volumetric losses while external losses are solely mechanical (friction in bearings and seals). Hydraulic losses are caused by disk friction in the impeller, loss due to rapid change in flow direction and change in velocities throughout the pump. The Best Efficiency Point (BEP) is the point of operation where the combination of losses is minimal.

In practical dredging applications, the pump will only operate a small amount of time at its best efficiency point. This has no practical implications only a higher energy consumption and less efficient pump are to be expected. Further calculations for pump de-rating will incorporate various dependencies on flowrate versus flowrate at BEP so the method of determining BEP will be explained below.

The flowrate at which the pump is most efficient occurs at the flowrate corresponding to the maximum of the efficiency curve. Given the shape of the curve, determining at which point on the curve the derivative is equal to zero will provide Q_{BEP}. The points of best efficiency are illustrated by a dot on the pump curves in figure 3.3.

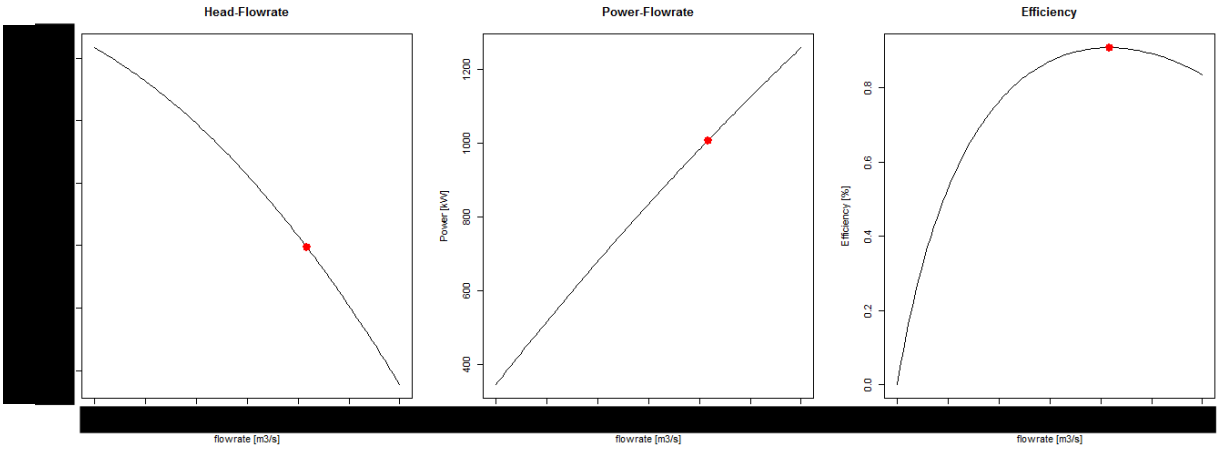

Figure 3.3: Theoretical Pump Curves for current impeller of Pallieter. (180 RPM equivalent - 4 Bladed - closed 2250 mm twisted blade design)

3.4 Effect of solids on pump performance

During dredging, ever changing soil conditions are encountered and must be handled by the dredge pump. If the mixture is a combination of water with another substance, being clay or sand, the performance of the pump is influenced. Dependant on the composition of the mixture, a different behaviour can be expected in pump characteristics when only the density changes or when also the viscosity is altered.

The adverse effects on pump performance originate because the suspended solids are not able to transmit any pressure energy. The particles can only acquire kinetic energy and are unable to fully transform this energy back to pressure energy. This effect is less pronounced when less solids are present and a higher viscosity is reached. For both effects are de-rating methods available although more knowledge is present with respect to solids influence.

Dependant if the governing correction is equal for all flow rates or varies accordingly, the obtained correction factor will be multiplied with the head value for water as shown in the equations below.

$$H = H_w * C_H \qquad Q = Q_w * C_Q \qquad \eta = \eta_w * C_\eta \tag{3.14}$$

3.4.1 Solids concentration effect

Dependant on the rheological characteristics of the mixture, more pronounced effects exist on head or power. Because impeller design was improved over the past years, less effect of solids exist on head while an increase in power is still to be expected.

The presence of solids in the mixture will have a large negative effect on the pump efficiency due to increasing hydraulic losses as discussed earlier. Various reduction formulas are developed for predicting the increasing losses. According to Stepanoff (1965), the ratio between pump efficiency in water and efficiency in slurry can be determined by the following relation. This relation includes the effect of particle size, d_{50}, and delivered concentration, C_{vd} Matoušek (2004). It is also possible to use this reduction factor as a measure of pressure reduction and output power reduction according to the following formulas:

$$P_{man,m} = P_{man,w} * \frac{\rho_m}{\rho_w} * f_c \qquad P_{out,m} = P_{out,w} * \frac{\rho_m}{\rho_w} * f_c \qquad \eta_m = \eta_w * f_c \tag{3.15}$$

with according to Stepanoff (1965):

$$f_c = 1 - C_{vd}(0.8 + 0.6 log d_{50}) \tag{3.16}$$

This reduction factor is then used to predict the pump input power and efficiency in slurry conditions based on the known water characteristics. It can be seen there is a direct relation between fluid concentration, particle size and performance reduction (figure 3.4). Because the relation is depending on the logarithmic value of the particle size, influence from small particles will be minimal while large/coarse particles will practice large influences on the characteristics. Experimental and field results were researched and concluded that impeller diameter is also of large influence on pump performance reduction according to Miedema 1999. This lead to a improved Stepanoff equation as stated below.

$$f_c = 1 - \frac{C_{vd}(0.466 + 0.4 log d_{50})}{D_{impeller}} \tag{3.17}$$

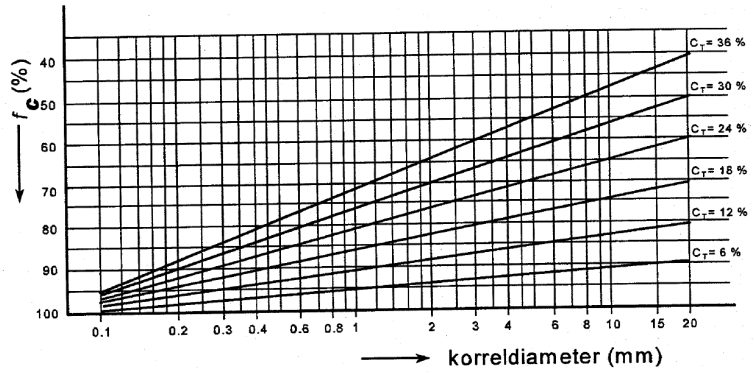

Figure 3.4: The relation between particle size (x-axis), delivered concentration (c_T), and reduction parameter according to Stepanoff (1965).

3.4.2 Viscous effect

Performance impairments also occur when the pump is handling fluids with much smaller particles. When very fine particles are present in the fluid, they might settle very slowly or not at all. When this is the case, the medium can be assumed homogeneous and rheological characteristics are different from water. Most of the liquids handled in this case are characterized by a non-linear flow curve including a initial yield stress to overcome internal friction (Non - Newtonian fluids). The viscosity at this point is much higher than for cold water and additional losses affect the pump performance. More about characterization in the following chapter.

Research on pump de-rating when handling non-Newtonian homogeneous fluids, started in 1927 by Gregory W.B. but the first significant research with correct conclusion in today's knowledge was by Walker and Goulas (1982). Here the importance of a complete rheogram was cited and the subsequent interpretation from rheogram to apparent viscosity μ_a or plastic viscosity μ_{pl}. To determine the correct efficiency reduction around BEP, various rheological parameters were used as governing de-rating parameters. At last, the conclusion was to relate pump de-rating to pump Reynolds number with plastic viscosity (determined at the highest available shear rate) as input value. Succeeding research determined other rheological parameters as governing during pump de-rating but conclusions should be interpret with care. As all mentioned literature was based on small centrifugal pumps, applicability to larger pumps is unconfirmed because the high cost and time consuming character of such experimental set-up.

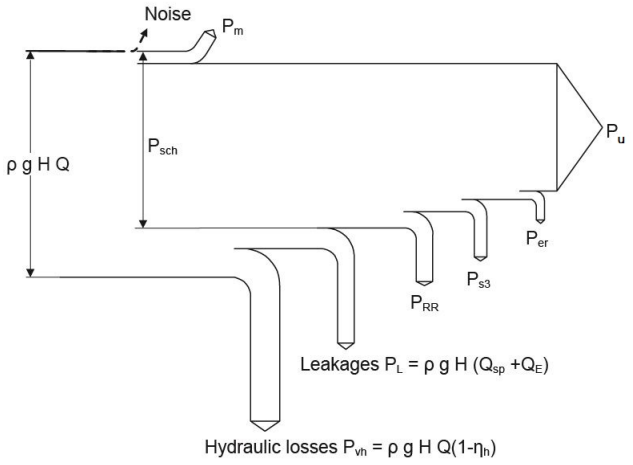

Figure 3.5: General energy balance of a centrifugal pump. P_m = mechanical power losses ,P_u = usefull power transfered to fluid ,P_{RR} = disk friction power ,P_{er} = specific erosion power ,P_{s3} = power loss dissipated in inter-stage seal (for multi-stage pumps)

To determine the factors responsible for these extra losses, let us take look at the energy balance of a centrifugal pump. As can be seem in figure 3.5, not all loss factors are dependant on rheological fluid parameters but some are. The most important loss factor is the disk friction. Disk friction losses grow with decreasing Reynolds number or increasing viscosity. The strong relation between disk friction and efficiency is responsible for large drops in efficiency as will be shown later.

Practical experience by Royal IHC (van den Berg and Stam (2013)) showed pump head was not greatly affected until the kinematic viscosity reached values 20 - 30 times higher than water. As the kinematic viscosity of water at 15 degrees Celcius is approximately $1.139*10^{-6}$ m^2/s, a kinematic viscosity of $6.5*10^{-6}$ m^2/s could occur in a silt mixture with a density of 1300 kg/m^3. Rules for the intermediate regime, when head is less affected, prescribe equal efficiency and linear density dependency. When higher viscosities are encountered, the de-rating method of Walker and Goulas (1982) was recommended.

By relating the pump performance to Reynolds number, the ratio of inertial forces to viscous forces is taken into account. With decreasing Reynolds number, the viscous forces grow and effects become governing. Measurements by Walker and Goulas (1982) found a significant efficiency reduction with Reynolds numbers below $2 * 10^6$ and reductions in head with Reynolds numbers below $7 * 10^5$.

$$Re_{pump} = \frac{\rho_m \ D_w^2 \ \omega}{\mu} \qquad [\text{-}] \quad (3.18)$$

with ρ in $[kg/m^3]$, D_w in $[m]$, ω in $[1/s]$ and μ in $[Ns/m^2$ or $Pa.s]$.

Successive research by Graham et al. (2009), Sellgren et al. (2000) and many more will be discussed into detail in the following chapters together with their adjustment to the de-rating methods as presented by Walker and Goulas.

effect on NPSH

Previous the phenomenon of Net Positive Suction Head was elaborated on and the importance of a margin between required and available NPSH was emphasized. As handling more viscous fluids than water result in extra losses, additional losses at the inlet of the pump will inevitably result in an increase of Required NPSH (sometimes also called $NPSH_3$).

Because the inlet losses can be calculated empirically, a safety factor was designed by Gulich (2008) including friction coefficients and inlet loss coefficient to give an estimate for the increased NPSH Required. This factor f_{NPSH} should be multiplied with NPSHR to take at least some additional losses into account.

Some de-rating procedures provide this factor although no excessive research results were found on NPSH effects when pumping highly viscous fluids. Again, the vacuum pressure at the pump inlet need to be monitored with care as a combination of air and viscosity is manifest for pump performance and air induced by cavitation cannot be mitigated by a degassing installation.

3.5 Pump sealing

Two locations in a centrifugal pump need to be sealed. The first location is the shaft side where a seal is necessary on the rotating shaft, powering the pump impeller. This will be later referred to as ''gland' flushing (figure 3.6b). The second location exist on the suction side of the pump (figure 3.6a). Due to an axial gap between impeller and casing, back-flow could occur and results in excessive wear. Although this could be minimized by decreasing the axial spacing, other measures could be necessary.

Another method to reduce back-flow and reduce wear is by using an impeller with 'counter' blades, also referred to as expeller vanes. These blades induce a flow that is opposite to the direction of back-flow on the suction side of the impeller. Simultaneous radial blades could be present at the backside of the impeller which cause a higher pressure field to avoid intrusion of particles.

Lastly, a centrifugal dredge pump could be equipped with cover flushing system. Here water is injected behind the impeller seal at the suction side of the pump. With a high pressure jet pump, flushing water is injected at a higher pressure than could occur at the pressure side of the pump. Hereby intrusion of wear particles should be avoided. According to guidelines of van den Berg and Stam (2013), a minimum pressure is required equal to the maximum outlet pressure at a flow rate given by equation3.19.

$$Q = \frac{D^2\ n}{20} \qquad [\mathrm{m^3\,h^{-1}}] \quad (3.19)$$

where: D = impeller diameter [m] and n = nominal dredge pump speed [rpm].

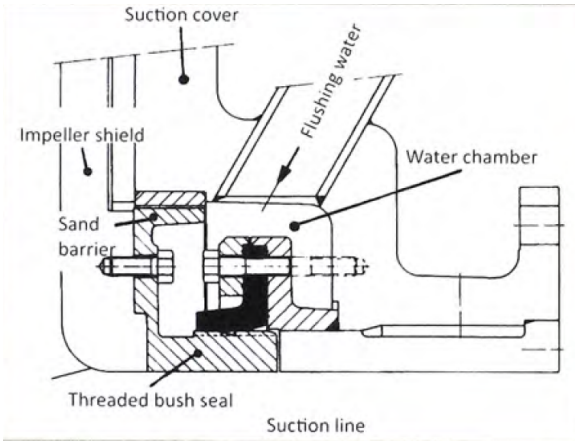

(a) Flushing water on suction side.

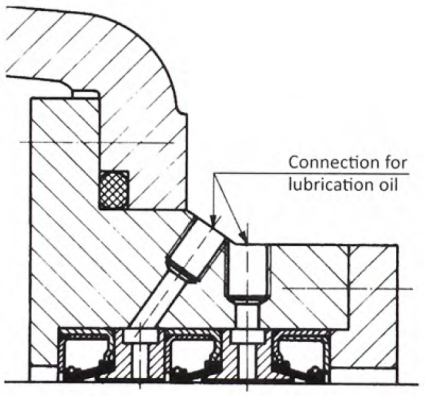

(b) Gland flushing on drive shaft.

Figure 3.6: Flushing methods for both suction side and back side of the impeller.

3.6 Measuring pump characteristics

In practice, to measure the corresponding head values over the spectrum of flow rates of a pump, a model test is carried out. In this test set-up a throttling valve is installed downstream of the pump to vary the flow rate at constant rotational speed. Note: If the valve was located at the inlet of the pump, risk of cavitation can disrupt the measured data due to presence of air in the mixture.

The experiment starts with a centrifugal pump driven at a constant circumferential velocity. During this stage a throttle valve downstream of the pump needs to be varied in opening to obtain H values for different flow rates (Q) by increasing the hydraulic resistance and thus lower the flow rate. All these readings plotted and interconnected on a graph is the Q-H curve as provided by the factory. For very large custom centrifugal pumps it is not always practical possible to conduct these tests. The manufacturer will in this case scale the values from geometrical similar pumps to the larger pump with affinity laws.

As for Pallieter, accepting the centrifugal pump as installed on board, pump characteristics were measured on board with separate equipment to validate theoretical performance. These parameters are used as starting conditions to give insight in current pump performance when handling water. The offset of the theoretical head characteristic is adjusted if necessary and new starting values are established for the further experiments.

The last parameter needed to establish a full characterisation of pump performance is pump power. As measuring shaft input power is not to difficult when the pump is electrically driven, accurate measuring a diesel direct is more complicated. To obtain the power parameter, a torque measurement was installed on the driving shaft powering the centrifugal pump. More information on the measurement set up for this research and water validation can be read in chapter 6.

3.7 General pump specifications

The pump installed on board of Pallieter (as seen in figure 3.7) was designed and made by Royal IHC in the Netherlands. A brief overview of pump and drive specifications will be given below.

- Brand: Royal IHC
- Type: HRMD 222-47-110
- Number of blades: 4
- Impeller diameter: 2250 [mm]
- Nominal speed: 195 [rpm]

This all is powered by two diesel engines from Wartsila through a two-speed gear box which switches between low and high gear with consequently one or two engines active.

- Motor manufacturer: Wartsila
- Type: 6L26
- Nonimal power: 2025 [kW]

- Gearbox manufacturer: Flender
- Gearbox type: GJZ 2600
- Reduction: 1000:195

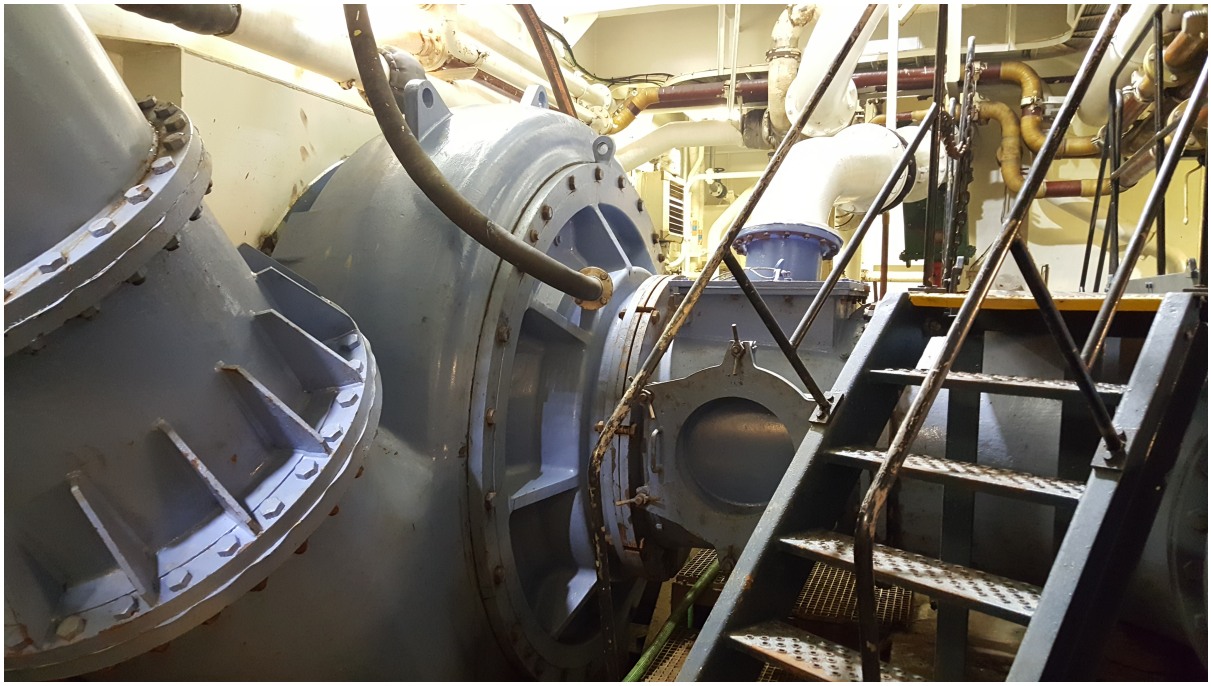

Figure 3.7: Single walled, high efficiency IHC Dredge pump on board Pallieter.

Chapter 4

Rheology

In this chapter the characterisation of the slurry will be discussed into detail. First, a general overview will be presented what full characterisation of mud encompasses. This is followed by elaboration on the determination and interpretation of the flow curve. Various methods are forehand to determine the rheogram but a dedicated protocol was used and will be presented. Lastly, other parameters which were measured to ensure full characterisation of the mixture are explained into detail.

4.1 Estuarine mud suspensions

As investigating the influence of viscous fluids on pump performance corresponds to maintenance dredging, samples are taken from several locations in the port of Antwerp where the TSHD Pallieter is dredging. All locations expect one are branches of the river Scheldt so the depositions are estuarine mud suspensions. The remaining sample was collected in a dock with no open connection to the river (further mentioned as location **A**) to be able to compare samples with a different salinity and origin. The relatively small solids fraction in the samples result in practically homogeneous samples as expected with sedimented material.

Estuarine mud suspensions are concentrated colloidal suspensions which behave as yield stress or viscoplastic fluids (Toorman (1995)). The suspensions are inelastic non-ideal Bingham fluids because of their deviation at low shear rates. At higher shear rates, the fluids shows a ideal Bingham behaviour. Looking at lower shear rates, a yield stress will be present when the concentration exceeds the gel point. At this point the gel will not flow until the internal shear forces exceed the yield stress of the structure and breaks up the network of particles into mobile aggregate particles. This research will mainly focus on the higher shear rates as occur inside the centrifugal pump during pumping. Lower shear rates will incorporate the effect of 'initial yield stress', 'Bingham yield stress' and related factors. If other parameters are further elaborated on, it will be for adequate characterisation of the slurry and possible future use.

In the past, various researchers have investigated characterisation methods based on samples from the river Scheldt as will be used in this research. Due to the previous research, methods are adopted and improved for this type of soil with respect to flow curves and mineralogical composition. As the assigned laboratory was the first to develop a new measurement protocol, this guidance will be used for the flow curves as encountered here.

4.2 Viscosity

When analysing liquid behaviour, as expected in pumps near solid boundaries, viscosity is an import property of the fluid as it is a measure of resistance to gradual deformation by shear stress and tensile stress. The resistance to deformation is caused by the inter molecular friction exerted when two layers of liquid want to slide by each other. Viscosity can be expressed in different units depending on the application. Below you will find the different measures of viscosity and corresponding (SI) units as encountered in standards and literature. As the available literature was written by researchers from different locations in the world, de-rating methods use various units so transition from one to another is often necessary.

4.2.1 Dynamic viscosity

When a thin layer of fluid is assumed which is kept between two parallel plates at a certain distance dy from another as shown in figure 4.1. A resistant force equal but opposite to F, will be the result of shearing under steady conditions due to the force of F. This resistance is caused by the liquid itself (Matoušek (2004)).

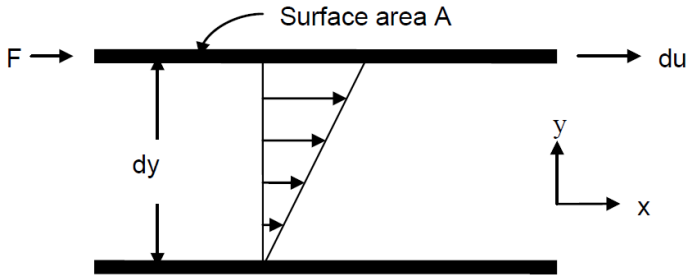

Figure 4.1: Schematic shearing flow at distance dy from each other.(Matoušek (2004))

In Newtonian fluids, this resulting shear stress ($\tau = \frac{F}{A}$) is linear related to the shear rate ($\dot{\gamma} = \frac{du}{dy}$) by means of the following relation:

$$\tau = \mu \left(-\frac{du}{dy} \right) \tag{4.1}$$

with μ in SI Units [Pa.s]

The coefficient μ is also known as coefficient of proportionality or dynamic viscosity. Dependence exist on temperature, pressure and nature of the fluid. The negative sign in equation 4.1 shows the resultant force due to shearing acts in opposite direction of the applied motion. In literature, various units are used dependant on geographical location or background from the author. Below is an overview presented for fast interpretation:

$$1 \text{ PI (Poiseuille)} = 1 \text{ Pa.s}, \qquad 1 \text{ P (Poise)} = 0.1 \text{ Pa.s}, \qquad 1 \text{ cP} = 0.001 \text{ Pa.s}$$

A plot combining shear stress with shear rate is called “flow curve” or rheogram with on the horizontal axis the shear rate and vertical shear stress. If the material can be simulated by a straight line passing through the origin of the graph, the material is classified as Newtonian with a dynamic viscosity μ equal to the slope of gradient of this curve.

When there exist a relation between shear rate and stress which is anything but linear through the origin, the fluid is classified as a non-Newtonian fluid.

4.2.2 Kinematic viscosity

When the density of the fluid needs to be taken into account, the kinematic viscosity can be used. This is the ratio between dynamic viscosity and density of the fluid as described by equation 4.2.

$$\nu = \frac{\mu}{\rho} \qquad [\mathrm{m^2\,s^{-1}}] \quad (4.2)$$

For example: the kinematic viscosity of water at 20.2° C equals 1 mm^2/s (E.T. (2017)).

$$1 \text{ St (Stokes)} = 10^-4\ m^2.s^-1, \qquad 1 \text{ cSt (centiStokes)} = 10^-6\ m^2.s^-1$$

4.2.3 Viscosity calculations

When non-Newtonian fluids are encountered, various models and units for viscosity can be used dependant on the application. Below can be found some of these units as encountered in de-rating literature as used.

Apparent viscosity μ_a

The apparent viscosity is expressed as the ratio of shear stress τ at a certain selected shear rate $\dot{\gamma}$. This value can be calculated for each point on the flow curve. This unit was first mainly used for de-rating purposes by Walker and Goulas (1982) and can be calculated as follows:

$$\mu_a = \frac{\tau_0}{\dot{\gamma}} \qquad [\mathrm{Pa\,s}] \quad (4.3)$$

At very low shear rates, apparent viscosity is also referred to as zero shear viscosity, μ_0, and infinite shear viscosity at very high shear rates, μ_∞ (Walker and Goulas (1982)).

Bingham plastic viscosity μ_{pl}

Also used in the work of Walker and Goulas (1982) is the Bingham plastic viscosity, μ_{pl}, which is defined as the local slope of the flow curve for any shear rate value. When the fluid is characterised as Bingham plastic, it can be calculated as follows:

$$\mu_{pl} = \frac{\tau_0 - \tau_y}{\dot{\gamma}} \qquad [\mathrm{Pa\,s}] \quad (4.4)$$

with τ_y = yield stress and $\dot{\gamma}$ the shear rate corresponding to the particular chosen shear stress τ_0.

When the fluid is characterised as Bingham plastic, the slope as calculated above (μ_{pl}) is equal to the consistency index K and is also called η or coefficient of rigidity.

4.3 Rheological models

Earlier it was already noticed not all fluids behave equal under varying flow conditions. Dependant on the fluid characteristics, viscosity can change due to shear rate or in time. Various models are developed in the past to best comprise the full behaviour for all shear rates. For each fluid, a different function was developed as will be presented:

$$\tau = f\left(\frac{du}{dr}\right) \quad (4.5)$$

4.3.1 Newtonian fluids

Newtonian fluids are characterised by a straight line on it's rheogram (figure 4.2) and only characterised by a single value, namely the dynamic viscosity. As discussed earlier, the slope of this straight line equals the dynamic viscosity μ. Mathematical this relation can be expressed as follows:

$$\tau = \mu * \frac{du}{dy} \tag{4.6}$$

where μ = coefficient of dynamic viscosity and $\frac{du}{dy}$ = shear rate.

Examples of Newtonian fluids are water, oil, glycerine and many more.

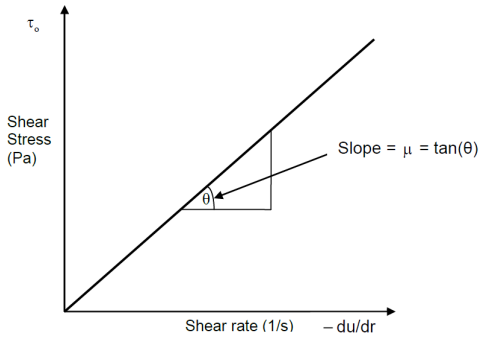

Figure 4.2: Flow curve of a Newtonian fluid. (Chhabra and Richardson (1999))

4.3.2 non-Newtonian fluids

Non-Newtonian fluids are characterised by flow curves which are non-linear or linear but don't pass through the origin of the rheogram (figure 4.3). In this case an initial force is necessary to initiate motion in the fluid. The apparent viscosity of a non-Newtonian fluid is influenced by many factors as temperature, pressure and flow-conditions (shear-rate) (Chhabra and Richardson (1999)).

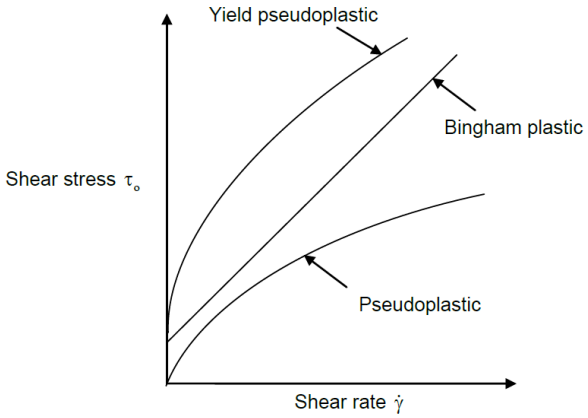

Figure 4.3: Flow curves of non-Newtonian fluids. (Chhabra and Richardson (1999))

In contrast to Newtonian fluids, many more models are available to characterise non-Newtonian fluids as can be seen in the coming sections.

4.3.3 Generalised model

Many models can be determined from a general constitutive model from which certain parameters need to be determined by rheological characterisation. From characterisation a value for yield stress τ_y, fluid consistancy index 'K' and flow behaviour index 'n' should arise. These parameters are related as follows:

$$\tau = \tau_y + K * \left(-\frac{du}{dr}\right)^n \tag{4.7}$$

Yield stress (τ_y)
A fluid comprises a yield stress when no flow occurs until the external stress exceeds a certain threshold value. If the stress is increased even further, the substance behaves again as a fluid. Yield stress thus equals a minimum value for sustainable fluid flow.

Dependant on the fluid characterisation and measurement method, different values can be obtained for yield stress. During this research, yield stress is encountered as follows:

1. Initial yield stress; τ_y
2. Bingham yield stress; τ_B
3. True yield stress, Peak yield stress of Static yield stress; τ_{peak}

Fluid consistency index (K)
A fluid consistency index represents the dynamic viscosity of a Bingham fluid. The same as for dynamic viscosity of Newtonian fluids, increasing the factor K equals a higher viscosity of the fluid.

Flow behaviour index (n)
This parameter in essence describes the curvature of the flow curve. Shear thinning fluids correspond to a 'n' value between 0 and 1 while shear-thickening corresponds to n > 1. When the index is equal to 1 (n = 1), the fluid shows Newtonian behaviour.

It gives an indication of "the rate of increase in shear stress with share rate", which also varies with concentration (Slatter (1986)).

A combination of all parameters is used by various researchers to characterise mixtures. Dependent on the behaviour of the medium one of models from Table 4.1 can be used. More models exist but Table 4.1 summarizes the most commonly used.

Fluid model	**Constitutive equation**	**Number of parameters**	**Parameters**
Newtonian	$\tau = \mu * \left(-\frac{du}{dr}\right)$	1	μ
Bingham plastic	$\tau = \tau_y + K * \left(-\frac{du}{dr}\right)$	2	τ_y, K
Power-law or Ostwald de Waele (pseudoplastic)	$\tau = K * \left(-\frac{du}{dr}\right)^n$	2	K, n
Hershel-Bulkley or Yield pseudoplastic	$\tau = \tau_y + K * \left(-\frac{du}{dr}\right)^n$	3	τ_y, n, K
Worrall-Tuliani	$\tau = \tau_y + \mu_\infty \dot{\gamma} + \frac{\Delta\mu\dot{\gamma}}{1 + \frac{\Delta\mu\dot{\gamma}}{\Delta\tau}}$	4	τ_y, μ_{infty}, $\Delta\mu$, $\Delta\tau$

Table 4.1: Overview fluid characterisation models.

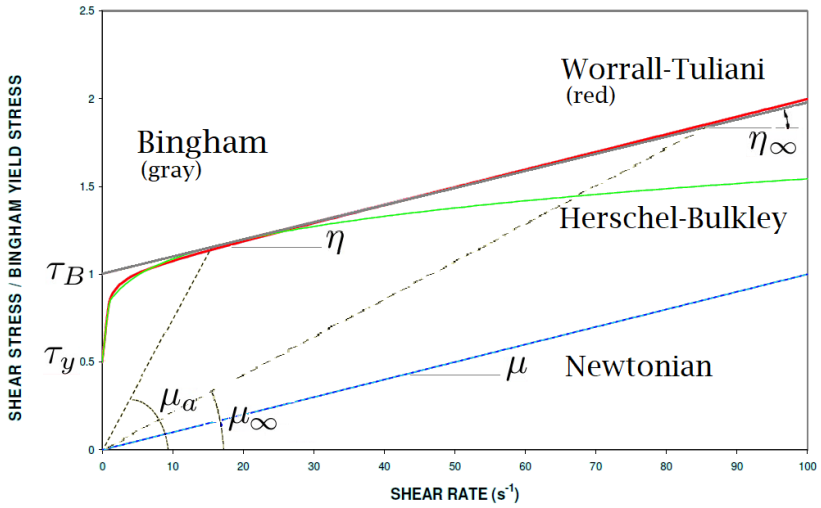

Figure 4.4: Flowcurve models comparison

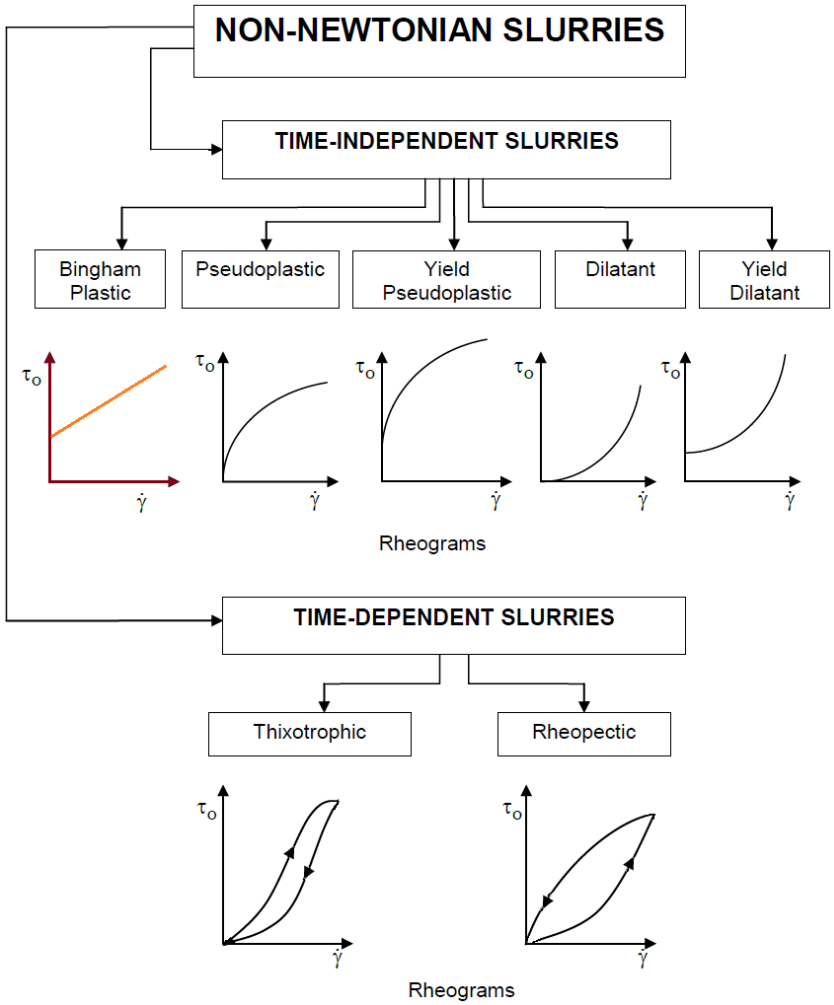

Figure 4.5: Overview of non-Newtonian flow curves according to Paterson and Cooke (1999).

4.4 Characterisation

To characterise viscous fluids, it needs to be determined how the shear stress relates to different shear rates. A curve combining both is also known as a rheogram or flow curve (see figure 4.4). If the curve holds a linear relationship, the fluids behaves as a Newtonian fluid. Non-Newtonian fluids, as the name suggests, don't hold a linear dependence and are characterised by phenomena as initial yield stress, shear thinning or thickening and other time dependant behaviours. To determine this flow curve, a deviant method is used from the most commonly used one. Below an overview.

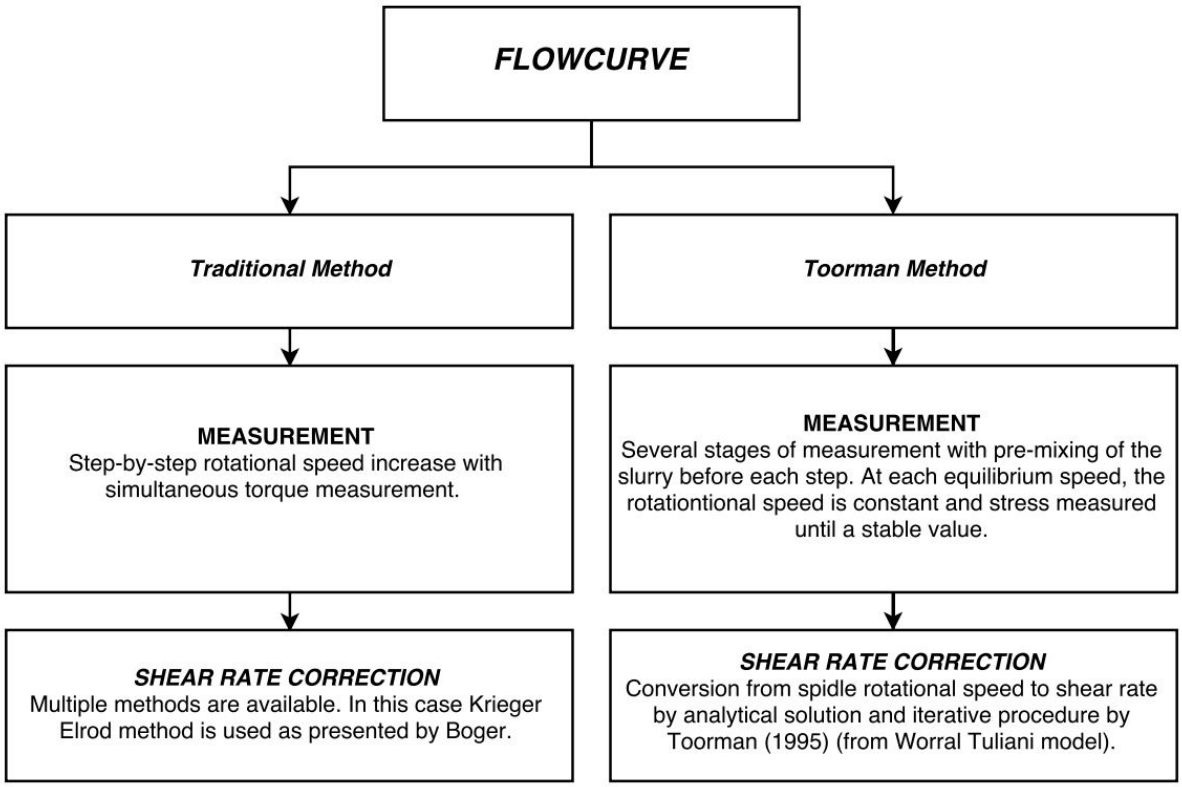

Figure 4.6: Overview flowcurve determination.

To determine a flow curve or rheogram, measurements are done by a rheometer or roto-viscometer. This apparatus measures only two quantities: the first being the rotational speed of the spinde and second the torque exercised on the spindle by the driving mechanism or fluid. To translate these quantities to the known flow curve, which gives the relation between shear rate [1/s] and shear stress [Pa], conversions should take place. The calculation of shear stress is done by calibrating the apparatus with fluids of which the viscosity is known. The calculation of shear rate however is less straight forward. Determining the radius to which influence of rotation extends or the exact velocity distribution in function of radius need more elaboration on. In consecutive order the measurement protocol and shear rate correction are explained.

4.4.1 Rheometer and Spindle

Measurements are conducted by an **Anton Paar Physica MCR301 rheometer**. The method used by the laboratory is a custom measurement protocol as will be explained.

The used rotating part in the rheometer is a vane spindle. The advantage of the vane compared to a cylinder is the minimal disruption of the fluid when immersing and reduced wall slip effect. Also the presence of larger particles are less of a problem when using a vane. Together with these advantages, disadvantages are present. Attention should be taken when analysing the measured data. Research by

Alderman et. al(1991) showed good agreement between cylinder and vane yield stress measurement at low concentrations. At higher concentrations, the vane yielded higher values compared to the cylinder. Other research at the KU Leuven revealed higher stresses for the vane at low rotation speeds and lower stresses at higher rotation speeds. This result in a Bingham viscosity (or limiting viscosity) which is lower than for cylindrical spindles. See the work of Toorman (1995) for further elaboration on the results.

The spindle used was: "**ST22-4V-40-SN11294**" with a diameter of **21.9 mm** and height of **40.3 mm**.

4.4.2 Measurement Protocol

To execute the rheological measurements, two laboratories were assigned with the task. For the determination of the flow curve, 'Waterbouwkundig Laboratorium' in Antwerp was chosen because of its experiences with equal mixtures in the past and adjusted measurement method. From this new protocol various rheological parameters could be obtained depending on the application. Not all parameters will be used for this research but will be shortly explained below.

The first parameter to determine by the protocol is the static yield stress or peak yield stress. Before the micro structure is broken down, an elastic deformation of the bindings could occur, resulting in bulk elastic deformation of the sample Claeys et al. (2013). When such elastic elements approach their critical strain the structure begins to break down causing shear thinning (strain softening) and eventually subsequent flow. At the transition of stress build up to strain softening, the maximal resistance to deformation can be measured, also known as peak yield stress. After breaking, the constant applied shear rate results in propagation of the shear stress to a equilibrium value (see figure 4.7).

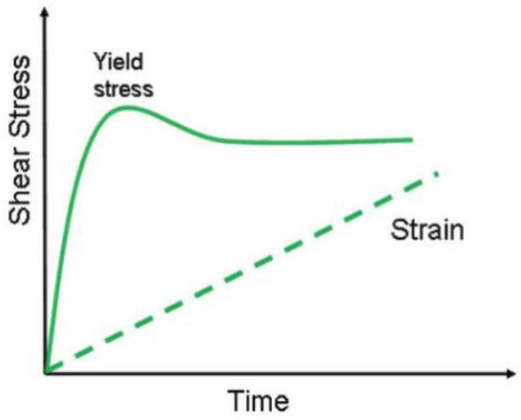

Figure 4.7: Stress evolution of a yield stress material at constant shear rate.

In practice, this part of the protocol will apply a rotational speed of 1 rpm to the *undisturbed* sample for a minimum of 30 seconds so the maximum yield stress is certainly met (lower rpm's will result in longer times before the maximum shear stress is occurred). This part of the protocol will not be repeated.

The next part of the protocol is the construction of the equilibrium flow curve (EFC). A newly developed protocol will be used a guidance for the experiments and is based on previously performed estuarine mud samples. The protocol contains three parts which will be repeated for every preselected rotation speed (EFC step).

1. The first step in the protocol is to pre-shear the sample until a stable starting condition is reached for the sample. The objective of this first phase is to destroy formed flocs and establish a stable starting condition for each step. Practically this is achieved by applying a constant rotation speed of 1000 rpm for 15 seconds.
2. Next is the first EFC equilibrium point. After pre-shearing the sample, before the floc structure is regained, a constant rotation speed of 112 rpm (will change for other EFC steps) is applied for 100 seconds. The stress is measured in time which is needed to maintain this rotational speed. This time-shear stress curve will be used for the calculation of the thixotropic parameters.

After each equilibrium point is recorded, a Dullaert test (Dullaert and Mewis (2005)) (method adapted by Styn Claeys, Antea Group (Claeys et al. (2013))) is performed to obtain the thixotropic parameters. The information obtained in this phase is purely additional and will only be used for better understanding of the mud encountered. In practice, the rotation speed of the spindle is decreased very rapidly from the previous speed to 0.001 rpm for 6 seconds. During this sample time, high sampling is required at 200 samples/second. As a result the retained stress is measured (i.e. time dependant behaviour of the mud in function of the shear stress).

After the Dullaert part, the sample is again pre-sheared to ensure equivalent starting conditions for the consecutive EFC step. This sequence is repeated 9 times in total for the equilibrium rotation speeds of: 112, 56, 28, 14, 7, 4, 2, 0.5 and 0.2 revolutions per minute. The overview of the measurement sequence can be seen in figure 4.8.

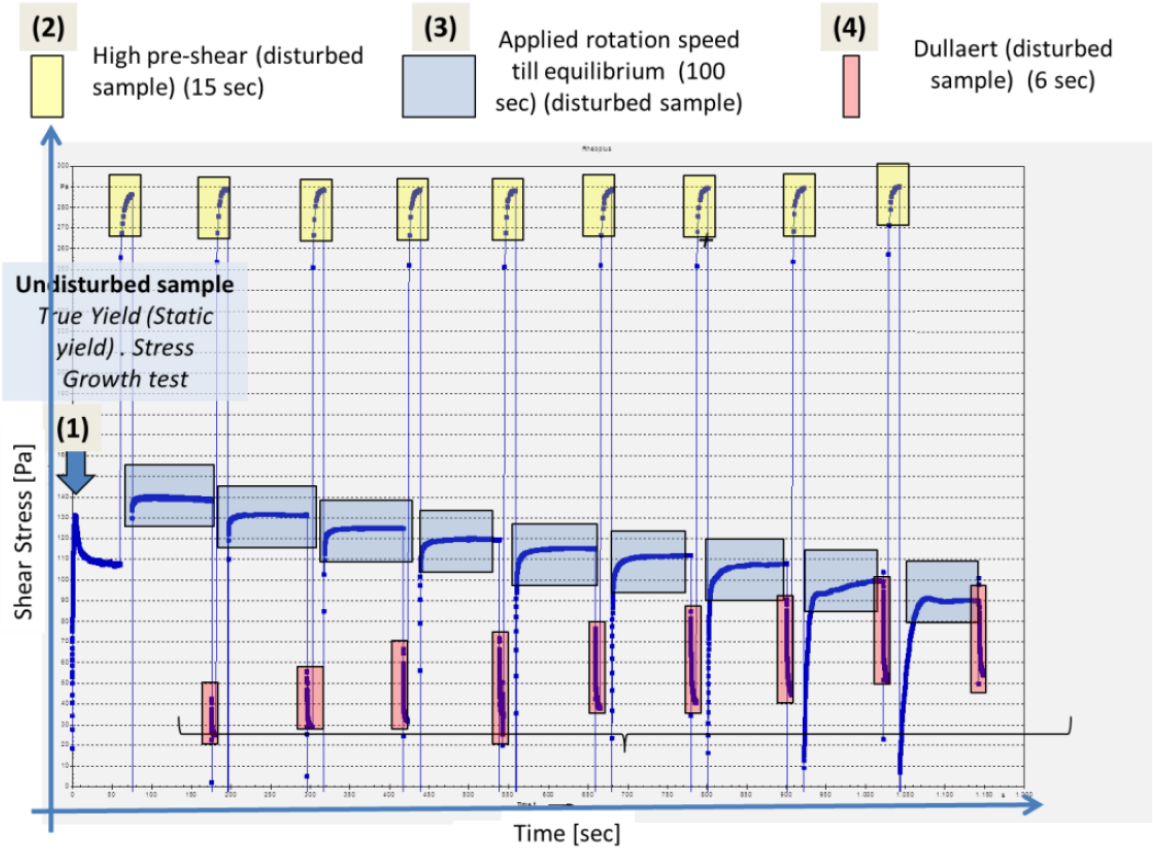

Figure 4.8: Overview measurement protocol as described above.

4.4.3 Shear rate correction

As can be seen in figure 4.9, the shear rate is not linear distributed over the sheared gap. Knowledge of the shear rate distribution is necessary to calculate the correct shear rate from the applied bob rotation speed. This is not evident, given the non-linearity of the rheological behaviour which makes that the shear rate is not solely depending on the geometrical parameters but also depend on the rheological parameters. To obtain the correct shear rate, two methods are presented. Due to practical limitations, measurements are conducted according to the Equivalent Flow Curve protocol and processing/shear rate correction by use of Krieger Elrod/Fisher method.

Toorman correction [Toorman (1995)]

To determine a correct flow curve, which is also comparable with previous researches, the correct shear rate needs to be calculated starting from the vane's rotation speed. Given the dependence on rheological parameters a vicious circle problem arises. All existing methods for concentric cylinder viscometers are based on a shear rate correction method as proposed by Krieger and Elrod (1953). Further elaboration on this preliminary research proposed a correct solution for the condition of plug flow, only requiring knowledge of the magnitude of the yield stress but further independent on the rheological parameters.

A different approach was proposed by E.A. Toorman in 1994. The use of a analytical solution for the flow field exist for only few model fluids with mostly dependence on the rheological parameters. The rheological model, for which an analytical solution is forehand and which also describes well the behaviour of the fluid is the Worral-Tuliani model. With the use of a iterative procedure, in which the rheological parameter estimates are improved, it is possible to obtain the proper shear rate correction for a non-Newtonian fluid. The advantage of working with the exact solution is the deduction of geometrical limitations. This is very useful regarding the requirement of gap width which needs to be 30-100 times the largest particle size.

1. Initially the Krieger solution can be taken as a first approximation (even starting from the Newtonian solution works fine). The parameters of the resulting rheogram are determined using a least squares fitting (LSF) of the data points to the Worrall-Tuliani model for its four parameters (see Appendix B of Toorman (1995)).

2. The integration constants A and B, as well as the yield radius r_y are computed iteratively.

3. The shear rate at the rotating surface is calculated with the Worrall-Tuliani model with the iteratively determined parameters as input. A new flow curve can be drawn.

4. Again a LSF is performed. The initial parameters are updated, by using a relaxation method, necessary to guarantee convergence.

5. Steps 2 to 4 are repeated until convergence.

The convergence behaviour of this scheme is slow and depends strongly on the initial values. Therefore, some relaxation is necessary, but not too much, otherwise the scheme becomes unstable. The iterative procedure is further fully described in the work of Toorman (Toorman (1995)) if of interest.

Although the method is theoretical closing, practical implications could still lead to improper results. To ensure the results are comparable with previous research, the correction method of Toorman (1995) was not used but instead the original model by Krieger and Maron (1952).

Krieger and Maron 1952 Krieger and Maron (1952)

The method developed by Krieger and Maron is applicable in a cup where the radius exceeds the yield radius and thus not all fluid inside the cup will be sheared. For this case they developed a method to determine the shear rate based on the spindle rotational speed (angular velocity) and shear rate given by:

$$\dot{\gamma} = \frac{2\ \Omega}{n} \tag{4.8}$$

$$n = \frac{dln\ T}{dln\ \Omega} \tag{4.9}$$

where 'n' represents the local gradient of the line connecting measurement points on a log-log scale representing torque on the y-axis and angular velocity on the x-axis.

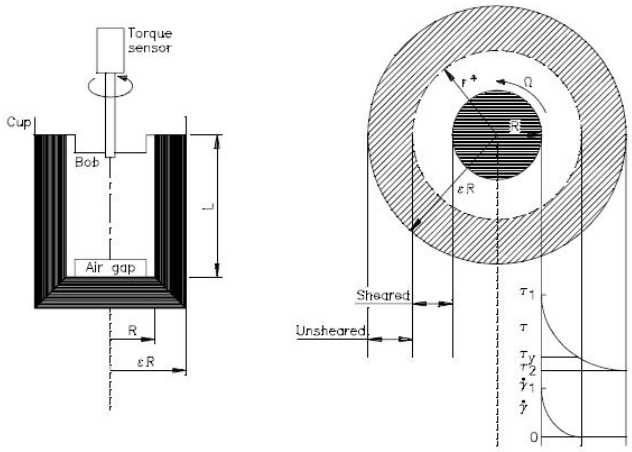

Figure 4.9: Shear stress distribution over the shear gap in a roto-viscometer.

As can be seen in the figure above, fig 4.9, the shear stress extends into the medium dependant on the yield stress. If the requirement of wall shear stress is fulfilled, the equations are valid and can be used.

4.5 Additional soil parameters

As changing the soil parameters will result in a different characteristic of the pump, analysing these parameters to which the measurement data relates, is of great importance. Soils which will be dredged can be characterized apart from flow curve by particle size distribution (PSD), Atterberg limits, organic content, water content and mineralogy.

For the purpose of this thesis research project, representative in-situ soil samples are collected from four different locations in the port of Antwerp with an assistant vessel from the TSHD Pallieter. The use of these samples is to obtain information about the type of soil, their properties and composition. All samples are taken with the use of a "Van Veen Grab" because all properties are possible to determine from a disturbed sample. From this grab, the slurry was directly transferred into an air-tight bucket for storage until laboratory research. To determine all the above characteristics, collaboration with two laboratories was necessary to ensure accurate results. Detailed information about all experiments can be found in chapter 6.

The first company is "Waterbouwkundig" Laboratory in which the following parameters are analysed:

1. **Particle size distribution**
   Determination of particle size distribution with the use of Laserdiffraction. Samples are loaded into the **Malvern - Mastersizer 2000** by an autosampler. Next diffraction patterns are converted into particle size distributions.

2. **Wet density**
   Determining the density of the soil can be measured in various ways. Depending on the viscosity and maximum particle size, an appropriate method was chosen by the laborious. The density was determined with the use of a oscillating U tube. This apparatus determines the density by the measuring the frequency of oscillation. The apparatus used was a **Anton Paar - DMA 500**.

3. **Carbon content**
   The amount of organic carbon is possible to determine with the use of burning the sample corresponding to the Dry Oxidation method requirements. The apparatus used was a **Precisa - prepASH 229**.

Other parameters to complete the soil characteristics are measured at the laboratory of the company "Qmineral" in Heverlee. Completed tests are:

1. **Mineralogical composition**
   The mineralogical composition of the sample was investigated by means of x-ray diffraction. With this method, both bulk mineralogical as well as clay mineralogical content of the clay fraction ($< 2\mu$m) are investigated.

   From this mineralogical composition, the amount of Smectite minerals present in the slurry is determined.

2. **Atterberg limits**
   Information about the limits.

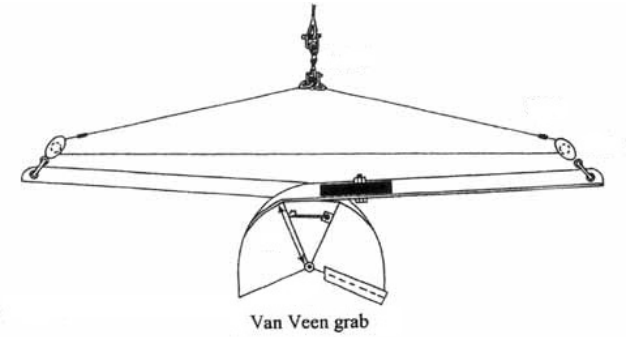

Figure 4.10: Van Veen Grab - Illustration of sampling device as used.

4.5.1 Particle size distribution

An important property of the soil is the Particle Size Distribution (PSD), characterising the distribution of particle sizes relative to the total amount of particles. This size of the particles affects the settling characteristics of the fluid and can thus determine if the fluid can be assumed as homogeneous or as a settling fluid in the prevailing circumstances.

As the sample is characterized by silt and clay, an appropriate method is the laser diffraction, giving a measure of volume. Other measurements include sedimentation, hydrometer of microscopy but were not chosen due to suitability or price of the method. The apparatus used was a Mastersizer 2000, Particle Size Analyser. An example of a Particle Size Distribution can be seen in figure 4.11.
Visualisation is done with the horizontal particle size-axis in LOG scale and vertical volume-axis expressed in cumulative percentage.

4.5.2 Mineralogy

The analysis starts with drying of the sample at 60 degrees for at least 24 hours. After drying both Bulk and mineralogical content of the clay fraction are determined.

Bulk mineralogical analysis. 10% of an internal standard material (Zincite, ZnO) was added to a representative part of the sample. This is done to create diffraction peaks with known position and height to correct the measurement. The powder was than mixed and ground in a McCrone micronising mill in ethanol. After drying, the sample was loaded in a sample holder by side-loading and measured by x-ray diffraction (using CuK α radiation). The subsequent quantification was performed by using a combination of the Rietveld method and of the PONKCS method. The quantitative mineralogical composition of the samples is shown in table 7.1.3. The corresponding diffraction pattern is displayed in figure10.6.

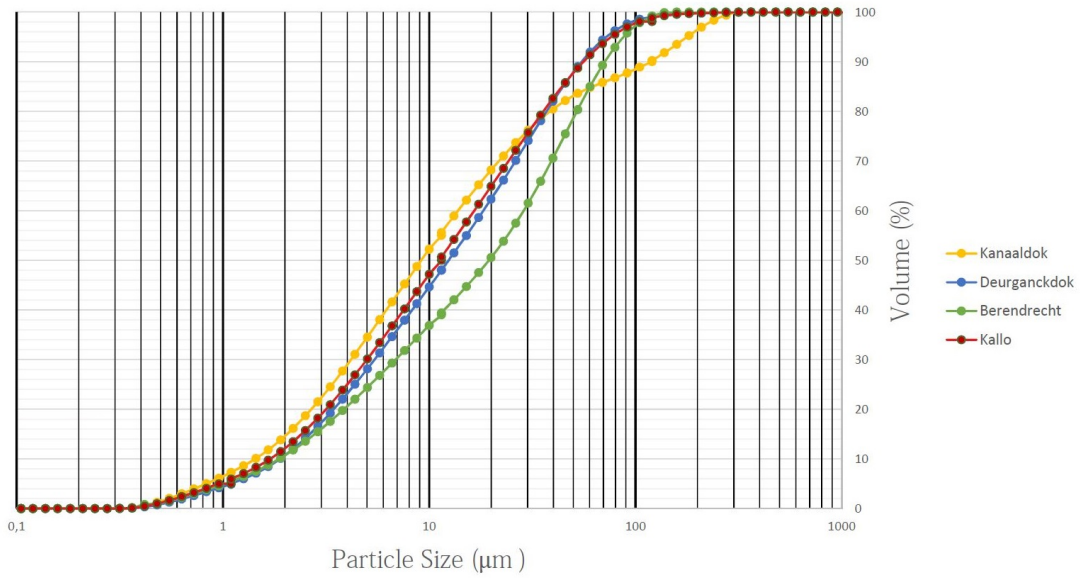

Figure 4.11: Particle Size distribution measurements - Overview

Using the 'Rietveld' method, diffraction structure patterns as measured are compared to known patterns from literature to identify the mineral. The PONCKS (Partial of no known crystal structures) is used when no identification was possible by the 'Rietveld' method. More information can be found in Scarlett and Madsen (2006).

4.5.3 Organic Content

Various methods are available to determine the amount of organic content in the sample. To quantify the amount of dissolved gas the soil is able to produce, the amount of organic content had to be determined. The samples of all four locations were subjected to the **Dry Oxidation Method** where the sample is heated to certain characteristic temperatures. Based on the weight loss due to combustion of organic content at these temperatures the amount can be determined.

Measurements are executed based on the standardization of EN 12879:2000 (Characterization of sludges - Determination of the loss on ignition of dry mass.) EN12879 (2000) prescribing the temperatures and organic constituents. First the sample is dried at 105 degrees to extract all water content. At this point the amount of dry mass can be weighed. After weighing, the sample is heated further on **550** degrees whereafter the sample is again weighed. The loss at this stage is characterised as "loss on ignition" and is calculated as follows:

$$w_V = \frac{m_b - m_c}{m_b - m_a} * 100 \tag{4.10}$$

where:

w_V is the loss on ignition of the dry mass of a solid sample, in percentage
m_a is the mass of the empty crucible, in grams
m_b is the mass of the crucible containing the dry mass, in grams
m_c is the mass of the crucible containing the ignited dry mass, in grams

After determining the weight percentage of organic matter, the sample is heated further to 800 degrees for estimating the loss on ignition due to lime content/ calcium carbonate ($CaCO_3$). Further heating the sample after this temperature can result in loss of water out of the crystal lattice leading to inaccurate results.

4.5.4 Atterberg Limits

Determining solely the parameters above, as particle size distribution and mineralogical parameters are not sufficient to fully describe the behaviour of the clay. Also important to determine are the liquid and plastic limit - also known as the Atterberg limits.

When a clay soil undergoes transition from dry to wet, great amount of water is absorbed by the soil. During this transition from dry to liquid it undergoes distinguishable changes in behaviour and consistency. As the water content increases in the soil, four states may be defined for cohesive soils: solid, semi-plastic solid, plastic and liquid van den Berg and Stam (2013). The transition between states is rather gradual although arbitrary limits are defined for convenience (Atterberg Limits). Important to know is that Atterberg limits are determined on well mixed uniform mixtures and give no representation or indication about particle fabric or residual bonds between particles as can be encountered in natural soils.

The difference in consistency is related to the water content. Obtaining this parameter can be done by drying the soil sample at approximately 100 degrees and measuring the difference in weight due to the evaporation of water. The Natural Water content (WN), liquid limit and plastic limit can be determined by using this method.

The Liquid Limit (WL) is the moisture content at which the soil ceases to be liquid and becomes plastic according to ASTM-standard D4318. It can be determined by a Cassagrande apparatus which spreads the material in a bras cup, lifts and drops the cup in a standardized way and counting the repetitions needed to close a handmade groove in the sample. The plastic limit is determined differently. According to ASTM D4318, the plastic limit (WP) is the water content at which clays rolled to strings of approximately 3 mm on a glass plate start to break. Here the transition takes place from solid to semi-plastic solid.

The last parameter completing the Atterberg Limits is the Plasticity Index (IP) expressing the difference in water content between the liquid limit and plastic limit. For example, a soil with low plasticity requires only a small amount of water to turn from solid into liquid state. Also, the closer the natural water content is to the liquid limit, the faster the clay goes in suspension. This is represented by the Consistency Index (IC) = (Wl - WN)/IP.

The Atterberg results for the different locations can be found in the experimental results section.

4.6 In-situ gas presence

A combination of gas and liquid is referred to as multi phase flow. The complex interaction of viscous fluid, various gasses and the hydraulic system is difficult to quantify but will be taken into account.

Composition The composition of the gasses in the dredged material can vary widely in space and also in time! As the gas is a result of a bio-organic process, the composition and quantity vary during the process. Most of the time the mixture will be a composition of air and methane gas. Methane (CH_4) is a flammable product as the result of decomposition of organic material (Carbons) in the absence of oxygen. Organic material can be the remains of many sources as remains of fish, other water animals, debris of plant or trees, etcetera. In some cases the mixture can contain also carbon dioxide (CO_2), hydrogen sulphide (H_2S) and others which originate from industrial process remainders dumped in the rivers. The H_2S product can be observed due to the smell of "rotten eggs" alike.

The gasses can be present in two ways:

1. Dissolved in the transportation liquid: Dissolved in the water which transports the solids through the pump. All of the above mentioned gasses can be dissolved in the liquid depending on the liquid temperature and pressure.

2. Trapped in the soil: As the soil contains gas cavities, which are kept in the soil due to high internal soil stresses (viscosity dependant), the gas due to organic process is kept in the soil which will be dredged.

Note: As the dredging areas which are investigated are dredged on a regular basis, the time between dredging campaigns and the governing water temperature are effecting the biological processes and thus the possible gas content in the liquid and soil.

It is possible to observe the in-situ gas as bubbles appearing at the surface as this is rather exceptional. Most of the time the gas can't be noticed. However during the dredging process, the in-situ soil and water conditions are disturbed resulting in a pressure and composition change. Sucking the soil from sea bottom to the entrance of the dredge pump frees most of the gas and causes it to expand dramatically. Expansion of gasses and solubility can consequently be estimated by the "Law of Boyle-Gay Lussac" and "Law of Henry". A brief overview of both is given below as well as a quantitative example to demonstrate the origin of the measured Gas Volume Fraction by the "Sonartrac".

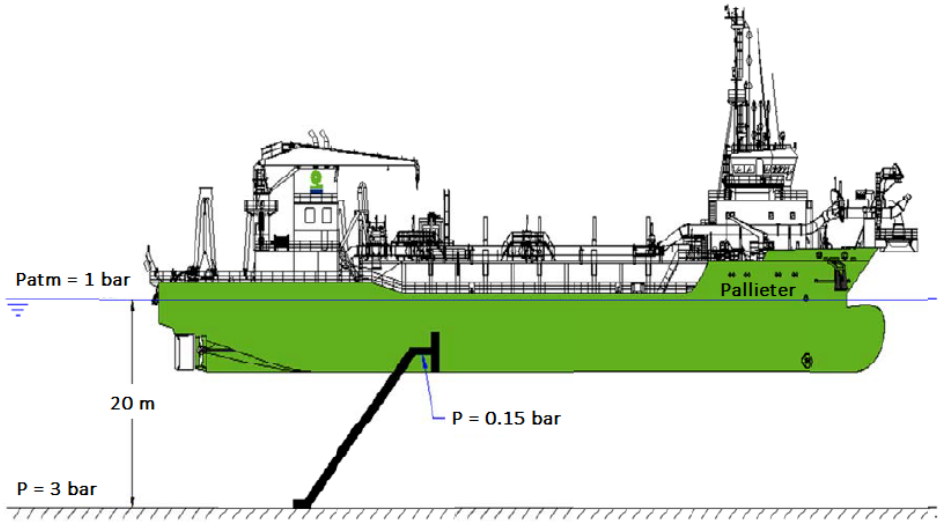

Figure 4.12: Field example when dredging at a depth of 20 meters.

4.6.1 Law of Boyle - Gay Lussac

A change in pressure is the cause of expansion of the trapped gasses. A exact volume of trapped in-situ gas is very difficult to predict but based on the expansion law of Boyle/Lussac several scenario's can be calculated.

As a example, the dredging depth in Deurganckdock is 15m below water level and the atmospheric pressure is 1 bar. This leads to an (absolute) in situ pressure of 2.5 bar. At the suction side of the pump, a convincingly vacuum value of 0.85 bar occurs. This is an absolute pressure of 0.15 bar. According to the law of Boyle - Gay Lussac, the product of absolute pressure and volume equals a gas constant times the absolute temperature of the gas. The temperature can be assumed constant leading to a direct relationship between pressure and volume.

$$p.V = R.T \tag{4.11}$$

The example of Location B, a small gas bubble of 1 cm^3 will expand to a volume of: (2.5/0.15) * 1 cm^3 = 16.66 cm^3 at the suction side of the pump.

A volume of 1 dm^3 of gas per m^3 (1 % of volume) will become 16.66 dm^3 of gas per 1.1566 m^3 (14.5 % of volume) going from 2.5 bar to 0.15 bar absolute.

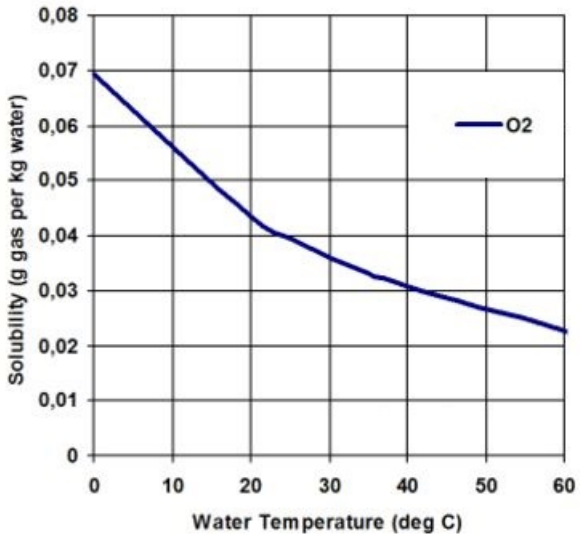

Figure 4.13: Solubility of O_2 in water with varying water temperature.

What the exact amount of trapped gasses in the soil are is very difficult to predict but due to the high amount of organic content (as measured), large gas fractions are likely to occur at these locations. Depending on the efficiency of the degassing installation on board and the amount of gas, residual gasses will be present after the dredge pump and will be measured by the "Sonertrac". Analysis of these measurements will be dealt with further on in the report.

4.6.2 Law of Henry

What also needs to be taken into account is the solubility of the occurring gasses in water. Depending on the circumstances, temperature, pressure and gas characteristics the amount of gas which can be solved in water changes. When the pressure of this liquid changes as in previous example, the solved gas will also expand according to the law of Boyle / Gay Lussac, proportional to the partial pressure of the gas.

At the standard characteristic condition (0 degree, 1 bar), $33dm^3$ methane gas can dissolve in 1 m^3 of water according to the law of Henry. Carbon dioxide dissolves somewhat better, other air components less good. Some gasses related to industrial processes such as sulphur dioxide and ammonia dissolve much better Wikipedia (2017). After a certain time extend, equilibrium will be reached meaning the liquid is maximal saturated with gas. Attention: The law of Henry only applies to saturated solutions of gas in water. No gas will come free from the solution until the solution is saturated.

Saturation of water in the river Scheldt is a important parameter for various ecosystems. The amount of oxygen in water is a result of 1) physical oxygen exchange with the atmosphere, 2) oxygen created due to photosynthesis by for example: algae, 3) consumption of oxygen due to respiration or due to decomposition of organic content. The latter is measured by determining the carbon content of the samples. The estimate is rather rough but can give a good insight (Maris et al. (2014)).

To illustrate this with a example, saturation of the river water needs to be known. 100 % saturation will never be met exactly but vary throughout the year. The nett effect of the above mentioned biological processes will result in saturation changes depending on the oxygen producing or consuming processes. In the summer, supersaturation could occur due to excessive algae grow resulting in small bubbles rising to the water surface. Also is saturation faster reached in higher water temperatures due to lower solubility.

Calculation example: As the river Scheldt will hold a combination of salt ocean water and fresh river water, also known as brackish water, the solubility changes based on the salinity. For this case, a solubility of oxygen will be used of **8.5 ml/l** brackish water (8.5 dm^3 oxygen per m^3 water). At higher pressure, more gas can be solved according to the Law of Henry. Going from 1 bar (atmospheric) to 2.5 bar (1 bar atmospheric and 1.5 bar due to 15 meter of water column = dredging depth) the maximum amount of dissolved oxygen is (2.5 bar/1 bar) * 8.5 dm^3 = **21.25** dm^3 per m^3 water. To calculate the remaining amount of solved oxygen when this water body is transported from sea-floor to pump entrance, the law of Boyle-Gay Lussac is used. Going from 2.5 bar absolute to 0.15 bar absolute, (0.15 bara/ 2.5 bara)* 100% = 6 % will remain dissolved. This leads, with these conditions, 94 % of the 21.25 dm^3 will free itself from the water = 19.975 dm^3. Expressed in volumetric percentage, in the same way Sonartrax measures the GVG, 19.975 dm^3 equals 1.975 %. When no degassing installation would be present in this case, this is the amount which will need to pass the dredging pump with all subsequent consequences.

Figure 4.14: Bubbles arising from the mixture when discharged in the hopper. - 'Pallieter'

Chapter 5

Centrifugal pump de-rating

Pumping a different medium than water results in a different behaviour and characteristics of the centrifugal pump. When pumping fluids with a viscosity much higher than water, additional losses will affect the performance of the pump. For this reason, pump characteristics given by the manufacturer cannot be applied in a viscous environment without applying an applicable correction method. These environments may be as encountered in high concentration clay dredging for example. For correcting the water curve, several empirical methods are available based on laboratory test data. These correction methods all result in a correction factor for the viscous environment based on the known water performance. The corrected units depend on the method used, but in general the flow rate, head and efficiency are scaled according to the following factors.

$$f_Q = \frac{Q_v}{Q_w} \qquad f_H = \frac{H_v}{H_w} \qquad f_\eta = \frac{\eta_v}{\eta_w} \tag{5.1}$$

A valid generalisation, although dependant on the viscosity, is that head and flow rate will normally decrease with increasing dynamic viscosity. Due to increasing losses and friction forces, the power will increase as well as the net positive suction head (NPSH3). Starting conditions of a pump in a viscous environment are not considered as the dredging operation is always started in water conditions.

Prior to elaboration on the present de-rating models, the following should be clear to the reader. Almost all de-rating experiments used different pump / impeller models at which the model is calibrated and verified. To this extend no general de-rating model is available and applicable for all pumps as encountered, at this time. Attempts have been made to relate a de-rating model to dimensionless parameters in order to cover all centrifugal pumps regardless of operating range or geometry.

Other than various empirical procedures for estimating the viscous performance of a pump, a detailed loss analysis could also be conducted. In contrast to the empirical procedure, where only few parameters are necessary as input, the detailed loss analysis requires full knowledge of impeller/pump geometry and flow regime. This is not always known in detailed terms so caution is required when interpreting the results of this method.

Another parameter influencing the performance of centrifugal pumps is the presence of gas in the mixture (two-phase flow). Also for this problem no general solution is forehand but the magnitude of influence will be researched in combination with the rheological parameters of the mixture. The governing soil parameter is expected to be the yield stress of the fluid as this resembles the resistance the mixture exhibit on the release of air. A detailed analysis can be read further in this chapter.

Lastly, all published de-rating standards are designed for pumps handling Newtonian fluids. Various researchers have searched for a rheological characterisation of non-Newtonian fluids to extend the current de-rating-model range outside Newtonian fluids alone. The differences in prediction and rheological parameters were researched in combination with various de-rating standards and methods. The same will be done here, only for much larger pump dimensions as currently encountered in literature.

5.1 Factors influencing losses

Prior to determining the reduction in pump performance and efficiency, it is important to identify the factors influencing pump behaviour when pumping viscous fluids. Various physical phenomena are involved which determine the magnitude of the losses to be expected. The following individual losses together with all secondary losses determine the power balance of the pump. It is possible that a combination of effects will result in a same nett performance due to contradictory influences.

$$P = function\left(\frac{\rho g H Q}{\eta_{vol}\eta_h}\right) + P_{RR} + P_m \tag{5.2}$$

where

P: power input at the coupling of the pump
η_{vol}: volumetric efficiency
η_h: hydraulic efficiency

1. **Mechanical losses (P_m):** These losses are not governed by the medium in the pump and thus should not be taken into account when correcting the characteristics for viscous fluids.
2. **Leakage losses:** These are the losses due to backflow trough the annular seal of the pump. The phenomena is natural as a fluid tends to flow from a high pressure area (outlet) towards the low pressure area (inlet). To reduce this effect some impellers are equipped with expeller vanes. The leakage losses generally decrease with increasing viscosity or decreasing Reynolds number.
3. **Disk friction losses(P_{RR}):** This is one of the governing factors in determining the reduced performance of the pump. The disk friction influence on efficiency is very important, especially for low specific speeds (n_q).P_{RR} represents the sum of all disk friction losses on the impeller side shrouds and axial thrust balancing drum or disk. The disk friction part contribution will increase with decreasing Reynolds number or increasing viscosity.
4. **Hydraulic losses:** These losses are situated at the inlet of the pump, impeller and diffuser, made up by friction losses and turbulent dissipation. Detailed quantification of all loss factors will be discussed further.

5.1.1 Disk friction losses

It is known that roughness increases the resistance to flow in turbulent conditions. It is however only the case when the rough surface is extending outside the laminar sub-layer. With increasing Reynolds number the boundary layer thickness decreases and the permissible roughness for a hydraulically smooth condition, drops as well. This results in vortex shedding due to the roughness peaks and the exchange of momentum with the main flow.

The same is valid when considering a impeller with two "straight" side-walls rotating in a (viscous) fluid. The power consumed by the disk follows the relation $P_{RR} = function(\rho * \omega^3 * r_2^5 * c_f)$ as this relation follows from the integral of torque exerted by friction on the rotating impeller. Where the friction coefficient c_f depends both on the Reynolds number and surface roughness. A combination of Reynolds number and surface roughness will give insight in the flow regime and determine whether the actual surface roughness is of significant importance or not. As many other factors are of influence on the disk friction losses, a brief summary will be given below.

1. Reynolds Number
2. Roughness of the rotating disk
3. Roughness of the casing walls
4. Axial side wall gap (s_{ax})
5. Shape of the casing and size of the impeller side wall gap
6. Leakage flow
7. Fluid between the impeller and side wall

To quantify the disk friction losses, empirical formulas and relations are available based on friction losses of rotating disks or cylinders in a particular fluid. Starting with the Reynolds number to include viscosity of the fluid in the equation is followed by surface roughness, impeller sidewall gap and rotating wetted surface. From these quantities friction coefficients are calculated resulting in power consumption per side of a rotating disk. If all other quantities are kept constant while altering the kinematic viscosity, the ratio between disk friction and total power consumption can be visualised by the figure below (figure 5.1).

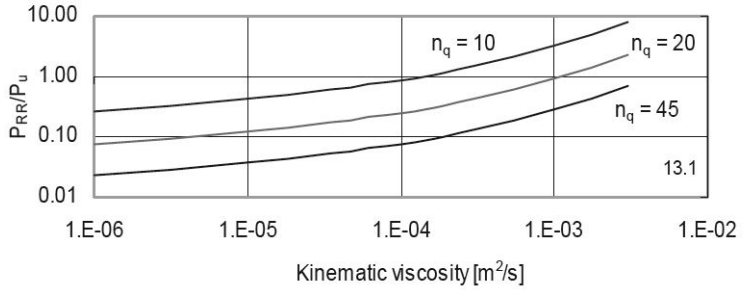

Figure 5.1: Relation between disk friction power P_{RR} and usefull power delivered to the fluid P_U.

To obtain the relation as depicted above in figure 5.1, the relation from Gulich (2008) is used and can be found as eq. 3.5.12 and 3.5.13 in his work. The equations can also be found below with equation 5.3 for turbulent conditions (Re $> 10^5$) and equation 5.4 for all other cases.

$$\frac{P_{RR}}{Pu, opt} = \frac{770\ f_{R,La}\ f_L}{n_q^2\ \Psi_{opt}^{2.5}\ Re^{0.2}\ f_q} \tag{5.3}$$

$$\frac{P_{RR}}{Pu, opt} = \frac{38500\ k_{RR}}{n_q^2\ \Psi_{opt}^{2.5}\ f_q} \tag{5.4}$$

where: $f_{R,La}$ = influence of roughness by roughness rotating disk, f_L = influence of leakage flow, n_q = specific speed, Ψ_{opt} = head coefficient at BEP, f_q = number of impeller eyes (= 1).

As explained is the main cause of power an increase friction between fluid and the rotating surface. This should be kept in mind when examining the disk friction losses of an impeller equipped with expeller vanes. Expeller vanes are used to reduce the amount of backflow i.e. flow through the annular seal from the high pressure outlet area to the low pressure inlet area. As this results theoretically in a surface roughness with a order of magnitude from 50 to 100 mm, losses would be disproportional and should thus be avoided when pumping viscous fluids.

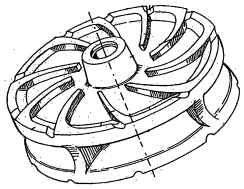

Figure 5.2: Impeller equipped with expeller vanes on the rear sidewall.

Surface Roughness

Altering the surface roughness could result in contradictory effects. Although a higher disk friction is to be expected with a corresponding increase in required pumping power as explained before, also a higher flow turning could be expected i.e. higher theoretical head. Due to a thicker boundary layer as the result of a higher surface roughness, the difference between c_{2u} and u_2 (see velocity triangles) is reduced

and a higher theoretical head is achieved. Also transition in boundary layer flow pattern near solids boundaries from fully rough to hydraulically smooth can be responsible. These effects were confirmed by tests which revealed slightly higher heads when a disk with higher roughness was used. The effect is not always visible and depends if the magnitude exceeds the losses caused by the roughness. (Guang (2000))(Stoffel et al. (2002))(Guang (2014))

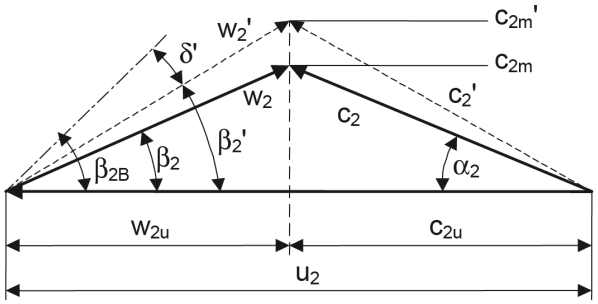

Figure 5.3: Centrifugal pump velocity traingle for impeller outlet. u_2 = circumferential velocity of the impeller, w_2 = particle relative velocity, c_2 = absolute velocity, c_{2u} = Circumferential component of absolute velocity, α_2 = absolute outlet angle without blockage. Dotted line indicate outlet blockage.

5.2 De-rating models

In the past, various researchers have searched for a comprehensive relationship between viscosity and pump head and efficiency reduction. Also new research has improved empirical relations used in older models for pump derating. Because the research was mainly conducted on smaller centrifugal pumps (max 630 mm (Sellgren et al, 1999)) and high rotational speeds (1200 - 1900 rpm), applicability to dredge pumps is until now unknown and the older models will still be taken into account in this research. Because of uncertain effects on larger pumps, validation of all preliminary models will be discussed. All models below are used in the R Studio script used for analysing the live data of TSHD Pallieter on the river Scheldt.

5.2.1 Newtonian pump de-rating

All available de-rating models are designed and validated for Newtonian fluids. An example is the method of the Hydraulic Institute, which like all others, provide pump performance prediction when handling Newtonian fluids. It is only possible to provide this prediction for handling a viscous mixture when the particular performance characteristics for water are known (Hydraulic Institute (1983)).

All methods obtain after the calculation correction factors for head, flow rate and efficiency which can be multiplied with water characteristics as provided by equation 5.1. De-rating methods available at this moment are:

1. 1983 - Hydraulic Institute (Hydraulic Institute (1983))
2. 1989 - KSB Krieselpumpen lexicon (Kreiselpumpen KSB (1989))
3. 2004 - Hydraulic Institute 9.6.7 (ANSI and Hydr (2004))
4. 2008 - Gulich pump handbook (Gulich (2008))
5. 2009 - Graham (Graham et al. (2009))
6. 2015 - ANSI / HI 9.6.7 (ANSI (2015))

The procedure and equations necessary for de-rating can be found in the following chapters with inclusion of alternative approaches as presented by various researchers. As the procedure is relatively equal for each method, it will only be demonstrated for the Hydraulic Institute (1983) de-rating equations.

Hydraulic Institute (1983)

The method of Hydraulic Institute (1983) was developed and based on preliminary research in the field of Newtonian centrifugal pump de-rating. Only when the performance data of the pump is known when water is pumped, the method can be applied. The method is designed to fit the body of research data from the past with the use of the factor 'B'.

The procedure as was published yielded correction factors in function of Q, H, ν and q*. The factor of B_{HI} includes implicitly Q, H and ν what results in a dimensionless parameter with the following relationship $B_{HI} \sim 1/Re^{0.5}$. Only disadvantage of this method is exclusion of the pump specific speed which proved to be of influence. Also at higher specific speeds ($n_q > 20$), over-prediction of power is very likely while under-prediction at $n_q < 15$ according to Gulich (2008).

With all parameters in SI-Units unless otherwise stated. Subscripts 'w' are used for characteristics in water while parameters with subscript 'v' are intended for viscous pump performance.

First the parameter B is calculated based on the water performance at BEP.

$$B_{HI} = \frac{480\ \sqrt{\nu}}{Q_{BEP}^{0.25}(g\ H_{BEP})^{0.125}} \tag{5.5}$$

Next the factor f_Q is calculated to correct flow rate at BEP in a viscous environment.

$$f_Q = e^{-0.11(logB_{HI})^{5.5}} \tag{5.6}$$

Previous determined correction factor can only be applied at BEP, at all other flow rates equation 5.7 should be used. $q*$ is given by $q* = \frac{Q}{Q_{BEP}}$.

$$f_{q*} = 1 - 0.014(B_{HI} - 1)(q* - 1) \tag{5.7}$$

The flow rate when operating in a viscous environment (at BEP or elsewhere with consequent f_Q or f_{q*}) is than given by:

$$Q_v = f_Q * Q_w \tag{5.8}$$

The correction factor for head is calculated as follows and is independent from flow rate.

$$f_H = (0.25 + 0.75 f_Q) f_{q*} \tag{5.9}$$

Head characteristics in a viscous flow are given by:

$$H_v = f_H * H_w \tag{5.10}$$

Although some researchers made a distinction between pumps with or without impellers equipped with expeller vanes, Hydraulic Institute (1983) doesn't take this into account.

$$f_\eta = e^{-\alpha(B_{HI} - 0.5)^{1.08}} \tag{5.11}$$

where:

$$\alpha = 0.05 e^{0.04\sqrt{B_{HI} - 0.5}} \tag{5.12}$$

When all correction factors are calculated at a particular flow rate, expected power consumption can be calculated as follows:

$$P_V = \frac{\rho_v\ g\ Q_v\ H_v}{\eta_v} \tag{5.13}$$

All of the equations above were transformed into a nomogram by the Hydraulic Institute for easy usage. The graph is called 'Hydraulic Institute Chart' and referred to many times in literature. Equal to the procedure above does the graph contain a lower part where based on BEP values for water a starting point is created. Hereafter viscous correction values can be read for head, flow rate and efficiency for **Newtonian fluids** (Hydraulic Institute (1983)).

Kreiselpumpen KSB (1989)

The procedure as proposed by the KSB Krieselpumpen lexicon is generally equal to the Hydraulic Institute 1983 apart from that it includes the influence of specific speed in the parameter B. When the specific speed is equal to 15 , the parameters B and B_{HI} are equal. Another point of difference is the exception for the case of expeller vanes. Also a limit was set when the correction factor for efficiency and cannot be less than 0,4 according to the formula. An overview of the formulas specific for the KSB method can be found in table 5.1.

Although the procedures are quite similar, much different results are to be expected in some areas. Because the influence of specific speed is dominant, large drops in efficiency occur when the specific speed deviate from 25 a 30. Generalization of this method was questioned as validation was only done with the use of one test at $n_q = 46$ as reported by Mollenkopf (1978).

KSB-Kreiselpumpen-Lexikon. 3. Aufl	
B factor	$B_{HI} = \sqrt{\frac{\nu}{Q\ n^{(s)}}}(g\ H)^{0.25} = B_{HI}\sqrt{\frac{15}{n_q}}$
Correction factor for flowrate at BEP. .	$f_Q = \left(\frac{15}{n_q}\right)^{0.013B} \quad e^{-0.165(logB)^4}$
Correction factor for flowrate ratio.	$f_{q*} = 1 - 0.014(B_{HI} - 1)(q * -1)$
Correction factor for head. .	$f_H = (0.25 + 0.75 f_Q) f_{q*}$
Correction factor for efficiency. .	$\beta = 0.083 B^{0.59}$
Correction for efficiency. .	$f_\eta = B^{-\beta} - \Delta n_q$
Correction for efficiency (With expeller vanes.)	$n_q < 25 : \Delta n_q = 0.005(25 - n_q)$ $n_q > 30 : \Delta n_q = 0.005(n_q - 30)$
Correction for efficiency (Without expeller vanes.)	$f_{\eta,0} = 0.4 + 0.6\ f_\eta$
Power	$P_v = \frac{\rho_v\ g\ Q_v\ H_v}{\eta_v V}$

Table 5.1: De-rating method and formulas according to the KSB-Kreiselpumpen-Lexikon - third version.

Gulich (2008)

Another method available for viscous pump de-rating is established by Gulich (2008). Gulich (2008) emphasised the strong relation between viscous pump performance de-rating, Reynolds number and the specific speed. The combination of both influencing factors resulted in a modified Reynolds number as given in equation 5.14 below:

$$Re_{mod} = Re\ \omega_s^{1.5}\ f_q^{0.75} \tag{5.14}$$

To quantify the expected losses, a correlation was established between preliminary test data and an analytical detailed loss analysis. Test data used for this research was found in:

1. Hergt and al (1981)
2. Mollenkopf (1978)
3. Hamkins and al (1987)
4. Saxena and Et al (1996)

An overview was presented by plotting all measurements from the researchers above, in combination with the loss analysis against the modified Reynolds number (equation 5.14). The optimal correlation

between both equals the following formulas in Table 5.2.

Gulich 2008	
Reynolds number	$Re = \frac{u r_2}{\nu} = \frac{\omega {r_2}^2}{\nu}$
Modified Reynolds number	$Re_{mod} = Re\ {\omega_s}^{1.5}\ {f_q}^{0.75}$
Correction factor for head H_{opt}.	$f_{H,opt} = [Re_{mod}]^{-\left(\frac{6.7}{{Re_{mod}}^x}\right)}$
Correction factor for efficiency .	$f_\eta = [Re_{mod}]^{-\left(\frac{19}{{Re_{mod}}^y}\right)}$
Correction factor for flow rate	$f_Q = f_{H,opt}$
Correction factor for head at $q*$ not equal to 1.	$f_H(q*) = 1 - (1 - f_{H,opt})(q*)^{0.75}$
	$q* = \frac{Q}{Q_{BEP}}$
Power consumption	$P_v = \frac{\rho_v\ g\ Q_v\ H_v}{\eta_v}$
Correction factor for Power	$f_P = \frac{f_Q\ f_H}{f_\eta}$
Correction factor for required NPSH3	$f_{NPSH} = 1 + \zeta_E \frac{c_{f,v}}{c_{f,w}} \frac{{c_{1m}}^2}{2\ g\ NPSH_3}$

Table 5.2: De-rating method of Gulich (2008) based on prior research data and loss analysis.

Due to some spread in measurement data, the exponent 'x' in the correction factor for head and efficiency is chosen between some minimum and maximum value. For $f_{H,opt}$ the exponent is minimal 0.68, mean 0.735 or maximum 0.81. Consequently for efficiency between 0.65, 0.705 and 0.77 can be chosen.

ANSI/HI 9.6.7 2004 de-rating method

Further development of de-rating theories in combination with more test data available has led to an improvement of Hydraulic Institute (1983) and resulted in ANSI/HI 9.6.7 - 2004. The method is still based on a starting parameter 'B' but now is supplemented with specific speed as can be seen in the following equations.

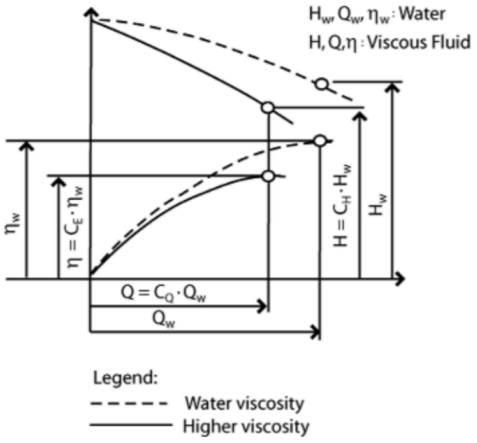

Figure 5.4: Schematic overview of corrected head and efficiency curves for water and viscous service.

The de-rating procedure provided by ANSI 9.6.7 - 2004 is shown in detail here:

Step 1: Determine the factor B on the water characteristics of the pump. In this case, the water characteristics are provided by the pump manufacturer (IHC) in the form of a measurement test report.

NOTE: If the factor B < 1, the influence of viscosity on head, flowrate and efficiency is negligible and all correction factors will be equal to 1. In this case viscosity will only have influence on required pumping power. If B > 40, correction factors include high uncertainty and will result in inaccurate predictions.

Step 2: Calculate the correction factor corresponding to flow rate by the following formula.

$$Q_v = C_Q * Q_w \tag{5.15}$$

Using the above formula, there is a correction value obtained for flow rate at BEP. This correction value is also valid for head at BEP as demonstrated by the following formula.

$$H_{BEP-v} = C_{BEP-H} * H_{BEP-w} \tag{5.16}$$

Step 3: Now the correction values are obtained for both flow rate and head at BEP, the correction value for head outside BEP can be determined. In contrast to flow rate, the correction factor for head is depending on flow rate and thus not constant over the flow rate range.

$$H_v = C_H * H_w \tag{5.17}$$

Step 4: The penultimate parameter which need to be corrected when pumping a viscous fluid is the efficiency of the pump. How the efficiency is calculated for a water regime can be read in section 3.6.

$$\eta_v = C_\eta * \eta_w \tag{5.18}$$

Step 5: The final parameter, for a complete pump characteristic overview, is the pump shaft input power. This parameter is also corrected when pumping a viscous fluid. The result of a reduced efficiency is a increase in required input power with other parameters kept constant.

$$P_v = \frac{\rho_v \; g \; Q_v \; H_v}{\eta_v} \tag{5.19}$$

With Q in m^3/s, head in m, shaft power in kW and efficiency (η) in %. The parameter s is specific gravity which can be calculated as follows:

$$s = \frac{\rho_{viscous}}{\rho_{water}} \tag{5.20}$$

A summary of the used equations can be found in Table 5.3. It should be noted that this procedure is also an empirical method, similar to Hydraulic Institute (1983) and Kreiselpumpen KSB (1989). Therefore the origin of measurement data could be of great importance. The results were established with relatively small centrifugal pumps, single-stage and a maximum Reynolds number of $4 * 10^6$ should be expected in water service.

ANSI / Hydraulic Institute 9.6.7 - 2004	
Parameter	$B = \frac{480\ \sqrt{\nu}}{Q^{0.25}(gH)^{0.125}} \left\{ \frac{n_{q,ref}}{n_q} \right\}^{0.25}$ where $n_{q,ref} = 20$.
Correction factor for flow rate.	$f_Q = e^{-0.165(logB)^{3.15}}$
Correction factor for head at BEP.	$f_{H,BEP} = f_Q$
Correction factor for head at $q*$ not equal to 1.	$f_H(q*) = 1 - (1 - f_{H,BEP})(q*)^(0.75)$
Correction factor for efficiency.	$f_\eta = B^{-\beta}$ with: $\beta = 0.0547B^{0.69}$
Power at coupling.	$P_v = \frac{\rho_v\ g\ Q_v\ H_v}{\eta_v}$
Correction factor for NPSH3.	$f_{NPSH} = 1 + A_1 \left\{ \frac{1}{f_{H,BEP}} - 1 \right\} \left\{ \frac{n_{ss,Ref}}{n_{ss}}, \right\}^{1.33}$

Table 5.3: De-rating method presented by ANSI/HI 9.6.7 in 2004.

For pumps with radial inlet: $A_1 = 0{,}5$. The factor $n_{ss,Ref} = 200$. Apply the f_{NPSH} at constant flow (i.e. without shifting the flow by factor f_Q).

ANSI/HI 9.6.7 2015 de-rating method

The next update in American national standard for rotodynamic pumps was issued in 2010 and improved the ANSI 9.6.7 - 2004 by increasing the test data used to validate the model. Further improvements were made again and in 2015 the latest version became available. Only 2015 will be discussed due to minuscule difference between the both. Although this method only differs in small detail from 2004 also, the differences will be discussed briefly.

A first improvement was made by adjusting parameter 'B' from 2004 to 2015. This to fit the larger body of test data. Next a small factor was added to the equation for efficiency reduction due to new research knowledge in power requirement. Executing the method is equal to ANSI 9.6.7 - 2004 and can be found in the previous section.

ANSI / Hydraulic Institute 9.6.7 - 2015	
Specific Speed	$n_s = \frac{N*(Q_{BEP-W})^{0.5}}{(H_{BEP-W})^{0.75}}$
Parameter B	$B = 16.5\ \frac{v_v^{0.5}, H_{BEP-W}^{0.0625}}{Q_{BEP-W}^{0.375}, N^{0.25}}$
Correction factor for flow rate.	$C_Q = (2.71)^{-.0165*(log_{10}B)^{3.15}}$
Correction factor for head at BEP.	$C_{BEP-H} = C_Q$
Correction factor for head at $q*$ not equal to 1.	$C_H = 1 - \left[(1 - C_{BEP-H}) * \left(\frac{Q_W}{Q_{BEP-W}} \right)^{0.75} \right]$
Correction factor for efficiency.	$C_\eta = B^{-0.0547*B^{0.69}}$ (for $1.0 < B < 40$)
Power .	$P_v = \frac{Q_v * H_v * s}{367 * \eta_{vis}}$

Table 5.4: De-rating method presented by ANSI/HI 9.6.7 in 2015.

5.2.2 non-Newtonian pump de-rating

The models available for pump de-rating to date are all based on **Newtonian** fluids as can be seen in the previous section. It should be clear that all research conducted in the field of non-Newtonian fluids included the search for an appropriate input parameter to validate the applicability of the Newtonian models when handling non-Newtonian fluids. The search for this parameter was approached differently by the researchers and in time.

As read in the section about rheological parameters, Newtonian fluids are characterized by only one parameter (i.e. the dynamic viscosity/kinematic viscosity, μ). To translate the various parameters characterising a non-Newtonian fluid into a single value, can be approached differently depending on which parameters are thought to be of influence. For example, if there is chosen for apparent viscosity at a low shear rate, there will exist a high influence of yield stress. The effect of yield stress is however ruled out when use is made of the Bingham plastic viscosity (= coefficient of rigidity η).

The methods currently available are developed by Walker and Goulas (1982), Sery and Slatter (2002), Kabamba (2006) and Graham et al. (2009). Although only these methods are available, the method statements which were developed can be applied to other de-rating methods as well. As only the method is verified for the slurry as used during laboratory research at small pump scale, no method is excluded at this point due to unknown effects in large centrifugal pumps.

Below can be found an overview of all research combining centrifugal pumps with non-Newtonian fluids. Table 5.5 gives a summary mixtures used during the research as well as pump and approach used.

	Walker and Goulas (1984)	**Sery and Slatter (2002)**	**Kabama (2006)**	**Graham (2009)**	**This Thesis (2017)**
Centrifugal pump used	Hazleton 3 in B CTL and Warman 4/3	Warman 4/3	GIW 4/3 and Warman 6/4	GIW 4/3 and Warman 4/3	IHC HRMD 222 - 47 - 110
Material tested	Coal dust and kaolin clay	Glycerine and kaolin clay	CMC, kaolin and bentonite	CMC and Ultrez 10	Estuarine mud suspensions*
Approach used	Walker and Goulas	Walker and Goulas	Walker and Goulas	Graham et. al.	Hydraulic Inst. 1983 KSB Krieselpumpen Graham et. al. 2009 Gulich 2008 ANSI/HI 9.6.7
Reynolds number	$1 * 10^7$ (max 1200 rpm)	$1 * 10^7$	$1 * 10^7$	$1 * 10^5$ (max 1400 rpm)	$2.5 * 10^7$ (max 195 rpm)

Table 5.5: Overview on non-Newtonian pump de-rating research and used method statement.

Walker and Goulas (1982)

Walker and Goulas were one of the first to stress the importance of a full rheological characterisation of the mixture in relation the pump de-rating. Repeating pump performance tests with a mixture only characterized by volumetric percentage of clay could lead to very different results due to incomplete rheological information. Research earlier than Walker and Goulas, i.e. (Herbich (1959), Bonnington (1957)), did include rheograms but only from samples made after testing or no complete rheogram at all. Therefore it was not possible to give a qualitative interpretation of these results.

It was found that slurries with a lower SG (Specific Gravity) of 1.248, but high yield stress, didn't result in a large head or efficiency difference around BEP compared to the water characteristics but started to deviate tremendously at low flowrates. The influence around BEP is still valid to date but deviation at low flow rates was found to originate from the accumulations of air pockets in the low pressure regions of the impeller (see Furlan et al. (2016)). Higher SG fluids can result in large drops on efficiency and moderate on head.

Regarding the applicable shear rate to use for the calculation of apparent viscosity, potential flow calculations in the blade passage of a radial vaned impeller are used. According to Vavra et al. (1960), the apparent viscosity should be calculated with a characteristic shear rate, radial velocity gradient, of 2Ω (with Ω in rad/s leading to $\dot{\gamma}$ in s^{-1}). This assumption replaces the recommendation of Duckham (Duckham (1971)) to use a shear rate between 100 s^{-1} (for pseudo-plastic and Bingham plastic) and 1000 s^{-1} (for dilatant materials) what was already found quite a vage assumption by Walker and Goulas. It is an idealization but is assumed to be a good starting estimate. The substantiation to use the apparent viscosity rather than plastic or limiting viscosity is to include the influence of yield stress as this is the dominating factor in head reduction. This latter finding was disintegrated by Furlan et al. (2016) as the yield stress was not the cause of head reduction at low flow rates and will be discussed later.

Walker emphasized the danger of a deviant head curve at low flow rates (at this point in time still assigned to rheological parameters). It can result in multiple operating points which should be avoided at all times as can be seen in figure 5.6.

The proposed relationship between head reduction and pump Reynolds number was successful considering the variation in apparent viscosity, pump speed, solids SG and particle size. Most important was the lack of dependence on either the solids SG or the particle size. The correctness of the **homogeneity** assumption was confirmed by the fact that the physical properties of density and viscosity were enough to fully represent the slurry characteristics.

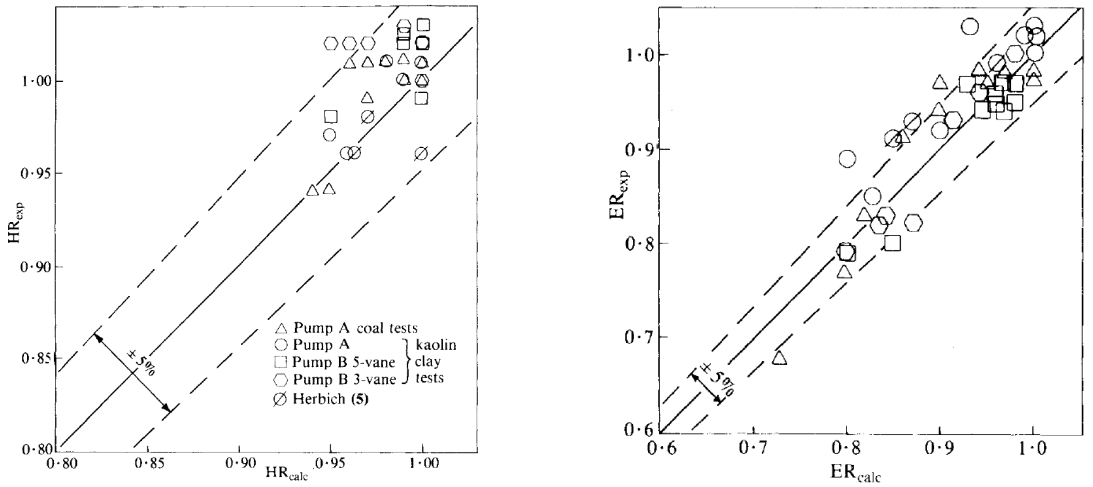

(a) Measured HR by WG 1984 versus HI de-rating.

(b) Measured ER by WG 1984 versus HI de-rating.

Figure 5.5: Experimental results by Walker and Goulas (1982) versus HI de-rating predictions.

Calculation of HR and ER near BEP was done by using the plastic viscosity. This viscosity parameter in turn was determined at the maximum measured shear rate (i.e. between 100 and 1500 s^{-1}). It was concluded that the correction method of Hydraulic Institute 1969 for Newtonian fluids was well accurate near BEP when the plastic viscosity (μ_{pl}), calculated at a shear rate of 1500 s^{-1}, was used instead of the dynamic viscosity (μ). In this particular experiment, it was possible to predict pump de-rating within 5 % for head and efficiency as seen in figure 5.5.

The trend in Efficiency Reduction (ER) is indicating that there are less losses experienced by higher specific speed pumps. This is due to the fact that low specific speeds pumps have narrower passage and larger diameter impellers than high specific speed pumps. Relatively narrower passages and larger disk diameters result in consequently larger skin friction losses and disk friction losses.

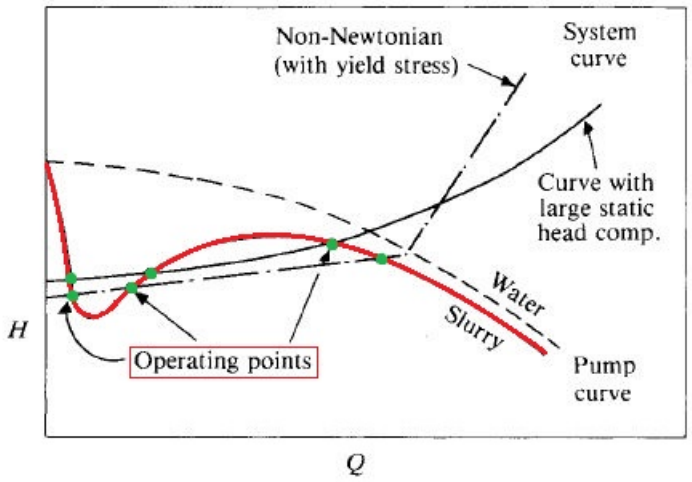

Figure 5.6: System operating points when handling non-Newtonian fluids in combination with deviant Head curve. Walker and Goulas (1982)

Sery and Slatter (2002)

Also based on the method of the Hydraulic Institute, Sery and Slatter (2002) conducted laboratory research on viscous pump de-rating. The mixtures used in this research were glycerine and kaolin slurries pumped by a Warman 4/3 centrifugal pump. To verify the measurement with a Newtonian de-rating method (Hydraulic Institute (1983)), use was made the Bingham plastic viscosity (ν).

Results showed a linear correlation between prediction and measurements within a 20 % bandwidth for head and 10 % for efficiency.

Kabamba 2006

Research by Kabamba (2006) continued and expanded the research field from Sery and Slatter (2002) by testing more mixtures with two different pumps. The pumps which were used are: GIW 4/3 and a Warman 6/4 centrifugal pump.

Mixtures were composed of three different materials namely: CMC solution, a bentonite mixture and kaolin. Different than Sery and Slatter (2002), de-rating was only calculated at a high shear rate regime (around BEP). This resulted in the following dependencies:

1. GIW 4/3 pump: head and efficiency both within 15 %.
2. Warman 6/4 pump: head and efficiency consequently within 10 and 20%.

Also the Hydraulic Institute (1983) method was used with Bingham plastic viscosity as input for de-rating at high shear rates as occur around BEP.

Graham et al. (2009)

Similar to previous mentioned researchers, Graham et al. (2009) conducted laboratory pump experiments with non-Newtonian fluids. Two different mixtures were used namely: aqueous polymer solution of CMC and a mixture of Ultrez 10. These mixtures were pumped by two different pumps: GIW (KSB)(4/3 LCC-M80-300 - 310 mm) and Warman (4/3 AH - 245 mm). First a modification was researched on the Hydraulic Institute method of 1969 and second a modification on the Walker and Goulas (1982) method.

Modified Hydraulic Institute 1969

Firstly the correction method applied to the Hydraulic Institute 1969 de-rating. Essential is the input parameter of viscosity to pump de-rating. As the HI correction charts are designed for Newtonian fluids, consideration of the yield stress can be obtained by using the apparent viscosity at the appropriate shear rate. The complex flow throughout the pump is simplified by calculating the "equivalent pipe diameter". Given the flow through the pipe and equivalent diameter, an estimate can be made about the shear rate.

$$D_h = \frac{4w\pi D_{imp}}{2(\pi D_{imp} + w)} \tag{5.21}$$

With 'w' is the characteristic dimension which needs to be determined experimentally. For the experiments with a Bingham rheological model, good agreement was reached for $w/D_{imp} = 25$ %. Further is the velocity in the 'pipe' equal to:

$$V = \frac{4Q}{\pi {D_h}^2} \tag{5.22}$$

To calculate the apparent viscosity, a defined shear rate is necessary. If the flow encountered is laminar, the shear rate is calculated with the use of the Rabinowitsch-Mooney relationship as given by equation 5.23. If the flow is turbulent, a high shear rate viscosity (η_∞) is used, calculated at a shear rate equal or higher as 4000 s^{-1}.

$$\dot{\gamma} = \left(\frac{3n' + 1}{4n'}\right)\frac{8V}{D_h} \tag{5.23}$$

Lastly a new correction coefficient for the Hydraulic Institute method is calculated 'Cc'. With this value, and a table of newly determined coefficients (Graham et al. (2009)), the HR can be calculated by:

$$HR = A_0 + A_1 Cc + A_2 Cc^2 + A_3 Cc^3 + A_4 Cc^4 \tag{5.24}$$

Their research showed good agreement between the proposed correction and available test data as shown in figure 5.7. Most of the test points lie within a 10 % bandwidth of the predicted values for both used pumps. Later in 2011, a new paper was released with more validated data (Pullum et al. (2011)). For efficiency, also 10 % was mentioned as bandwidth although much less detailed results were presented.

The only downside to this method is that only values for performance are given at discrete points. It is than not possible to validate each measurement point without interpolating the method or determine a continuous fitted function. Because availability of other methods it was chosen to no validate this method quantitatively.

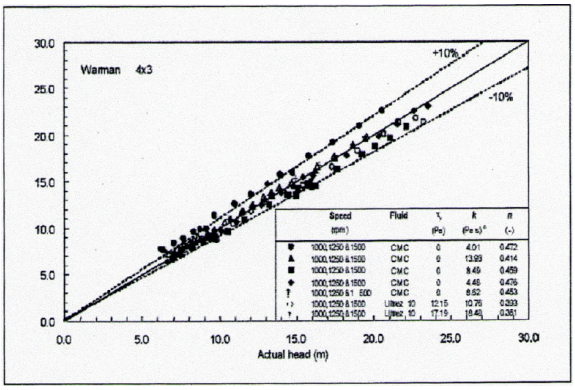

(a) Measured vs predicted for Warman pump.

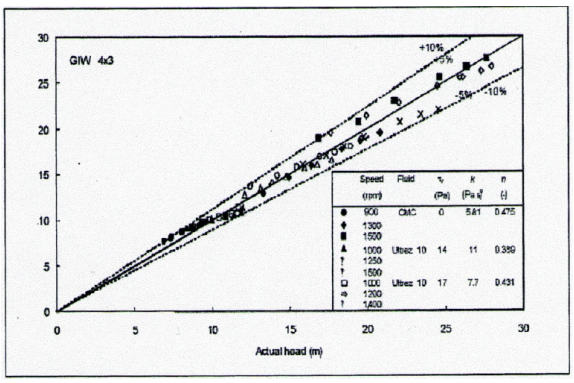

(b) Measured vs predicted for GIW pump.

Figure 5.7: Measurements presented by Graham et al. (2009) for head de-rating according to new method.

Modified Walker and Goulas 1984

Apart from the modified Hydraulic Institute method, an improvement to the method of Walker and Goulas (1982) was also suggested. The relation between head de-rating and pump Reynolds number was calculated using the Bingham plastic viscosity. To improve this relation, it was suggested to use the apparent viscosity (at a shear rate to be determined for different pumps, 4000 /s gave good results) instead of the Bingham plastic viscosity. Below the modified Reynolds number can be seen with apparent viscosity as dominator (eq 5.25). This was however not validated in great detail so large uncertainty should be taken into account.

$$Re_p = \frac{\rho \ \Omega \ D_{imp}^2}{\eta_a} \tag{5.25}$$

Furlan 2013, 2016 and 2017

The latest research with respect to viscous pump performance was published by Furlan et al. (2016) and summarized by Sellgren and Furlan (2017). The influence of air on head when pumping viscous mixtures at low flow rates was researched. Laboratory research in the past (Walker and Goulas (1982)) showed unstable head curves at low flow rates.

The research of Sellgren and Furlan (2017) gives a broad overview of de-rating methods currently available with respect to older literature, conducted mainly on kaolin slurries with a maximum particle size of 2 μm and de-rating of intermediate slurries as encountered in mining industries with particle sizes upto a few millimetres. Furlan started with expressing the importance of head and system curve to understand the changing operating point. Fine particle viscous slurries system head curves may often show a lower angle of interception between pump and pipeline curve. A small reduction in head due to de-rating, can therefore cause a large change in flow rate because this small angle. This results in a large flow rate range of operating.

Regardless of the changing perception on yield stress in the past, experiments resulted in a clear difference with respect to efficiency where only yield stress was altered. This difference was not noticed in the head characteristics. When two slurries with equal yield stress were tested, the mixture consistent of Phosphate clay showed a lower head and greater dependency on pump rotational speed as can be seen in figure 5.8.

Further is the method of Graham (Graham et al. (2009)) discussed and the fitting parameter "w'". As the purpose is to investigate the correctness of the previous methods when handling a combination fluid of non-settling and settling slurries, the parameter for "w'" is chosen to be the actual impeller width "w". The actual width is used for representing the shear rate and corresponding viscous influence in the two-component de-rating.

Also was noticed the absence of shift in BEP flow rate in contrast to the HI 2010 prediction. The experiment did also point out the strong effect of the yield stress on the de-rating factors when handling highly non-Newtonian fluids. The yield stress is accounted for when using the apparent viscosity parameter rather than plastic viscosity. Lastly caution was again mentioned regarding the backward sloping head curve in relation with possible air pockets inside the low pressure areas of the pump.

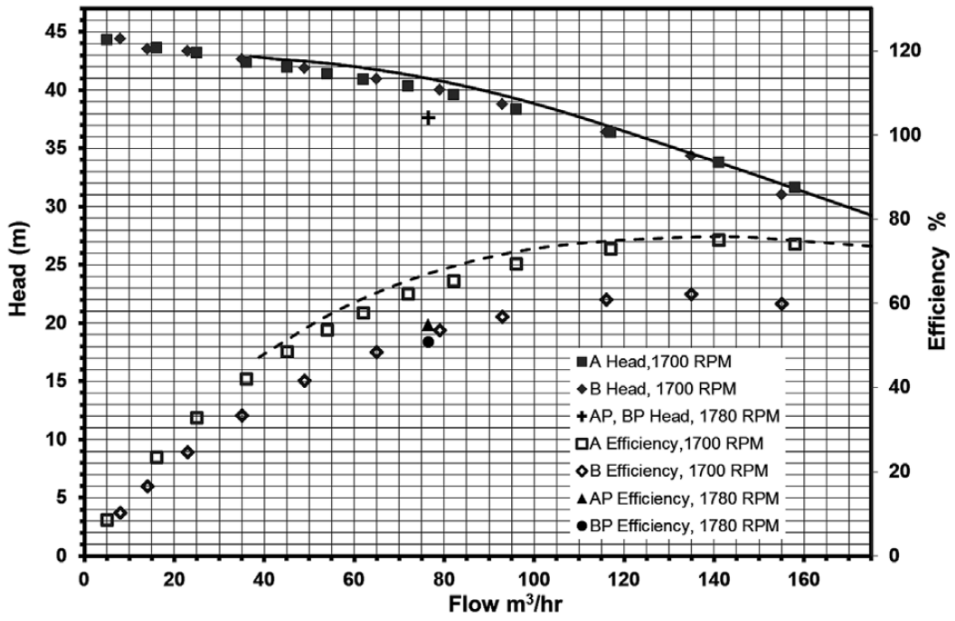

Figure 5.8: Head and Efficiency data, all scaled to 1700 rpm from Furlan et al. (2016). Solid line equals water performance.

5.2.3 Loss analysis

All methods presented until now are based on empirical laboratory pump performance data. Although good agreement could be obtained when the exact same experiment is conducted elsewhere, altering either mixture characteristics or centrifugal pump could result in deviant results. An example where a de-rating model proves to be insufficient, is when all parameters are equal except for impeller or casing surface roughness. This is not taken into account by present de-rating methods and could result in conservative performance predictions when the pump operates in a turbulent regime. Not only does a change in surface roughness require a loss analysis, a different Reynolds number has also influence on pump performance through the friction coefficient in hydraulic channels and consequent flow regime.

The disadvantage of a loss analysis is the requirement of complete geometrical knowledge of the pump. This is often not known by the user. If assumptions are required in this case, sensitivity of these assumptions should be guarded at all times.

All required information and equations to perform a partly loss analysis, namely calculate the expected increase in disk friction losses which literature suggest to be governing in viscous pump de-rating, can be found in appendix section 10.3.

5.2.4 Validity range

To summarise the section on existing de-rating models, an overview is presented of validity for each model. As the dredge pump used in this research exceeds the dimensions significantly from the centrifugal pumps used to validate the models from Table 5.6, this overview is particular useful to determine the validity of this research of future work.

OVERVIEW VALIDITY RANGE	
Hydraulic Institute 1983	- Newtonian fluids - Open or closed radial impellers - Q = 20 - 2000 m^3/h - H = 4 - 200 m
KSB Krieselpumpen 1989	- Newtonian fluids - Open or closed radial impellers - Q_{opt} = 1 - 10000 m^3/h - H_{opt} = 1 - 400 m - Kinematic viscosity: 1 - 4000 mm^2/s
Gulich 2008	- Newtonian fluids - Open and closed radial impellers - Specific speed (n_q): 7 - 50 - Kinematic viscosity: 1 - 4000 mm^2/s
ANSI 9.6.7 - 2015	- Newtonian fluids - Semi-open and closed impellers - Specific speed (n_q): 1 - 60 - Kinematic viscosity: 1 - 3000 mm^2/s (up to 4000 with increased uncertainty.) - B parameter: 1 - 40

Table 5.6: Validity range for most common de-rating models used for Newtonian fluids.

5.3 Influence of air on pump de-rating

Furlan et al. (2016)concluded that the influence of air on pump performance caused the backward sloping head curve as encountered in work of Walker and Goulas (1982) and others. As similar phenomena were noticed in preparation of this research, the effects of air were also included.

The handling capacity of a centrifugal pump to convey a multi-phase flow depends largely on the governing flow pattern. If the gas and liquid form a homogeneous mixture or tend to separate, different results should be expected. Small gas bubbles dispersed in the liquid can be considered as a quasi-homogeneous mixture but if there is any form of slip between the phases, small additional losses can be expected. Larger gas volume fractions introduce more significant problems. A higher amount of small bubbles tend to coalesce and form larger gas accumulations, especially in parts of the hydraulic system where separation is stimulated due to bends or valves. Apart from centrifugal forces, also buoyancy forces are acting on the gas bubbles together with a pressure difference between top and bottom of the pipeline. Due to this lower pressure at the top, accumulations at the top of the pipeline will also result in the coalescing of bubbles.

The performance reduction due to the presence of gas does generally originate from three sources. The gas either (1) present in the form of free gas (held captioned in the pores), (2) presence due to separation of dissolved gas (as explained before by the 'law of Henry') of (3) due to cavitation in local low pressure zones where the pressure is lower than the vapour pressure and imploding vacuum bubbles are present. The governing factor for performance impairment is the amount of free gas at the inlet of the pump.

In the present dredging installation, mitigations measures are already taken to reduce the amount of free gas entering the pump by the installation of a degassing installation. This system creates a low pressure

zone before the entrance of the pump with the use of high pressure jets and ejectors. This low pressure zone will attract free gas from the passing liquid and redirect it to a separation tank where the gas and liquid are further separated and reprocessed. The gas-free liquid is injected back into the flow before the dredge pump.

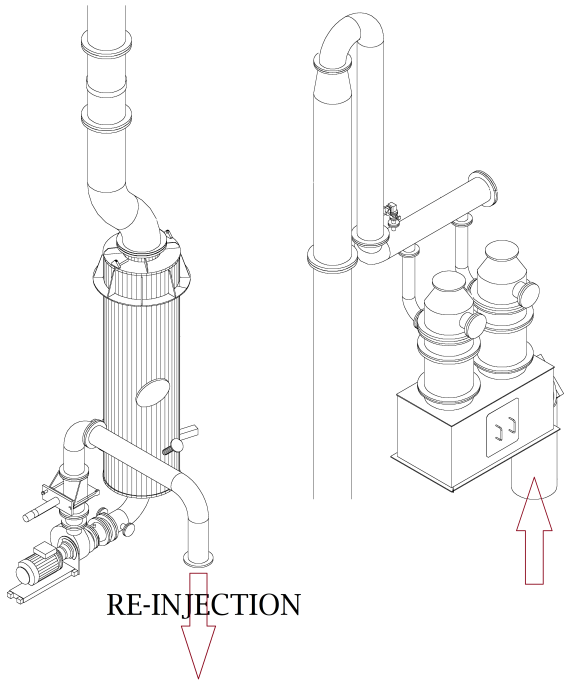

Figure 5.9: Overview degassing installation onboard Pallieter. left: Separation tank with slurry re-injection pump, right: Ejectors to create low pressure zone.

5.3.1 Factors influencing gas-handling capacity

Unsteady phenomena: The coalesced air pockets or smaller bubbles tend to accumulate in a low pressure area of the impeller and grow in time. Low pressure areas are mainly on the backside of a leading vane (dependant on flow rate, see fig 5.26) and in the eye of the impeller. Depending on the velocity and shear stress between the gas pocket and liquid, the pocket might be swept away or kept in place. As the hydraulic area is reducing due to the presence of the air pocket, the relative velocity increases. This phenomena of increasing pocket size, increasing velocity and finally removal of the pocket may result in surge-like phenomena. Laboratory test conducted by Tillack P. (1998) and Sauer M. (2002) revealed this unsteady surge behaviour. An increase of 1 % in GVF showed a water-head reduction of 50 % at times. This emphasizes the critical relationship between Gas Volume Fraction and pump performance. However to measure this surge-phenomena, the sampling rate and accuracy of the pressure transducers needs to high enough. As sampling on board of Pallieter is once every 2 seconds, no quantitative conclusions can be drawn to this extend.

Influence of viscosity: Increasing the viscosity of the carrier liquid will reduce phase separation effects as the drag is proportional to the viscosity of the carrying fluid as can be seen in equation 5.26 with ζ_W being the Reynolds dependant drag coefficient of the gas bubble. In literature, tests can be found varying the dynamic viscosity while keeping the Gas Void Fraction and measuring the resulting head. This research showed an improvement for two-phase pump performance mainly at flow rates higher than BEP (q* > 1). At lower flow rates the effect was less noticeable (Sauer (2002)).

$$c_A = \sqrt{\frac{4\ g\ d_B}{3\ \zeta_w}\left(1 - \frac{\rho''}{\rho'}\right)} \tag{5.26}$$

Influence of specific speed (n_q) A straightforward conclusion, as with the relation of disk friction/specific speed, is not possible with the two-phase performance of a centrifugal pump. The shape of the impeller is specific speed dependant and as such relates in some extend to the GVF handling performance of a centrifugal pump as seen in the research of Sauer (2002). However the phase distribution in hydraulic channels is influenced by many more factors.

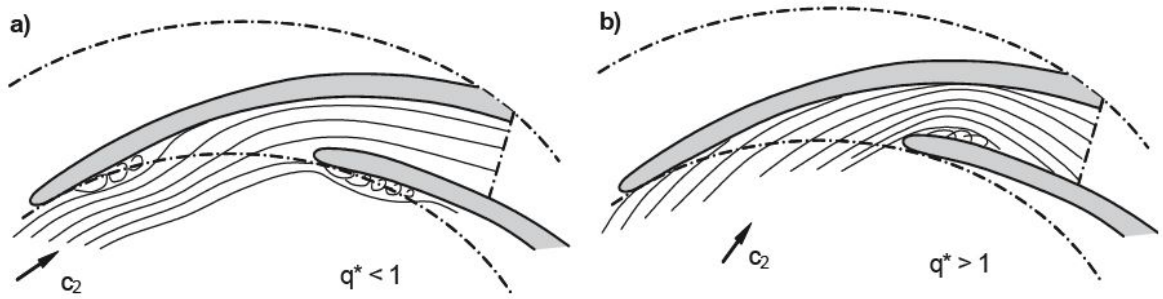

Figure 5.10: Flow pattern depending on flowrate. Recirculation areas where gas can accumulate are shown.

Effect of the sidewall gap (expeller vanes): As the space between the impeller and pump casing does not induce much radial flow, air tend to accumulate in these regions. On the front of the impeller, accumulation occurs at the annular seal and on the back around the hub of the rear shroud. It is possible in the dredging industry that a impeller is equipped with expeller vanes to reduce back flow through the side wall gap. This however is contra-productive for the gas handling as even less radial flow occur to carry gas bubbles away from the area. Also for handling viscous fluids this measure is not beneficial. On the other hand, the particular dredge pump is equipped with liquidine flushing and thus flow of water does happen at the rear impeller gap.

5.3.2 Performance reduction due to gas

Performance reduction due to presence of gas in centrifugal pumps is mainly governed by three phenomena. The first implication when gas is encountered in the fluid is the coalescence of bubbles at the impeller blades. The area covered by the bubble cannot fully transmit energy to the fluid. Also is the bubble reducing the hydraulic area in between the blades leading to a increase in relative velocity and consequently decrease in work transfer as calculated with the use of the velocity triangles. This effect might be responsible for the faster deviation at flowrates $q^* > 1$ than at partload ($q^* < 1$). Second is the exchange of momentum between the gas and liquid phase leading to additional energy consumption. Lastly are the gas accumulations in which pressure built-up is limited by the gas density due to the limitation on pressure rise in a closed gas volume. This last phenomenon is somewhat comparable to the solids effect on pumps. The presence of solids or gas is reducing the capability of the fluid to store and transport pressure energy as both are less or unable to store this form of energy and is thus lost. Figure 5.11 shows the measurements of Florjancic (1970) on the performance of a single stage centrifugal pump with a inlet pressure of 2.5 bar absolute to mitigate cavitation.

The results show a comparable trend for head reduction in function of GVF as can be found in literature by Walker and Goulas (1982). However, the percentage of gas at which severe reductions in head appear, is not consistent. In the research of Florjancic (1970), little influence on head was measured at a GVF of 2 % but started to deviate strongly at 4 %. The deviation relative to the GVF can be seen in figure 5.11.

It should be noted that the influence of dissolved gas on pump performance is very sensitive to several factors as rheological parameters, type of gas, operating point and many more. Parameters which are constantly changing during a dredging operation. It is therefore almost impossible to create a similar gas handling figure with accurate predictions for large centrifugal dredge pumps.

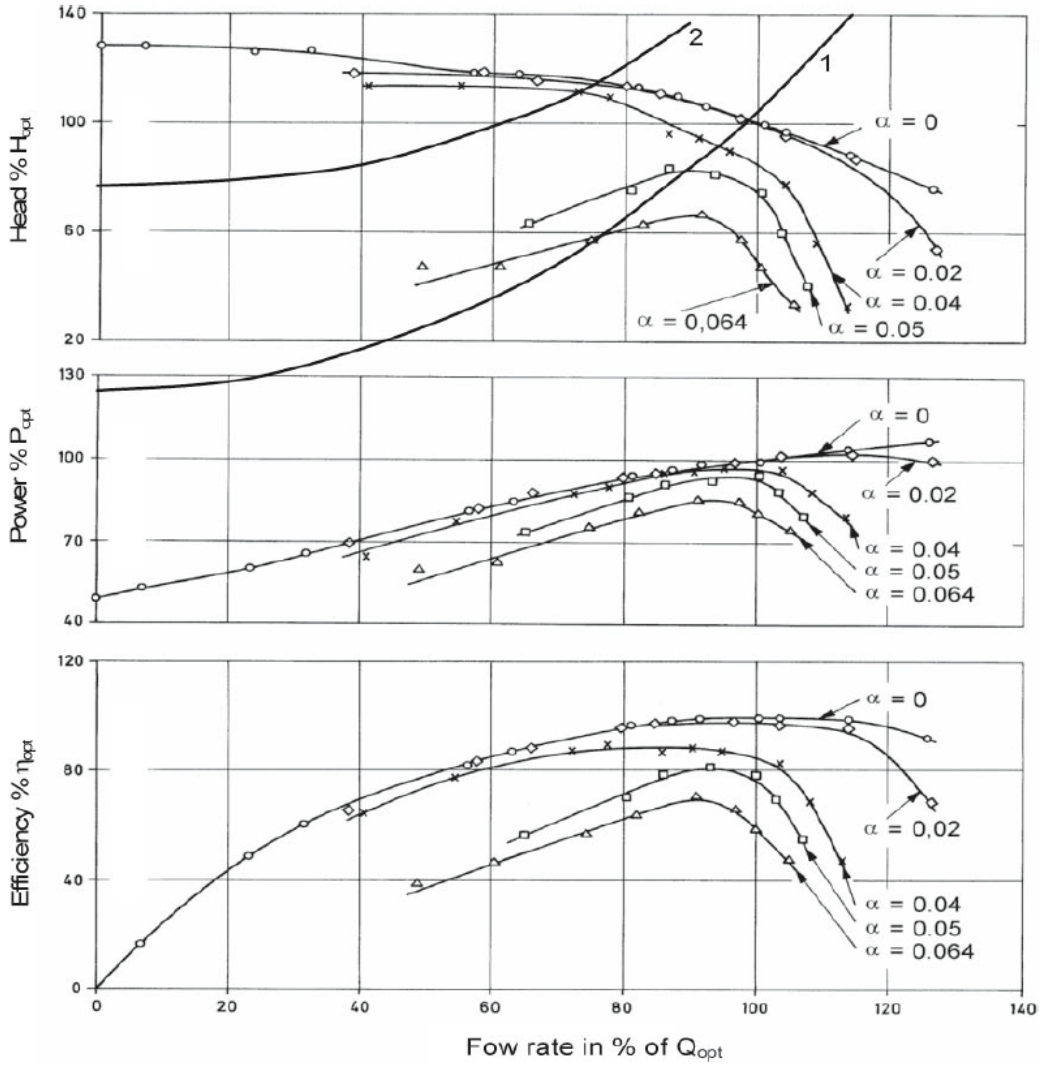

Figure 5.11: Head, Power and Efficiency curve measurements with a single-stage pump ($n_q = 26$) at various Gas Volume Fractions.

Chapter 6

Experiments

In the following chapter, all the aspects of measuring performance data of centrifugal pumps are described into detail. First the context of the measurements is explained, followed by the protocol which will guide the measurements, insures accuracy and repeatability of the results. Lastly, sample method and measurements to characterise the soil will be described. Detailed information with respect to the devices used and the installation can be found in Appendix 10.7.

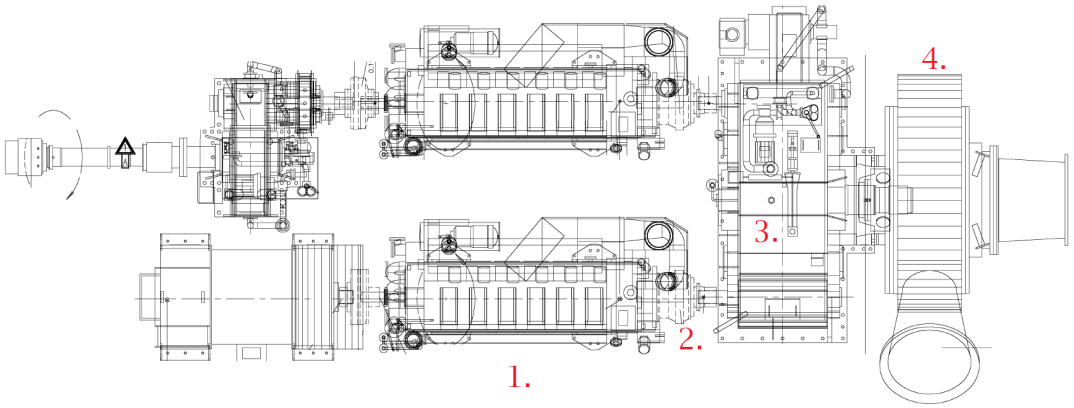

Figure 6.1: Engine-room layout Pallieter. Lower engine is referred to as MID engine. 1; MID Diesel Engine. 2; Pneumatic clutch and pump shaft with torque measurement. 3; Gear box (always operated in the same gear during research). 4; Dredge pump

6.1 Field Measurements

Measurements need to be conducted in order to obtain field pump performance data. This data will be processed in R Studio to obtain normalized performance data which can be compared to the theoretical predictions given by pump manufacturers. Measurements will be executed on board the Trailing Suction Hopper Dredger 'Pallieter' working in a mud environment. Other measurements, such as in-situ soil sampling to determine the soil characteristics, are executed from an assistance vessel of Pallieter, the "Multraship responder".

Parameters which are monitored on board exclusive for this thesis research are the pump shaft input-power and gas void fraction. Further in this chapter details are found about the applied equipment. As was concluded in the previous chapters, the visible phenomena are most probable caused by a combination of increased friction losses/disk friction due to increased viscosity of the mixture and a backward sloping head curve due to dissolved air in the mixture which was not removed by the degassing installation. To interpret the theoretical hypotheses, both shaft input-power and dissolved gas fraction (after the pump) need to be measured.

Repeatability and measurement accuracy are even more important when measuring outside a laboratory in the field. As the measurements are executed on board of Pallieter, relevant norms are followed as guidance for the test. The same norm applies as with performance acceptance test of the vessel, ISO 9906 (latest issue).

6.1.1 Torque measurement

Initially, the only recorded power input value was delivered engine power by measuring the fuel rack excitation. This resembles the linear relationship between diesel injection and engine power. Conversion happens based on fuel type and conversion parameters. This value is not accurate enough to investigate the increased power consumption when dredging viscous mixtures, so shaft torque measurements were executed. As can be seen in the overview drawing of the engine room, the layout of the dredge pump drive also includes a pneumatic clutch to be able to operate the engine without driving the dredge pump. To overcome this, pump shaft power is measured after the clutch so measured excitations were certainly transferred to the pump.

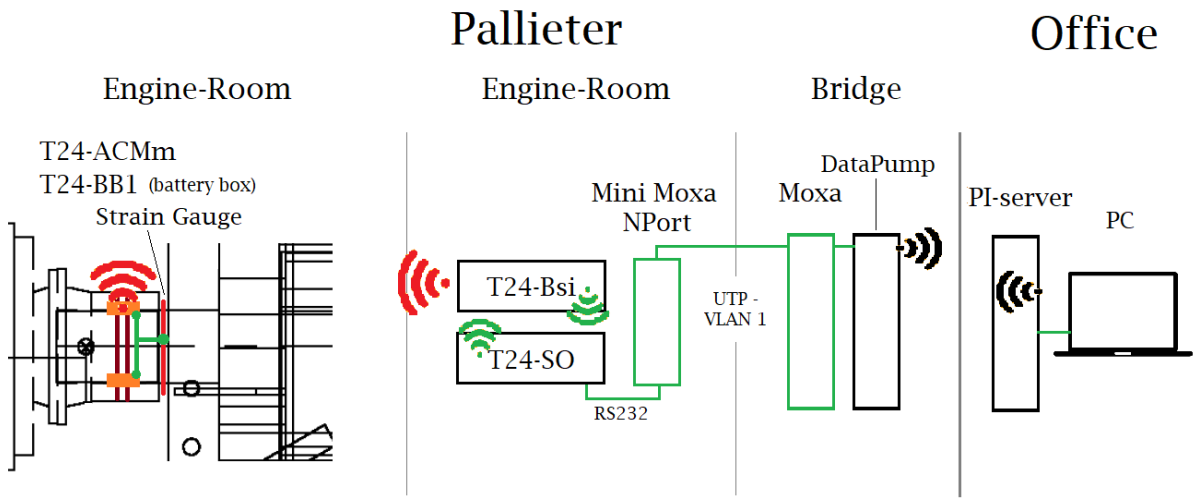

Figure 6.2: Overview measurement setup on board Pallieter.

On board of Pallieter, practical limitations on the installation of strain gauges are present. Pallieter is powered by 3 engines. From these three engines, the two outer engines are used for ship propulsion during trailing and the middle for powering the centrifugal pump. Because more pump input power is needed during pumping to shore, the dredge-pump is powered via a gearbox which can parallelize both the PS (portside) engine and the MID (middle) engine for increased power and speed. This arrangement is not of interest as we are only able to investigate the trailing status of Pallieter. Because of this arrangement on board, the available shaft length between the gearbox and pump is not sufficient and another location had to be found. Because only the middle engine is used during trailing, measuring the torque on the input shaft of this engine to the gearbox is a usable option. The only disadvantage of this option is that gearbox efficiency needs to be determined from the data of pumping water.

The setup of the torque measurement and apparatus used are as follows:

1. First of all, the strain gauge is glued to the shaft connecting the MID-engine to the gearbox. From the strain gauge (Micro Measurements 250US), the signal is transmitted through wires to the Mantracourt T24-ACMm Strain Acquisition box which will transfer the signal to the T24-Bsi.

2. Next the Mantracourt T24-Bsi (Basestation) is mounted near to the MID-engine and will receive the mV/V reading from the strain acquisition box on the rotating shaft. Because the T24-Bsi module was not able to generate a serial RS-232 message, a T24-SO module was installed.

3. The T24-SO module is specifically designed for serial RS232 or RS485 and will receive the mV/V signal from the basestation. In this module, a gain factor and offset can be programmed, but were left out to prevent mistakes at the source of the data. Processing of the data will be dealt with later.

4. To acquire the strain reading from the ship in the head office, it needs to be included in the DATALOG on the bridge of the ship. Transporting the signal could only be done with UTP via the Local Area Network. A mini Moxa N Port is installed next to the T24-SO module to convert the serial message to UTP. From here the VLAN1 network is used for further transportation and processing of the data at the bridge of the vessel. Data is accumulated in the data pump, packed and transferred to the head office of DEME via GSM network. At the office, further processing begins to store the sampled data.

The torque measurement sampling rate was chosen as 2000 ms because all other parameters are only sampled once every 2 seconds and the strain acquisition module is battery powered. Data points generated more frequent than 2 seconds will be lost. Sampling at very high frequencies will also result in regular battery changes which is not possible on the rotating shaft during vessel operation.

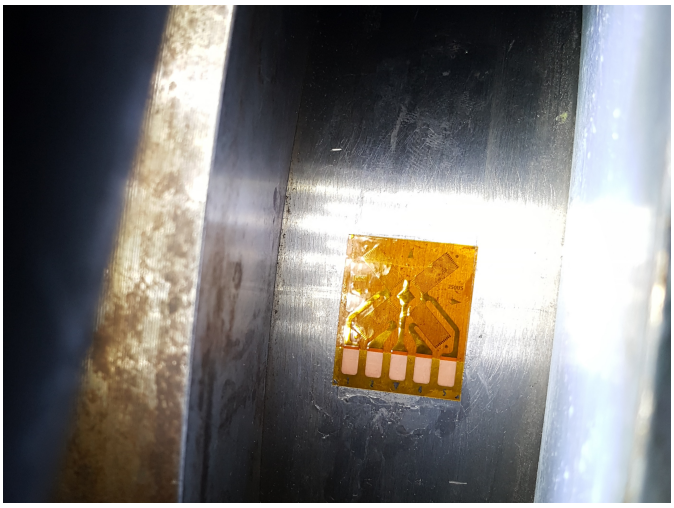

Figure 6.3: Strain gauge glued to pump input shaft.

As explained above, torque is measured by the use of a strain gauge glued to the ingoing engine shaft to the gearbox. From the strain in the shaft, torque needs to be calculated. Important for this calculation are the material properties of the shaft, measurement device specifications as well as dimensions. Transition from strain to torque can be calculated with the use of the formulas as given in Table 6.1 and material specifications as listed below.

1. **Strain Gauge**: Make (Micro-Measurement), Type (4-gauge, 90 degrees rosette), Factor K (2.11), Circuit bridge type (full bridge), Bridge factor B (4), Excitation voltage (3.33 V).

2. **Torque**: Nominal torque at measurement location (2025 kW = diesel engine specification), Nominal rpm of measurement shaft (1000 rpm).

3. **Material Specifications**: Material specification (CK35), Temperature (20 degrees), Young's modulus E ($211 * 10^9 N/m^2$), Poisson's ratio (0.3), Shaft inner diameter (0 m), Shaft outer diameter (0.185 m).

These input values in combination with the following formulas in Table 6.1, result in shaft torque.

Excitation - Torque conversion	
Nominal torque. T	
Shear Modulus. G	
Polar mass moment of inertia. J	
Shear stress at nominal torque.	
Shear strain at nominal torque.	
Relative output voltage.	

Table 6.1: Conversion calculation from strain in [mV/V] to torque in [kNm].

The result of this calculation is used for further processing the torque measurement. As can be seen from the latter equation, a nominal power input of 2025 kW corresponds with a strain gauge reading of 0.2022 $[mV/V]$. As explained before, the strain reading was not converted by measurement equipment and thus the raw measurement is used as torque input. After recording the zero value from the strain gauge (-0.0504 mV/V), the graph in figure 6.4 was established. Now each measured strain recording can be converted into a power reading by applying the equation as shown in the figure.

Figure 6.4: Calibration graph for strain - voltage reading.

6.1.2 Gas Void Fraction Measurement

The next part of the measurements on board of TSHD Pallieter is the measurement of the Gas Void Fraction after the dredge pump. For this, use was made of a CIDRA SONARtrac Volumetric Flow Monitoring System, Model VF-100.

The Sonartrac measures both the mixture velocity and gas void fraction at the same time in a passive and non-intrusive manner. By measuring pressure fields caused by the turbulent eddies with sonar arrays, the mixture velocity can be calculated based on the propagation speed of the eddies. Calibration was done based on a reference measurement from the conventional electro magnetic flow meter on board with in situ material as no theoretical requirement could be met on board. The theoretical calibration curve is based on flow measuremet and is a linear function of the inverse square root of Reynolds number as can be read in Rothman et al. (2007) and applied to dredging applications by Spek et al. (2016).

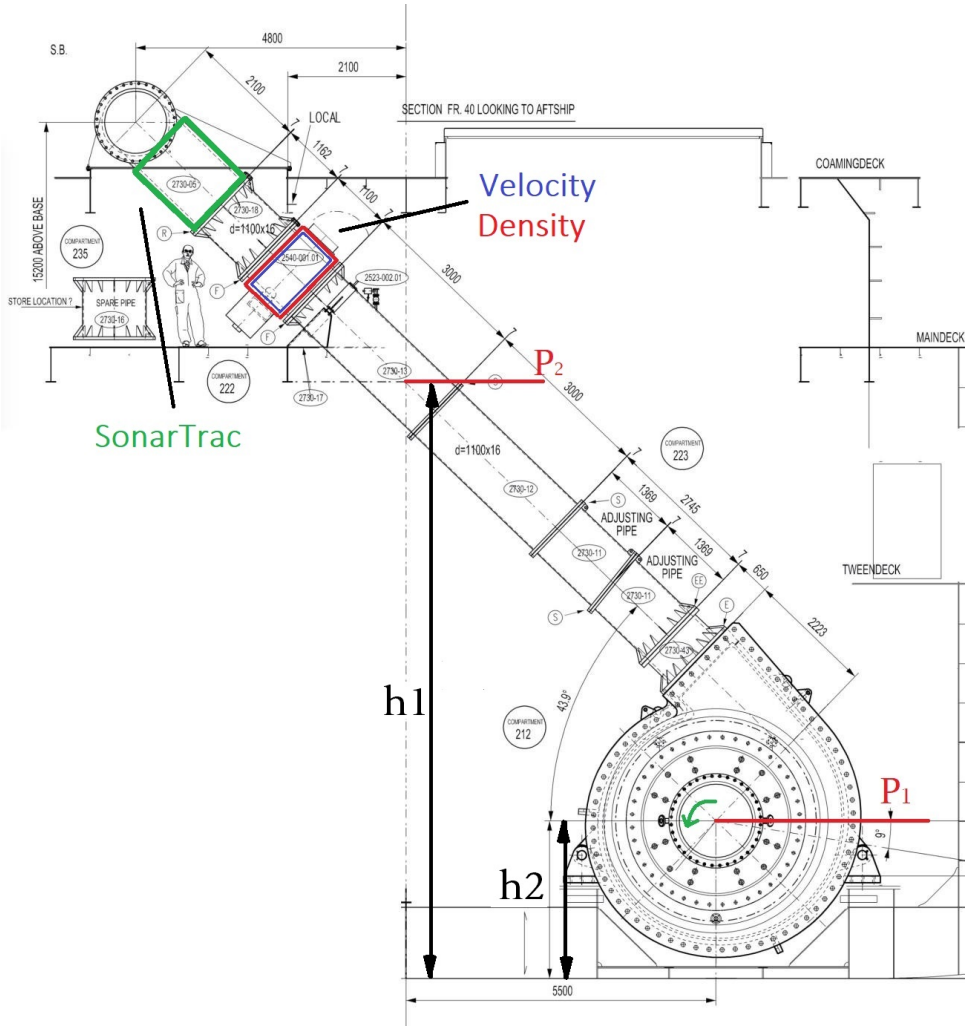

Figure 6.5: Measurement overview as executed on board TSHD Pallieter 2.

Important for this application is the possibility of gas presence in the mixture. Due to dredging in areas with high biological activity and sediment which can easily dissolve this gas, homogeneous dissolved gas can enter the suction process. A mitigation measure is the degassing installation but high density, rapid flow variation and high amounts of gas can result in malfunctioning of the installation and presence of gas after the degassing and dredge pump. Because the Sonartrac is able to measure the speed of sound in parallel to the mixture velocity in combination with a external mixture pressure measurement, the gas volume fraction can be calculated and used for compensation of the velocity measurement. The electromagnetic flow meter will over report the velocity in the same situation.

Figure 6.6: Sonartrac VF100 installed on board TSHD Pallieter.

6.1.3 Other parameter measurements

Other than the torque and GVF measurement, various parameters are measured to be able to replicate pump curves. Below there can be found a overview of parameters which were used during this research:

1. **Pressure:** Both the pressure before (vacuum) and after the dredge pump are measured.
2. **Velocity:** The velocity measurement is used from electro magnetic flow meter after the dredge pump. Because a difference in pipe diameter before and after the pump is present, a velocity difference should be calculated.
3. **Rotational speed:** The rotational speed of the dredge pump is measured on the outgoing shaft from the gear box. This value is used to scale all data points to one reference speed with the use of affinity laws.
4. **Density:** As the density is constantly changing, pump characteristics should only be compared at equal densities as different phenomena occur at different densities. Also the characteristics change with alternating densities.
5. **Location:** To compare measurements from different locations, geographical data is used to identify were the measurements are taken.

6.1.4 Measurement accuracy

Accuracy required by International Standard

Measurements will inevitably be subjected to some sort of uncertainty, even if there is full compliance with method statement and apparatus accuracy. To give a interpretation on this fault, various parameters can be calculated as well as following standards which describe this uncertainty. For this research, International Standard (2012) will be used as a guideline for measurement uncertainty.

Random Component: To estimate the uncertainty of a random component (i.e. for example a pressure transducer), placement of extra readings of the same unit is necessary with a minimum of three. From these readings, the relative value of uncertainty can be calculated from the mean and calculated standard deviation. **Note:** as on board no measurement is executed more than two times, this error calculation is solely as completeness.

$$e_R = \frac{100\ t\ s}{\bar{x}\sqrt{n}} \quad [\%] \quad (6.1)$$

Where: t is a function of n as given in International Standard (2012).

Instrumental measurement uncertainty: After all measures are taken to reduce the error to a minimum such as zero adjustment, calibration and proper installation of the device, there still exist an uncertainty. This systematic uncertainty is obtained during calibration according to international standards. To note, pressure transducers need to be calibrated until a error of less than 2 % exist (International Standards state a permissible uncertainty of 2.5 %).

Overall efficiency: The combination of random error with systematic uncertainty of the measurement apparatus result in the overall efficiency with the formula below.

$$e = \sqrt{{e_R}^2 + {e_S}^2} \quad [\%] \quad (6.2)$$

Also the combination of random error and measurement uncertainty are combined by ISO and displayed in the following table for all quantities needed for this research.

Measured quantity	**Symbol**	**Permissible overall uncertainty**
		Grade 2 and 3
Rate of flow	e_Q	3.5 %
Speed of rotation	e_n	2.0 %
Torque	e_T	3.0 %
Pump total head	e_H	3.5 %
Driver power input	e_{Pgr}	3.5 %
Pump power input (computed from torque and speed of rotation)	e_P	3.5 %
Pump power input (computed from torque and speed of rotation)	e_P	4.0 %

Table 6.2: Permissible overall uncertainty rates according to ISO 9906.

Efficiency uncertainty: As efficiency is calculated by a combination of factors, the individual errors need to be cumulated to obtain the overall efficiency uncertainty. To this extend a different formula will be used depending on the calculation method for efficiency (torque + speed or power input). For this research a combination of torque and rotation speed are used leading to the following relation:

$$e_\eta = \sqrt{{e_Q}^2 + {e_H}^2 + {e_T}^2 + {e_n}^2} \quad [\%] \quad (6.3)$$

When this method of cumulating is used, the influence of a dominating factor is carried through and will also dominate the solution (i.e. if the error on flowrate is significantly larger than other factors, the overall error will almost be equal to the flowrate error.). For the grade of application '3', a overall uncertainty of efficiency of $\pm$ **6.4** % is permitted.

Determining the instrumental uncertainty and application of calibration on the different measurement devices are discussed below. If no calibration was possible, other methods of error determination are followed as found in the next subsections.

Error propagation

Calculating a result with independent parameters having each an uncertainty influences the result. The same effect occurs when measuring pump behaviour with measurement equipment, especially pre-installed devices on-board. To determine the overall measurement uncertainty on the total head and power, the propagation of measurement errors will be elaborated on.

Calculation rules on error propagation:

1. **Addition or subtraction**
$$\delta Q = \sqrt{(\delta a)^2 + (\delta b)^2 + (\delta c)^2} \tag{6.4}$$

2. **Multiplication or division**
$$\frac{\delta Q}{|Q|} = \sqrt{\left(\frac{\delta a}{a}\right)^2 + \left(\frac{\delta b}{b}\right)^2 + \left(\frac{\delta c}{c}\right)^2} \tag{6.5}$$

3. **Raising to a power**
$$\frac{\delta Q}{|Q|} = |n|\frac{\delta x}{|x|} \tag{6.6}$$

With the following formulas, used to transform the measured quantity to total head, the measurement error will propagate through the following equations. As the calculated head is also scaled with the use of affinity laws, the error on rotational speed also needs to be taken into account.

$$\Delta P_{ref} = \left[(P_2 - P_1) + \rho\ g\ \Delta h + \frac{\rho\ (V_2^2 - V_1^2)}{2}\right] * \left[\left(\frac{n_{ref}}{n_{measured}}\right)^2\right] \tag{6.7}$$

Subtraction of non-error parameters, simplification and where V_1 is dependant on V_2, leads to the following:

$$\Delta P_{ref} = \left[P_2 - P_1 + \rho + \rho\ (V_2^2 - V_2^2)\right] * \left[(n_{measured})^{-1}\right] \tag{6.8}$$

To determine the overall error, a combination of the above propagation rules have to be used. The most efficient way is to divide the equation in soluble parts with each a solution, than combining the combined errors in a simplified formula. The accuracy errors of the used apparatus are given here:

Overall Uncertainty	
Measured quantity	Error*
Pressure sensor before pump	0.942 % (0.94 % + 0.065%)
Pressure sensor after pump	0.088 % (0.06 % + 0.065%)
Mixture density measurement	0.0 %
Mixture velocity measurement	1.53 %
Pump rotational speed measurement	0.33 %
*Note: The error as stated here is a combination of apparatus error and measurement error after calibration, also known as Overall Uncertainty by ISO 9906 : 2012.	

Table 6.3: Calculated uncertainty rates for all measurement devices.

Now using a combination of values when the pump operates around BEP, enables calculating the total measurement error.

Flow rate

On board of Pallieter a Sonartrac was installed. The device is able to passively measure the Gas Void Fraction as well as the liquid flow rate based on the wetted surface area times the velocity measurement. The Sonartrac is located just downstream of the existing electromagnetic flow meter and thus can be used to cross verify accuracy of the flow-rate measurement. Although this possibility exist, care should be taken as the electromagnetic flow meter was initially used to calibrate the Sonartrac apparatus. For the calculations of the thesis research, the velocity measurement of the electromagnetic flow-meter will therefore be used.

Pressure

A small variation in pressure measurement can result in large calculation errors. Also blockage in the small canal towards the measurement membrane can lead to inaccurate results. To make sure the measurement of pressure before and after the pump were measured correctly, both transducers were again calibrated. The apparatus used was a DRUCK DPI 610 - Pressure Calibrator.

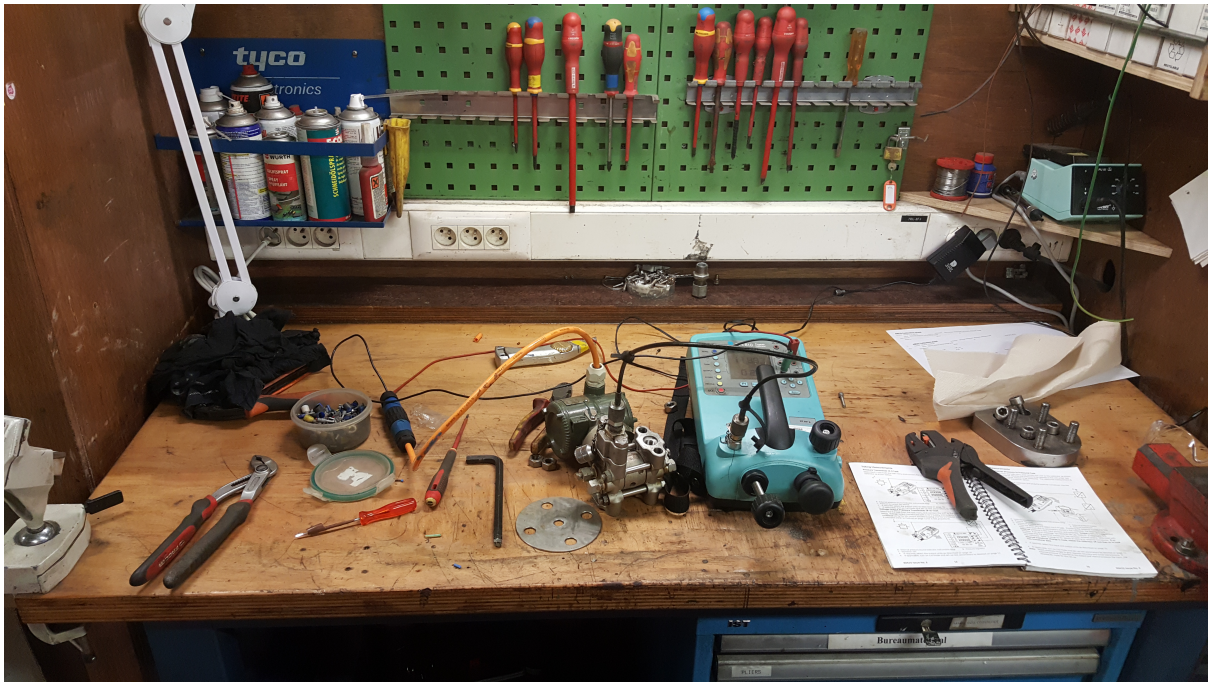

Figure 6.7: Calibration of pressure sensors.

Static Head

The last parameter of great importance is the geodetic height difference between the two pressure transducers. Acquiring this height from engine room drawings was not accurate enough as transducers are relocated. Measuring the height of both transducers relative to a reference plain (distance h1 and h2 on figure 6.5) was the only option.

6.1.5 Data processing

On board of TSHD Pallieter various parameters are logged which are processed in the office to obtain understanding about pump performance. The data consists of parameters for pressure, mixture velocity, location, mixture density, valve position, jet pump status and many more. From this combination of parameters, the pump manometric head curve can be calculated and compared to theoretical water curves or theoretical de-rating predictions. To do so, the program R Studio is used because the amount

of data which is analysed is out of scope for most Microsoft Office packages.

All data is imported into R STUDIO by combing all separate files into one data frame which hereafter is again combined with other data frames. The torque measurement on board is measured with the use of a separate apparatus which in turn put a time stamp on the data. All other measurements are processed simultaneous by the PLC in the engine room and obtain a time stamp from this PLC. To combine both sources of data, merging was done based on the time stamp. After thorough research, signals were not matching based on the time stamp due to different processing delays. Manual and visual manipulation was necessary to align both time signals in a correct manner. Below the time series of pump rpm and torque can be seen after calibration (figure 6.8).

Figure 6.8: Calibration to merge torque signal (red) with measured pump rpm (black).

An important parameter to analyse and compare different trips and locations are trip numbers. A trip number was not dedicated to the data so this was done by a logical operator which compares the status of the vessel in the previous time-step (trailing, dumping, sailing empty, sailing full,...) and the current status. From this , different phenomena in the pump curves can be designated to certain trips (different dredging operator) or different locations.

The next part of the calculation contains determination of the theoretical pump characteristics based on manufacturer data. The data file of the pump is composed of essential geometrical data about the impeller and housing, polynomial parameters for a dimensionless head and power curve and measurements supporting these parameters. From this data, the Best Efficiency Point is calculated as the maximum of the efficiency curve with the use of equation 3.9.

Data processing starts with determining a head-flowrate and power-flowrate curve for data points when pumping water. To determine these starting values, data is filtered on rotational speeds between 80 and 100 % of the maximum rpm ($170 < \text{rpm} < 195$), density is limited to 1050 kg/m^3 ($1000 < \text{density} < 1050\ kg/m^3$) and the dredging status should be 'trailing' or 'turning' to avoid data points when the pump was operated without the connection of the suction tube (as occurs during flushing of the hopper after dumping). Through these points a curve with similar h_2, h_1, p_3, p_2 and p_1 coefficients is plotted, only the offset is determined as the least squares solution through the data points. From this step, new dimensionless pump parameters arise as new starting values for the de-rating equations.

From this step: h_{0-new} to h_{2-new} , p_{0-new} to p_{3-new} and consequently eta were obtained.

With the use of these new parameters, new functions are constructed for water conditions which will be used as a start for the de-rating process. To compare all occurring values for flow rate, only continuous de-rating formulas can be used correctly. The continues models will be used to determine a R squared to obtain correctness of the fit. Other models can only be compared visually to the data and will be discussed separately.

In order to assign data points to the correct de-rating quantity (viscosity), a relation between density and viscosity is created as discussed earlier. In this way, based on the measured density, each data point can be reviewed. To do so, use was made of density classes for which each de-rating method was calculated. These classes will also enable to separate measurement logged during trailing, low density over board or flushing after dumping. The classes are equally divided, i.e. a density-class value of 1.2 corresponds to mixture density measurement ranging from 1.15 upto 1.25 t/m^3. The minimum value for the density-class is 1.0 and is ranging to a maximum of 1.5, although this a rather extreme value. Next, all de-rating methods should be calculated for various viscosities. For this a loop was made which calculated each de-rating method for a density, and consequently a viscosity of 1100, 1200, 1300 and 1400 kg/m^3. The formulas of concerning de-rating methods can be found in chapter 5.

The other facet of the research is about air influence on the pump performance and likelihood of occurrence dependant on the governing rheological characteristics. To research the effect of changing parameters, 4 locations were chosen to determine the rheological parameters in order to compare.

Filtering the data points on location was managed by building 4 geographical bounding boxes and assign the corresponding dredging area to those data points. After this filtering process, easily all locations could be compared with each other and with the pump performance data.

6.1.6 Standards for testing

The output of the experiment should include the data corresponding to the suction pressure, discharge pressure, flow, input torque and shaft speed. In order to obtain accurate experimental results, standards can be followed to ensure proper execution of the experiments and insuring comparability with other measurements. Testing standards which are applicable for testing centrifugal pumps are: ISO 2548 for standard centrifugal pumps manufactured in series; ISO 3555 for pumps used for conveying liquids, for injection and industrial power generation at medium outputs; ISO 5198 for model pumps in laboratories where very high measuring accuracy is demanded.

Great care should be used when conducting experimental data as incorrect data could cause misunderstanding while there is no reduction in pump performance. From measuring pump performance on board a dredging vessel equipped with a high efficiency pump, it's learned that more care is required to obtain test data on board compared to laboratory tests. Errors in measured data could mean loss of time and money due to attempts of locating sources of problems which are non-existent (van den Berg and Stam (2013)).

When a dredging vessel is delivered from shipyard to client, various acceptance tests are carried out to verify design criteria according to international standards. One of these tests is the pump performance acceptance test, carried out with water, which is the same medium as defined by the manufacturer performance tests. Testing centrifugal pump performance in order to affirm performance is done according to the governing/contractual norm for acceptance tests. For the case of accepting the centrifugal pump of Pallieter, ISO 2548 (Class C) was used as a guideline for testing. Over the years norms are updated but in essence prescribe the same method. The new version of ISO 2548, ISO 9906 will be used as a guideline where possible for conducting the measurements used for this thesis. Classification is done based on the application of the pump and shaft power of the pump. As the pump of Pallieter is deployed in slurry conditions and has a shaft input power of over 100 kW, the applicable grade is 3B.

6.2 Rheological Measurements

6.2.1 In-Situ sampling

To obtain samples from which the rheological parameters could be obtained, a sampling method had to be chosen for the river Scheldt and associated depth. The first option of sampling was directly from the hopper space when dredging in the particular area. On board is a sampling device installed to take samples directly from the hopper. This device can be described as small overhanging crane with a plastic bucket and manual winch to hoist the filled bucket. The location of this device however is fixed and sampling could only take place on this location. Samples taken with this method were researched and it's concluded that only low densities are measured as it was not possible to obtain samples from the lower regions in the hopper due to buoyancy of the bucket.

The next viable option was to sample from a vessel at the various locations with the use a Van Veen grab. Two versions were available, the first being a 10 L grab without extra weight and second smaller 5 L grab with added weight for deeper penetration. After testing and modifying both grabs, use was made of the 10 L version. Sampling depth ranged from 10 to 20 meters so a extension cord was attached to both the grab and release clamp.

After the sample was hoisted to sea level by hand, it was released in large 10 L airtight buckets for transport. From these large buckets, smaller but representative samples had to be taken for all laboratories. The content of the buckets was homogenized with a mixer and afterwards distributed over several smaller containers.

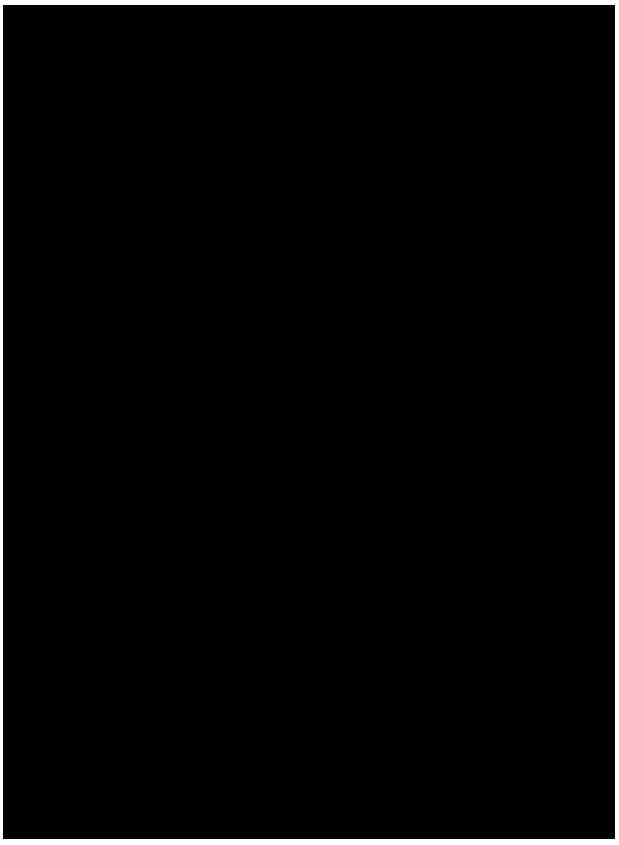

Figure 6.9: Sampling at Location D with the assistant vessel 'Responder'.

6.2.2 Particle Size Distribution

A Particle Size Distribution is established with the use of laser diffraction. Other methods would not be able to analyse the small fraction as present in the mud samples. Laser diffraction is based on the diffraction theory by Fraunhofer and relate the intensity of scattered light directly to the particle size.

All samples are tested with the use of a Malvern Mastersizer 2000 and are loaded into the machine by the 'autosampler'. Simultaneous to the measurement, light energy and obscuration can be monitored for the different light colors used during the research. From these diffraction patterns, a particle size distribution is compiled as can be seen in the Measurement Results section below.

6.2.3 Flowcurve

To determine the viscosity, which will be used as input to the de-rating methods, a flow curve had to be constructed. Measurements are executed with the help of an Anton Paar (Physica MCR 301) rheometer at the laboratory "Waterboukundig Labo Borgerhout". As explained in chapter 4, a vane was used in combination with a cylindrical cup.

During the dredging process, constant changing densities are being pumped due to varying in-situ conditions, operator interventions and ship/drag head movement. To be able to apply the de-rating methods to all these encountered densities, the flow curve is established for the density of 1.1, 1.2, 1.3, 1.4 ton/m^3 and in-situ density (between 1.15 and 1.25 t/m^3). Interpolation between these values will provide a viscosity value (apparent viscosity, tangent viscosity or yield stress) for the full range of dredged densities.

To obtain these densities, the sampled in-situ material had to be diluted and compacted as the supplied density is predominantly situated in the mid-range. The large buckets with the in-situ samples are being well mixed to obtain a homogeneous sample. After mixing, various small samples are taken for further research. These smaller samples, 16 in total (for each location 4 samples), are than diluted or compacted. Diluting is being done by mixing the sample with clear tap water. The process involved adding a small amount of water, measuring the density with the oscillating U-tube and correct if necessary. Compaction occurs naturally as the mixture will settle (although rather slow due to small fraction present) to a certain point. The water collected at the top of the sample was removed to obtain the correct density and again mixed to obtain a homogeneous sample. To obtain the highest required density of 1.4 t/m^3, settling was not enough and evaporation of water from the sample at room temperature was necessary. By removing the lid of the sample container for a certain amount of time, controlled evaporation could take place.

After obtaining the relation between torque exerted on the vane in relation to the rotational speed for each sample with the use of the custom measurement protocol (chapter 4), conversion is necessary to obtain the general accepted flow curve which gives the relation between shear stress [Pa] and shear rate in the mixture [1/s]. Only from this relation the tangent value or dynamic viscosity can be obtained in [Pa.s].

Correcting the shear rate

The correction of rotational speed to shear rate is based on the method as described in chapter 4. Putting the method into practice, every measurement point was plotted on a LOG-LOG scale where after the directional coefficient between each successive point was determined (see figure 6.11, factor n_1 and n_2). The gradient of the intermediate point which is considered was calculated by the mean of n_1 and n_2. This implies the loss of the two outer measurement points. This had no significant influence on the intended result. The graph on the left side shows both the initial measured point as well as the calculated corrected point.

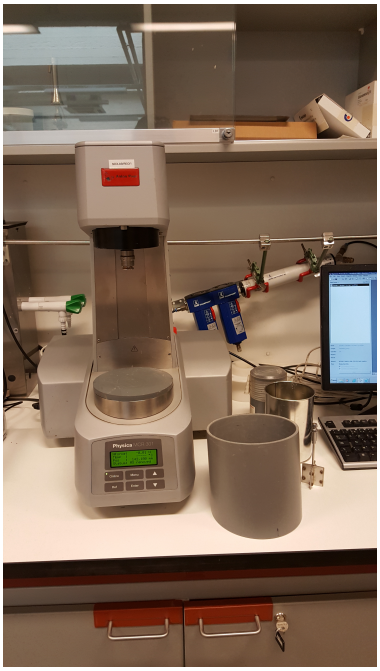

(a) The Anton Paar Rheometer used for the experiment.

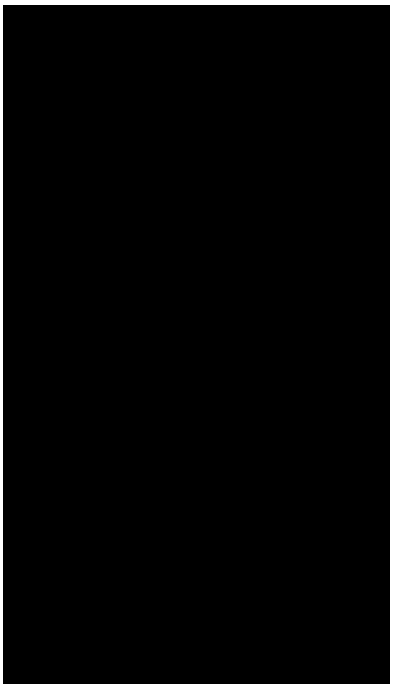

(b) A sample container with consolidated material.

Figure 6.10: Test set-up to determine the flow curves.

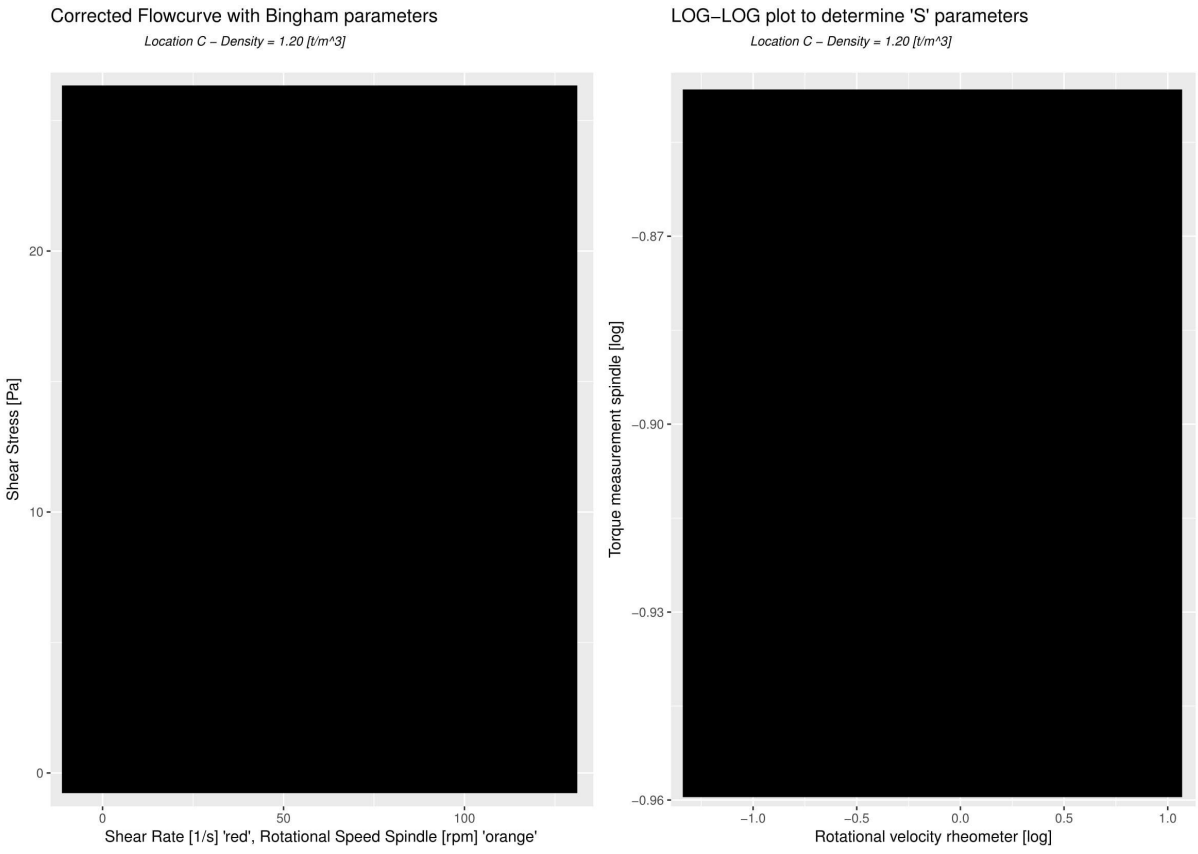

Figure 6.11: Conversion from rotational speed [RPM] to shear rate [1/s] by Krieger Elrod.

6.2.4 Atterberg Limits

The determination of Atterberg Limits was executed according to CEN ISO/TS 17892-12. Theoretical description of the limits can also be found in chapter 4. For this research the Plastic Limit, Liquid Limit and Plasticity Index were determined.

Determining the Plastic Limit was done by making a small thread of clay and rolling it out by hand. It needs to be done on a non-porous surface which in this case was a glass plate. The semi-dry sample is put on the glass plate, spread out until a workable state was reached. Than the sample is taken into hand and massaged into a roll. Now a thread is made and rolled out until the thread is 3 mm in diameter. If the thread did not break before 3 mm was reached, the sample was further dried out. This was repeated until the soil was dry enough to break at 3 mm. The broken threads are collected, dried for 24 hours in the oven and weighted to determine the moisture content. This determined the Plastic Limit.

To determine the Liquid Limit, use was made of a Cassagrande apparatus. The sample was prepared with dried clay material and water. Mixing both until a workable state was achieved. Now the sample is placed in the Casagrande cup and a groove is scraped to create a gap of 13 mm in the centre of the cup. The cup is now dropped from a height of 10 mm upon a marble surface while the number of drops is counted which were needed to close the groove made earlier. If less than 20 drops were necessary, the sample needs to be dried further. If more than 35 drop were necessary to close the gap, liquefy the sample more. Collect several samples from cups with drop counts between 20/25, 25/30 and 30/35. The wet weight was recorded, dried for 24 hours and measured again. Now the moisture content was plotted on a flow chart with x = LOG blows vs y = Water Content. A linear regression is established through the data points from which the slope is also called the flow index. The Liquid Limit is determined as the moisture content corresponding to a blow count of 25.

Important for the influence of the mixture on pump performance is the plasticity of the mixture. When clay is dredged with a relatively low natural water content, in the proximity of the plastic limit, a highly adhesive mixture can be expected. This will consequently increase disk friction with higher losses as a consequence. Also the combination of the Atterberg limits and water content determine how easily the soil will suspend in a watery environment. Only the combination of flow curve with mineralogical composition and Atterberg Limits will fully describe the mixture. The test results can be read in the following chapter.

6.2.5 Mineralogical Composition

The mineralogical composition of the samples is determined with the use of X-ray diffraction on dry samples. The process is complicated but will be elaborated on briefly. After drying the samples at 40 degrees Celsius and crushed by hand in a porcelain cup, further preparation commences. The crushed material is carefully loaded in a crushing cup together with a standard amount of ethanol to further reduce the maximum particle size to below 45 micrometer. After micronising in the McCrone mill, the sample is again dried and prepared for the XRD measurement.

In the measurement apparatus, x rays are created and during the research directed at the sample on various angles. When the crystal structure is hit at the right angle, diffraction of the ray happens and are reflected through the sample on the receiver module. Here the interpretation on the reflected x-rays is done with the use of Rietveld Method and PONKCS Method.

The generated diffraction pattern for all locations as well as the quantitative interpretation on the measurements can be found in chapter 7.

Chapter 7

Experimental Results

The chapter elaborates on the test results from experiments as explained in the previous chapter. First rheological test results are presented as the measurement of particle size, mineralogical composition and flow curves. Hereafter all results from measurements on board of Pallieter are presented together with the processed data.

7.1 Rheological experimental results

To determine the input viscosity to the de-rating models and interpret consequent soil characteristics, various laboratory tests were executed. Full characterisation is necessary to determine the in-situ conditions and behaviour when liquefied with salt water and pumped.

7.1.1 Particle Size Distributions

For the various locations several rheological parameters were determined to identify the samples as complete as possible. A general measure of soil classification is the particle size distribution as presented below. Visualisation is done by plotting the measured particle size in LOG scale on the horizontal axis versus the cumulative volume on the vertical axis as can be seen in figure 7.1.

Particle Size Overview			
Location of sampling	d(0.1) in μm	d(0.5) in μm	d(0.9) in μm
Location A	[redacted]		
Location B			
Location C			
Location D			

It can be concluded that locations do not differ significantly in terms of particle sizes present and all locations have a maximum particle size of 100 a 200 μm. According to general dredging classification tables are these samples containing a combination of cohesive clay and silt ($<$ 0.002 mm and 0.002 - 0.06 mm) together with a fine sand fraction (0.06 - 0.2 mm). Lastly a small fraction of organic matter was also found and identified by its black and brown color in combination with a organic smell. Quantification of this fraction is discussed separately.

Figure 7.1: Particle size distributions for the four sample locations.

7.1.2 Organic content

The amount of organic content is quantified by determining the carbon content of the samples. With the use of a 'prepASH 229' apparatus, the samples are heated and loss on ignition (LOI) is measured very accurately.

Organic Content Determination			
Location of sampling	Water Content *[%]*	Organic Content *LOI 550 degree C [%]*	Lime Content *LOI 800 degree C [%]*
Location A			
Location B			
Location C			
Location D			

Table 7.1: Water Content, Organic Content and Lime Content measurement overview.

The amount of organic content present in the sample is represented by the carbon content. By researching the differences in organic content between geographical locations, the likelihood of dissolved gas can be estimated. Measurements reveal higher carbon content levels at locations B and D. If there exist a direct relation between higher carbon content and dissolved gas will be discussed further in the section of field measurements.

7.1.3 Mineralogy

With the use of mineralogical research by X-ray diffraction, quantitative composition of the samples was obtained. From the analysis it became clear that samples were generally equal, especially from qualitative aspect. The exact qualitative overview can be found in table 7.1.3 below.

Mineral	**Theoretical formula**	Location A	Location B	Location C	Location D
NON-PHYILOSILICATES					
Silicates					
"Kwarts"	SiO_2	[redacted]			
"Alkali-veldspaat"	$Ca, Na)(Si, Al)_4O_8$				
"Plagioklaas"	$(K, Na)Si_3AlO_8$				
Carbonaten					
"Calciet"	$CaCO_3$				
"Mg-Calciet"	$(CaMg)CO_3$				
"Aragoniet"	$CaCO_3$				
"Dolomiet"	$CaMg(CO_3)_2$				
Fosfaten					
"Vivianiet"	$Fe_3(PO_4)_2.8(H_20)$				
Sulfiden					
"Pyriet"	FeS_2				
Oxiden					
"Anataas"	TiO_2				
Haliden					
"Halite"	$NaCl$				
Amorf					
"Opal"	$SiO_2.nH_2O$				
Total non-phyilosilicates					
PHYILOSILICATES					
Kaoliniet	$Al_2Si_2O_5(OH)_4$	[redacted]			
2:1 Kleimineralen (geschat perc. Fe-rijke 2:1 kleimineralen)	$K(Al, Mg, Fe)_2(Si, Al)_4 O_{10}((OH)_2, (H_2O))$				
Chloriet	$(Mg, Fe)_5Al(Si_3Al) O_{10}(OH)_8$				
Total phyilosilicates					

[redacted]

7.1.4 Atterberg Limits results

As explained before is describing the behaviour of the clay not complete without the Atterberg Limits. Below can be found the overview of measurement results

Atterberg Limits - Measurements			
Location of sampling	Plastic Limit w_p (in percentage)	Liquid Limit w_l (in percentage)	Plasticity Index (-)
Location A	[redacted]		
Location B			
Location C			
Location D			

Table 7.2: Overview Atterberg Limits results by "Q Mineral - Heverlee"

Based on the combination of plastic and liquid limit, samples can be characterised as follows based on general rules of thumb and ASTM standard. Having a liquid limit between 68.7 and 104.9 % results in 'soft clay', 'fat clay' and 'loam' with consequently 'plastic', 'soft' and 'plastic' classification characteristics.

7.1.5 Flowcurves

In this section the combined result of rheometer measurements and shear rate corrections will be presented. For all locations there were flow curves established at several densities to obtain a good insight in rheological characteristics. Because during the dredging operation several densities are encountered, it is only possible to process all data when for each density the viscosity is known. As various measures of viscosity are used in the derating methods, an overview is given below.

The measurement protocol by which all samples are processed together with the shear rate correction model can be found in chapter 4. Below the results are given as measured on the in-situ sample density, all other results can be found in the annex chapter at the end of the report.

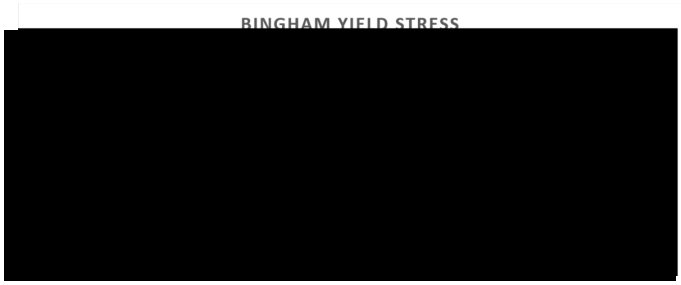

Figure 7.2: Overview Bingham yield stress in function of density for all locations.

Figure 7.3: Overview Bingham plastic viscosity in function of density for all locations.

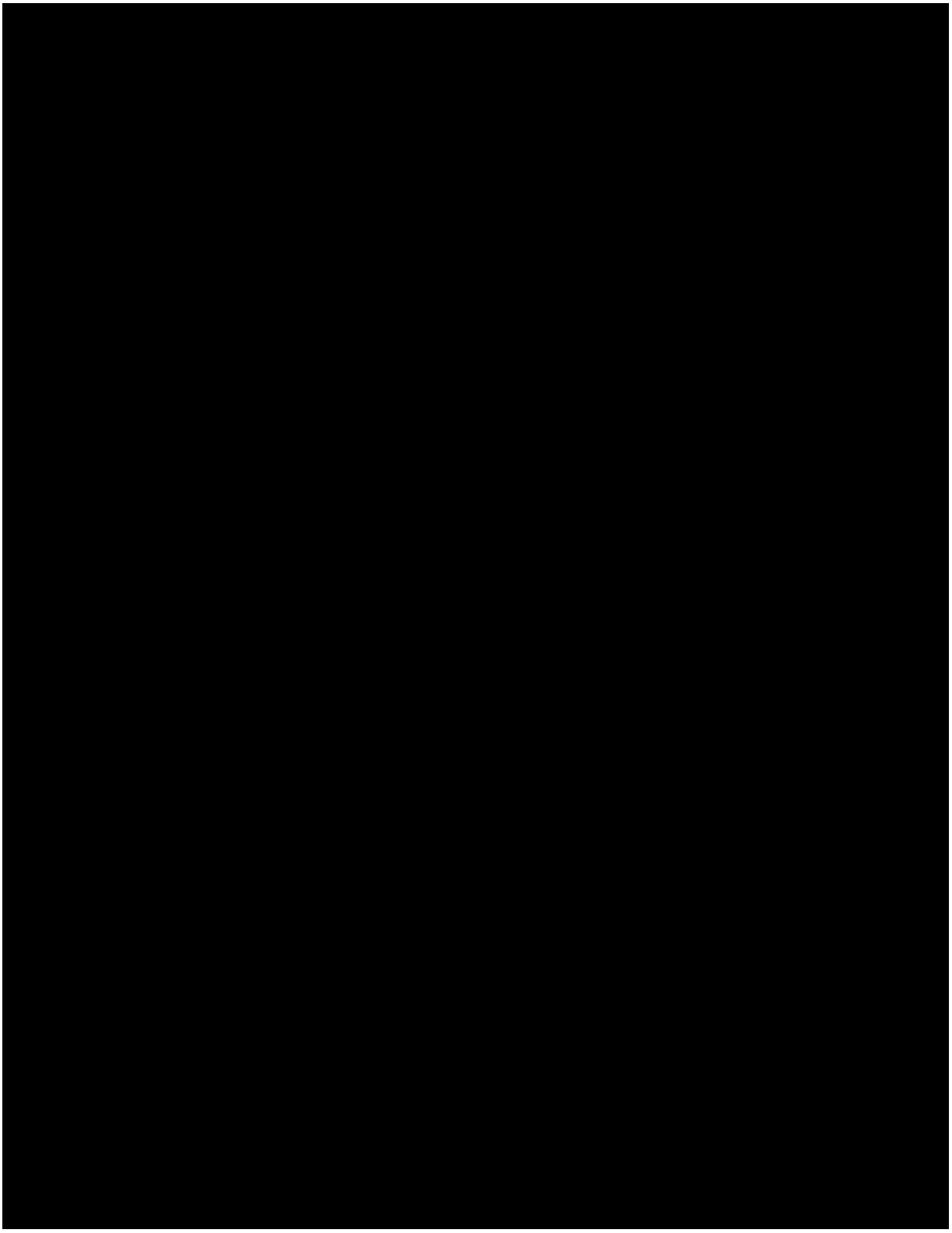

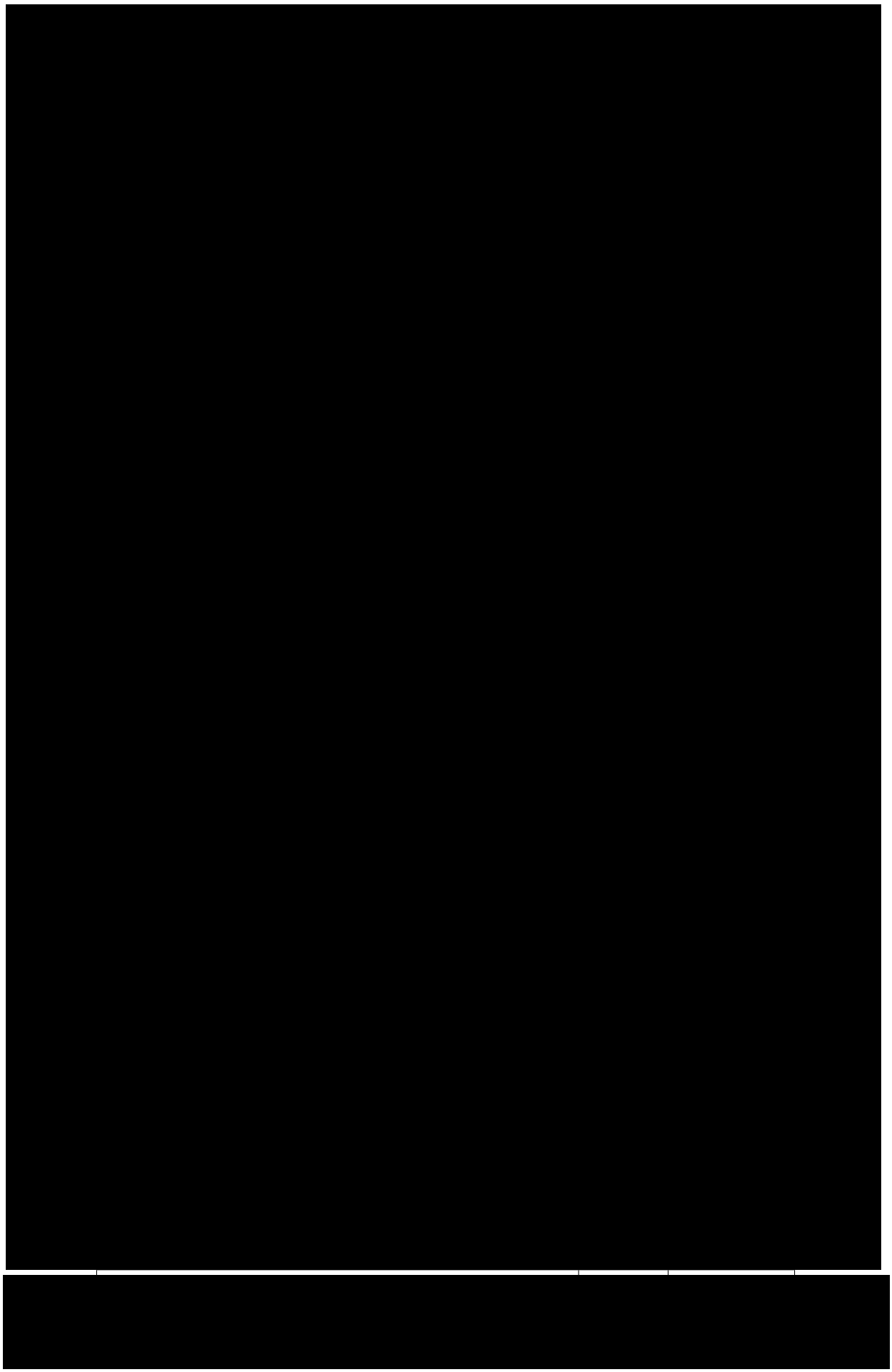

7.2 Field measurement results

In this section the measurements are presented as measured on board of TSHD Pallieter. Measurements on board are used to determine the influence of the pumped medium on large centrifugal pumps as used in the dredging industry. Pump characteristics relating head to flow rate, power to flow rate and efficiency to flow rate will be presented. Dependant on the location where the hopper was active after the installation of all measuring equipment, location dependant measurement results can be presented. Dedicated measurement devices installed on 'Pallieter' are the Mantracourt torque measurement and Sonartrac gas void fraction measurement. More information about the measured quantities can be found in chapter 6.

To compare the performance in clay and sand soils, two additional locations were chosen based on the availability of data from the particular location. The first sand location "Location E" was characterised by 'sand' while the other additional location "Location F" showed a varying classification between 'sand' and 'fine sand' according to the crew. It should be noted by the reader, all locations are in open contact with the river Scheldt except for location "A".

Gas void fraction measurements could only take place at locations where the vessel was active after the measurement device installation. Unfortunately, all locations except one were dredged after the installation of Sonartrac, resulting in unavailability of the data for "Location D" as can be seen in the table 7.2.1.

The same condition yields for the torque measurement. After the installation and calibration of the measurement device, Pallieter was only active in clay location "B" and sand location "F". Also these results will be presented in the following sections.

NOTE: For the sake of clarity in the report, only the figures corresponding to the analysis of Location 'B' and Location 'F' will be presented for power and efficiency due to data completeness at these locations. All other graphs can be found in the attachment section.

7.2.1 Location dependant GVF

Influence of dissolved gas on the performance of a centrifugal pump is obvious and will be quantified later. To determine which location has a greater natural dissolved gas content, the measurements of the Sonartrac are first analysed with respect to location and measured gas fraction in general. For all dredging locations the degassing installation was used so no difference in performance is assumed.

Apart from the four predefined locations, two extra locations were assigned in order to compare. These locations were characterised as "sand" by the dredging crew and project data. By comparing these different soils with each other, tendency of air presence can be related to the soil characteristics.

Associated box-plots can be found in figure 7.11.

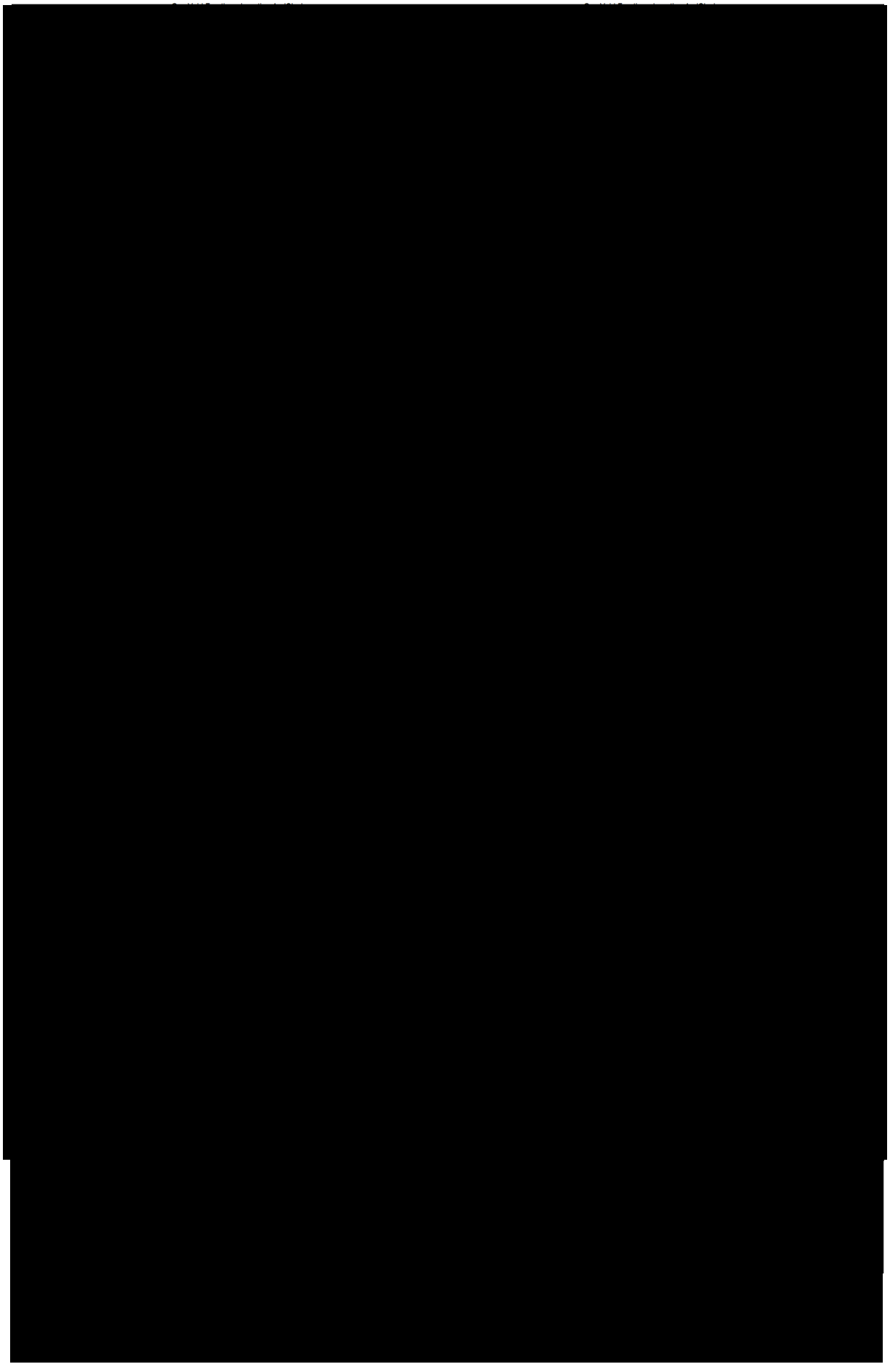

Figure 7.11: Boxplot visualizing the distribution of GVF occurrence at each location.

7.2.2 Head Flow-rate curves

As explained in the previous chapters, Head, Power and consequently Efficiency are simulated by measuring various parameters while dredging. The combination of both the pressure before and after the dredge pump, mixture velocity and density, pump rotational speed and torque on the input shaft result in the presented pump characteristics.

Influence on the head characteristics of a centrifugal pump was found to originate from two sources. A first source of de-rating which should be found is the presence of clay in the mixture which increases the viscosity of the medium and can be of great significance when very high viscosities are reached. Dependant on the measured density of the mixture, the amount of present clay can be calculated and consequently the expected viscosity. The second source of de-rating is related to the presence of air in the mixture. A higher viscosity and subsequent higher yield stress reinforces the resistance to separation. Both effects will be presented by filtering the data or changing the location where data is measured.

From this first figure, a general overview of measurement points can be seen with respect to head versus flow rate. Head was expressed in meters of slurry column to normalize head readings for different densities. Filtering was only done on density, as occasionally unrealistic values were recorded and RPM to determine when the pump was running. During the dredging operation a pump speed between 70 and 100 % is maintained.

Figure 7.12: Head Flowrate characterics for Location B. Head in meters of slurry column versus flowrate in function of BEP.

It can be seen that recordings follow the theoretical predicted trend although many outliers are also present (lower head). To determine the cause of these points, filters are applied and data is categorised according to density and measured gas fraction. As learned from previous chapters, an increase in viscosity should be characterised by lower head at high flow rates whilst an increase in gas fraction can be distinguished by a dropping head at low flow rates. To see if both rules are applicable to large centrifugal pumps, ordering of data was done accordingly.

Influence of rheology

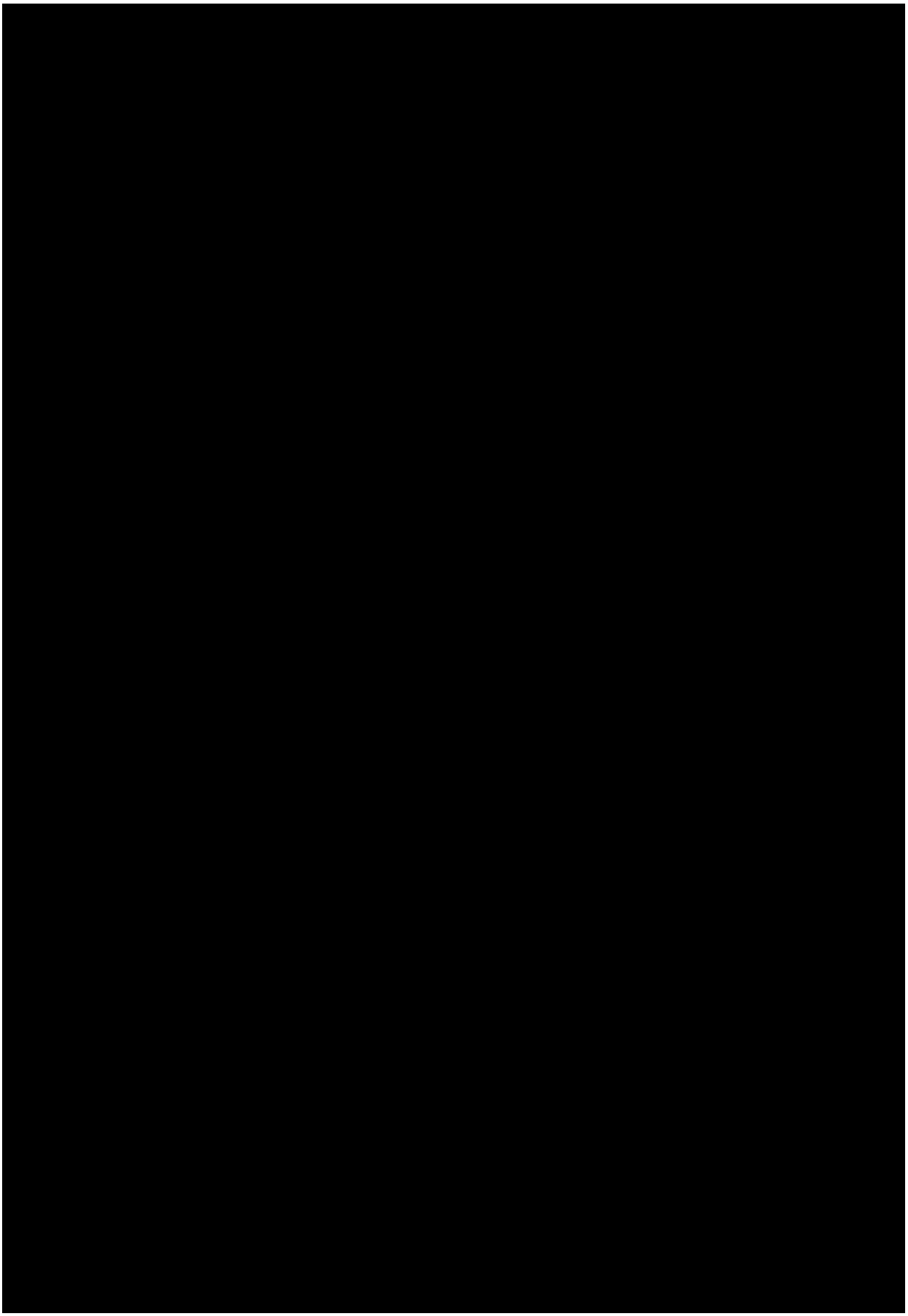

In the figures above (7.15 and 7.16) it can be seen that there exist a higher tendency for the clay location to deviate from the theoretical curve than for the sand location. It is possible for air to accumulate in the pump and be released again at a different point in time so negative effects of gas are noticed at a different moment.

Influence of gas void fraction

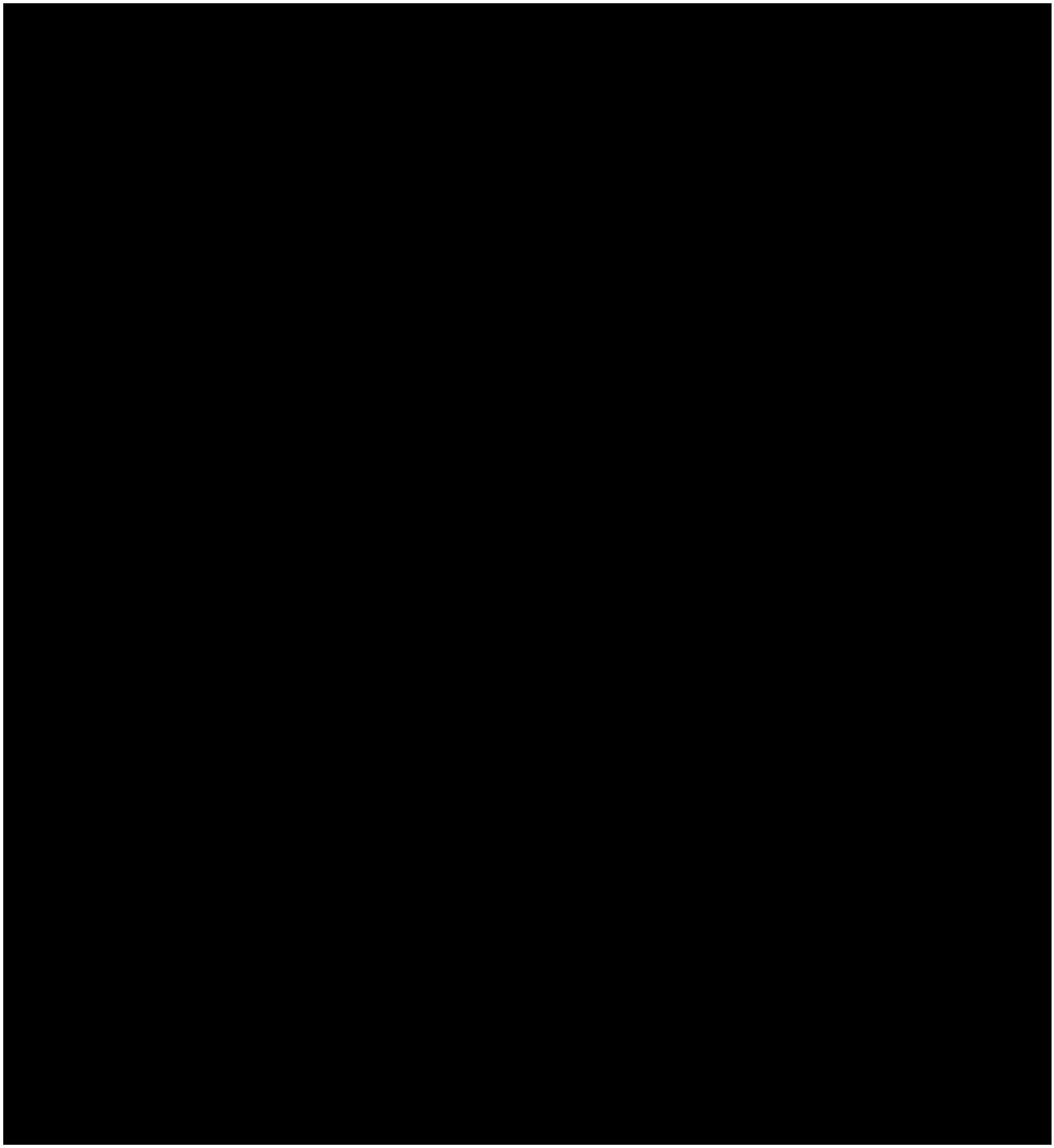

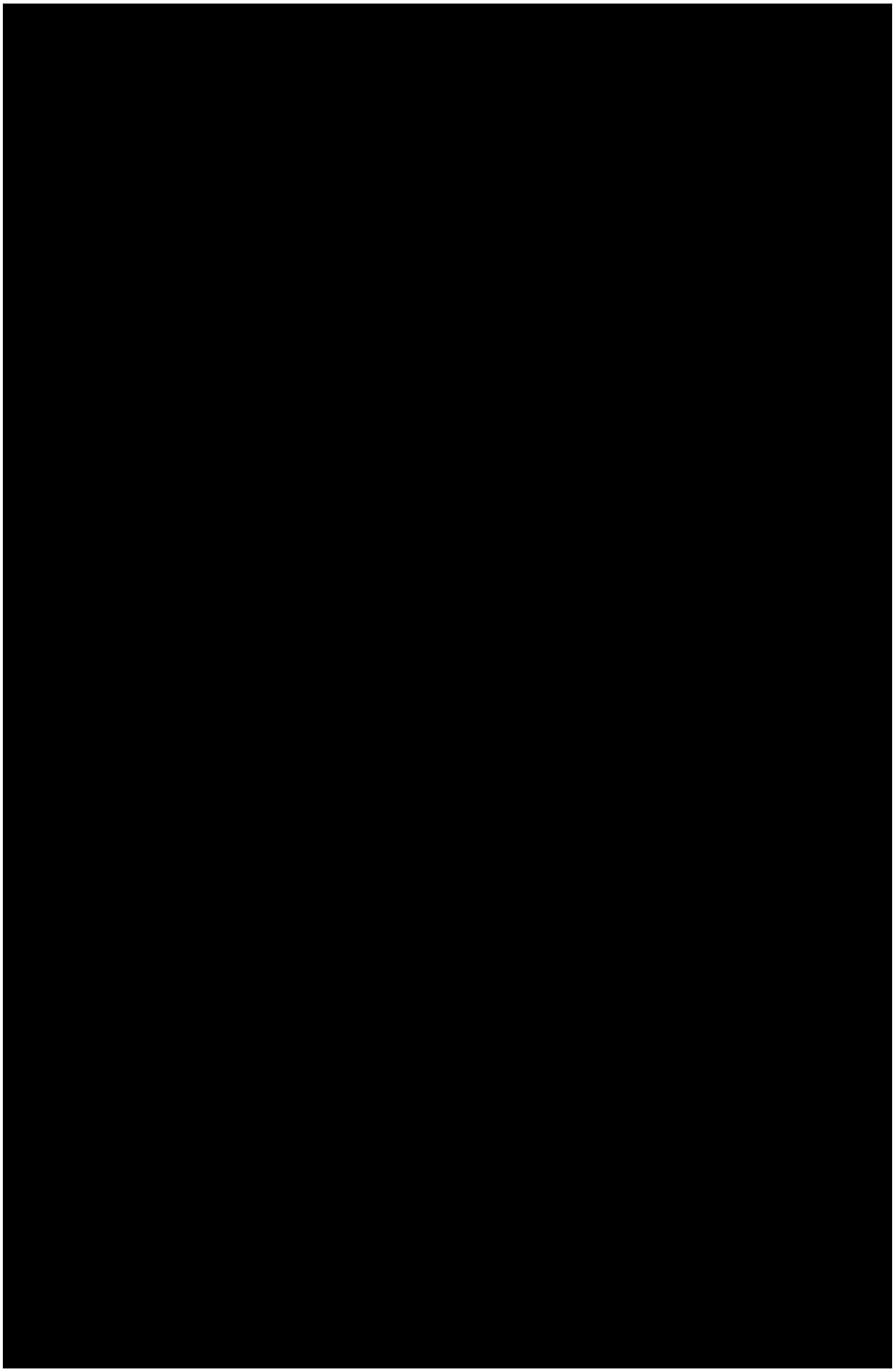

7.2.3 Power Flow-rate curves

Influence of rheology

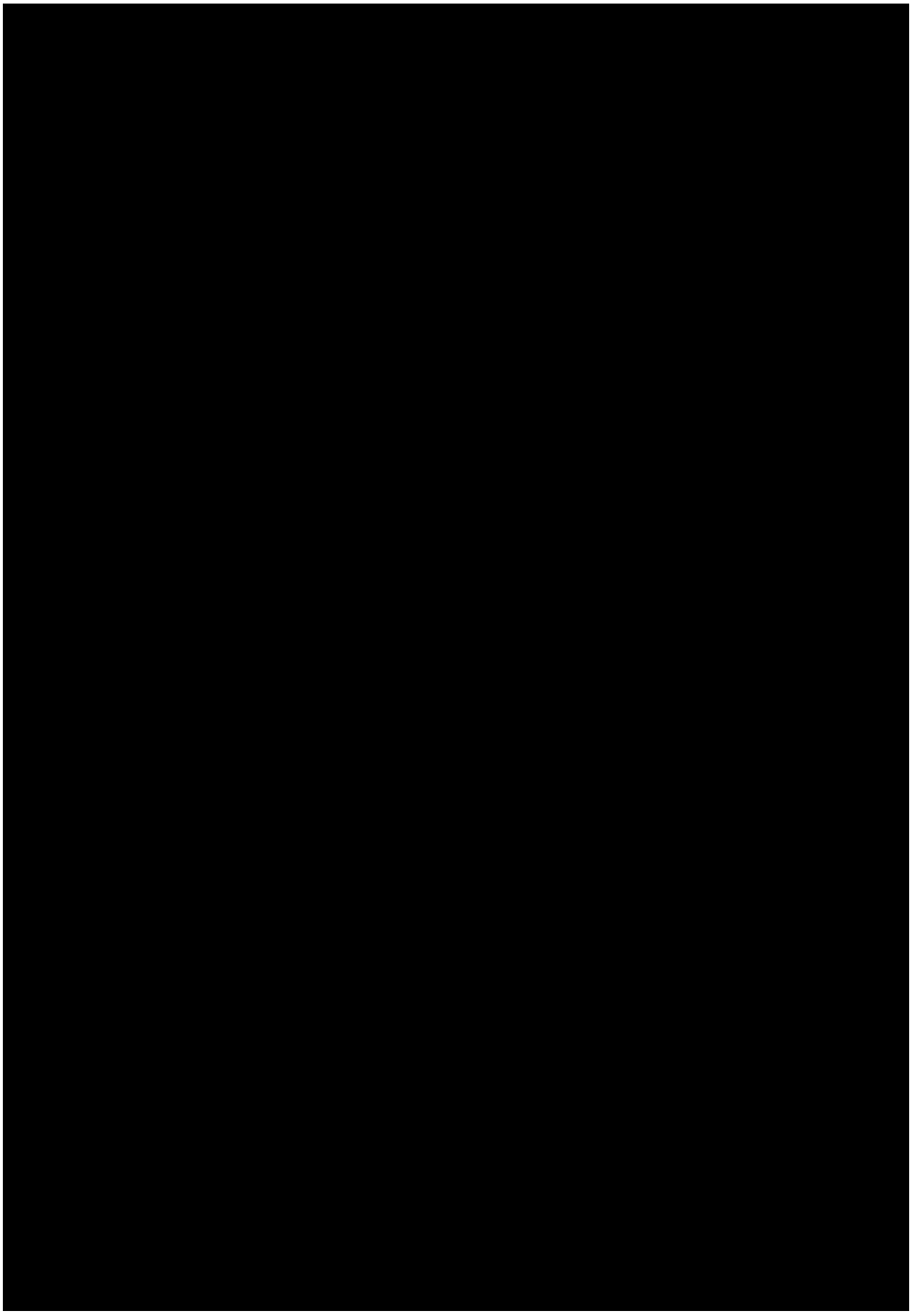

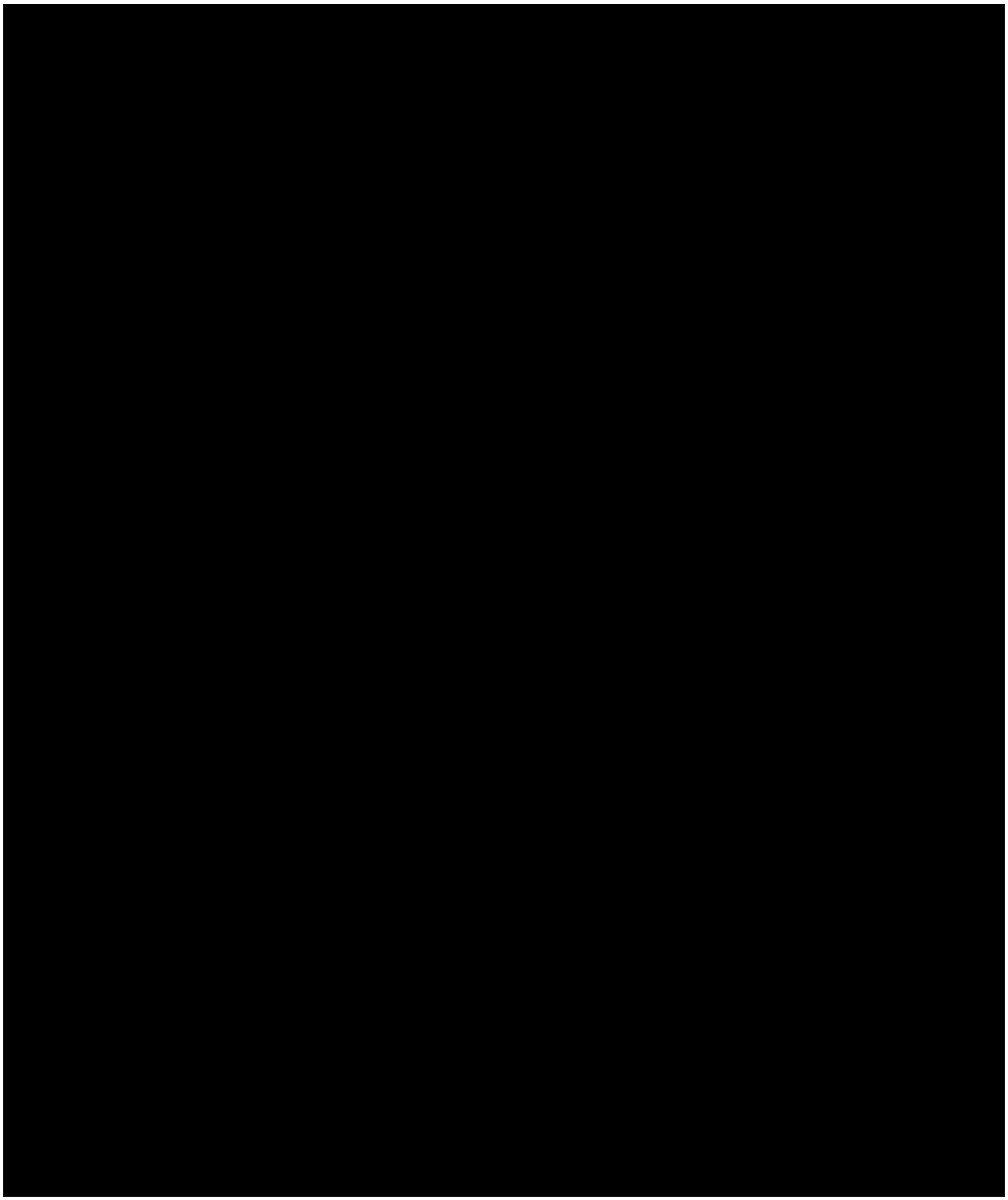

Chapter 8

Synthesis

In the past, models are developed for pumping highly viscous mixtures with centrifugal pumps designed for slurry applications. Although the methods are applicable based on the viscosity range as encountered in this research (< 4000 cSt) and specific testing parameters (i.e. 'B' for ANSI), no validation is available with a pump of similar dimensions as encountered in this dredging application.

In this section various models will be compared with the measurements from chapter 7 as measured on board of TSHD 'Pallieter'. Colours used in the coming plots is kept consequent for easy identification of each model.

1. **Black BOLD** (0): Power according to density-law.
2. Green (1): Model according to J.F. Gulich 2008 - Gulich (2008)
3. Red (3): Model according to Hydraulic Institute 1983 - Hydraulic Institute (1983)
4. Orange (4): Model according to KSB Lexicon - Kreiselpumpen KSB (1989)
5. Black (5): Model according to ANSI 9.6.7 (2015) - ANSI (2015)

Comparing the models with data is done by use of R Squared. R Squared or coefficient of determination quantifies the 'goodness' of the proposed fit or model to the data. Because the models are generated separately from the data points, negative R Squared are possible when a less good fit is present. If a negative R Squared result appear, the model does not follow the trend of the data well and a linear regression or horizontal line would better represent the data (University of New South Wales - Australia (2017)). Although negative, comparison between models is still possible by comparing the order of magnitude from R Squared. A more negative value resembles a less good fit.

$$R^2 = 1 - \frac{\sum_{i=1}^{n} {e_i}^2}{\sum_{i=1}^{n} (y_i - \overline{y})^2} \tag{8.1}$$

where: $e_i^2 = SS_{reg} = \sum_i (y_i - f_i)^2$

It should be clear to the reader that only data with a very low GVF is compared to the model as the models were developed with exclusion of gas presence in the mixture. Also the models were developed and tested during stable working conditions and constant mixture composition. During the dredging operation, non of these requirements are fulfilled and only filtering of data for a particular situation is possible.

Apart from comparing the models by means of R Squared, visual observations have proved to be equal beneficial. Conclusions regarding deviation when gas influences the pump performance will be based on a comparison between data points and a predefined bandwidth to estimate the deviance.

8.0.1 Models for Head

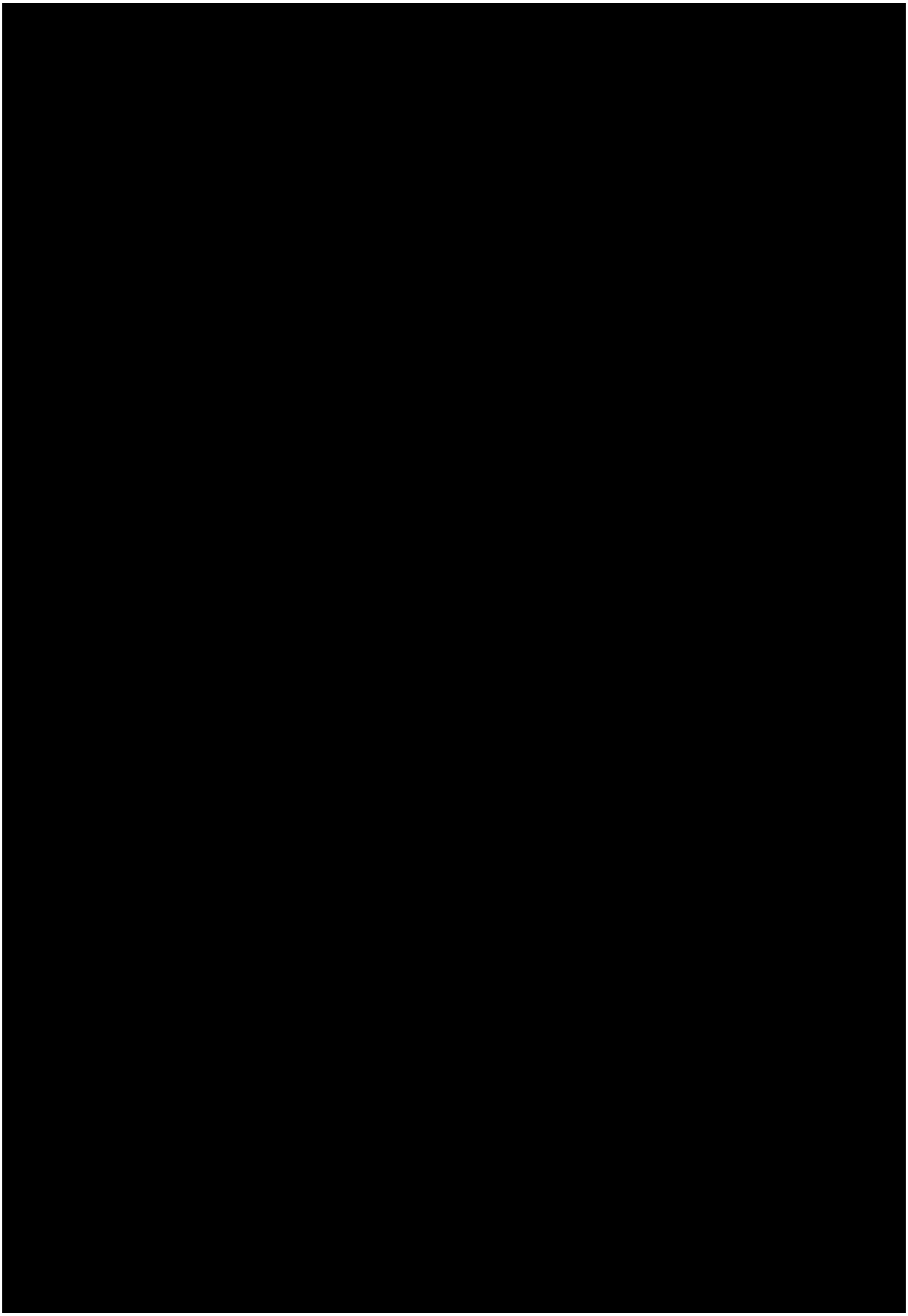

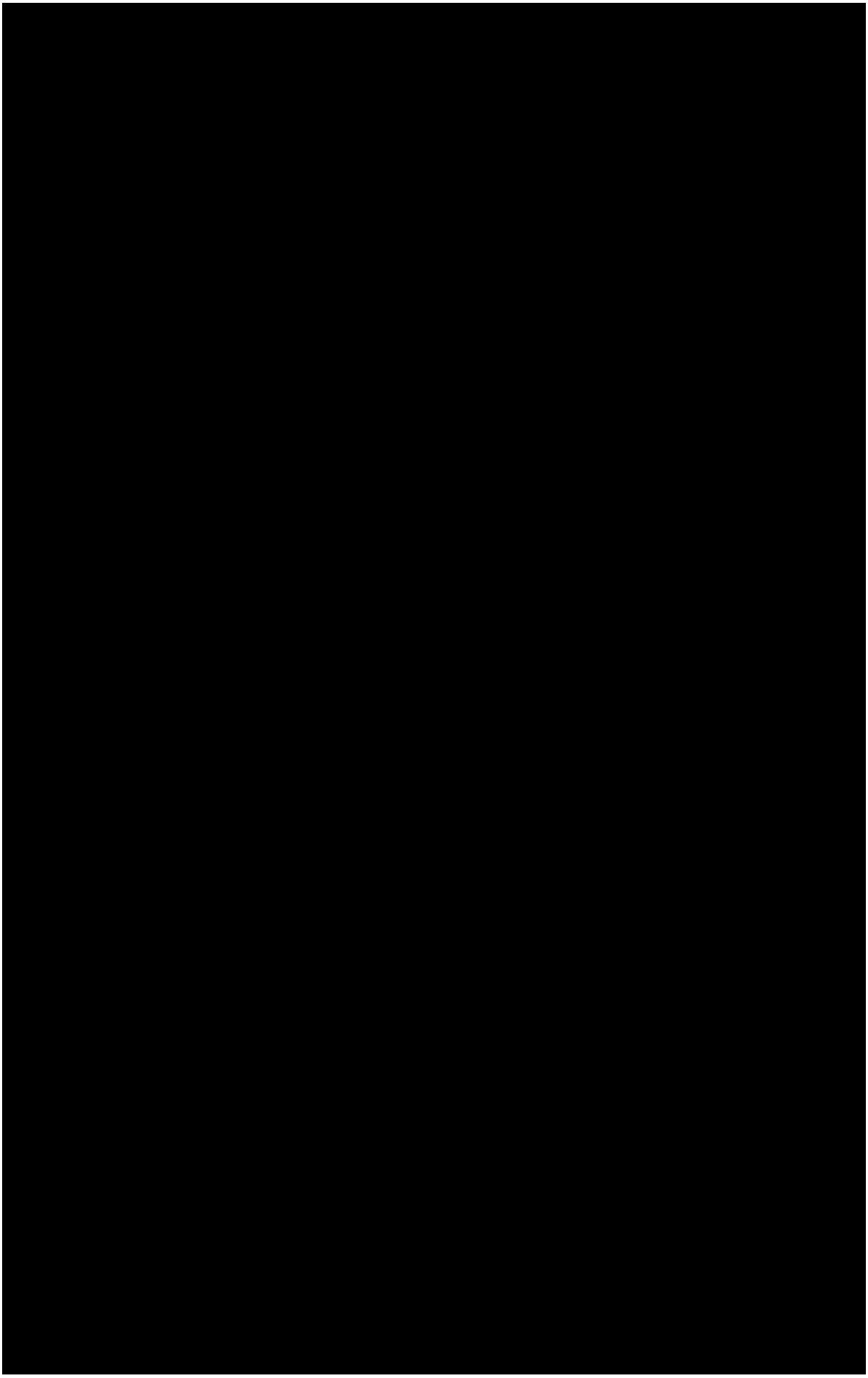

8.0.2 Models for Power

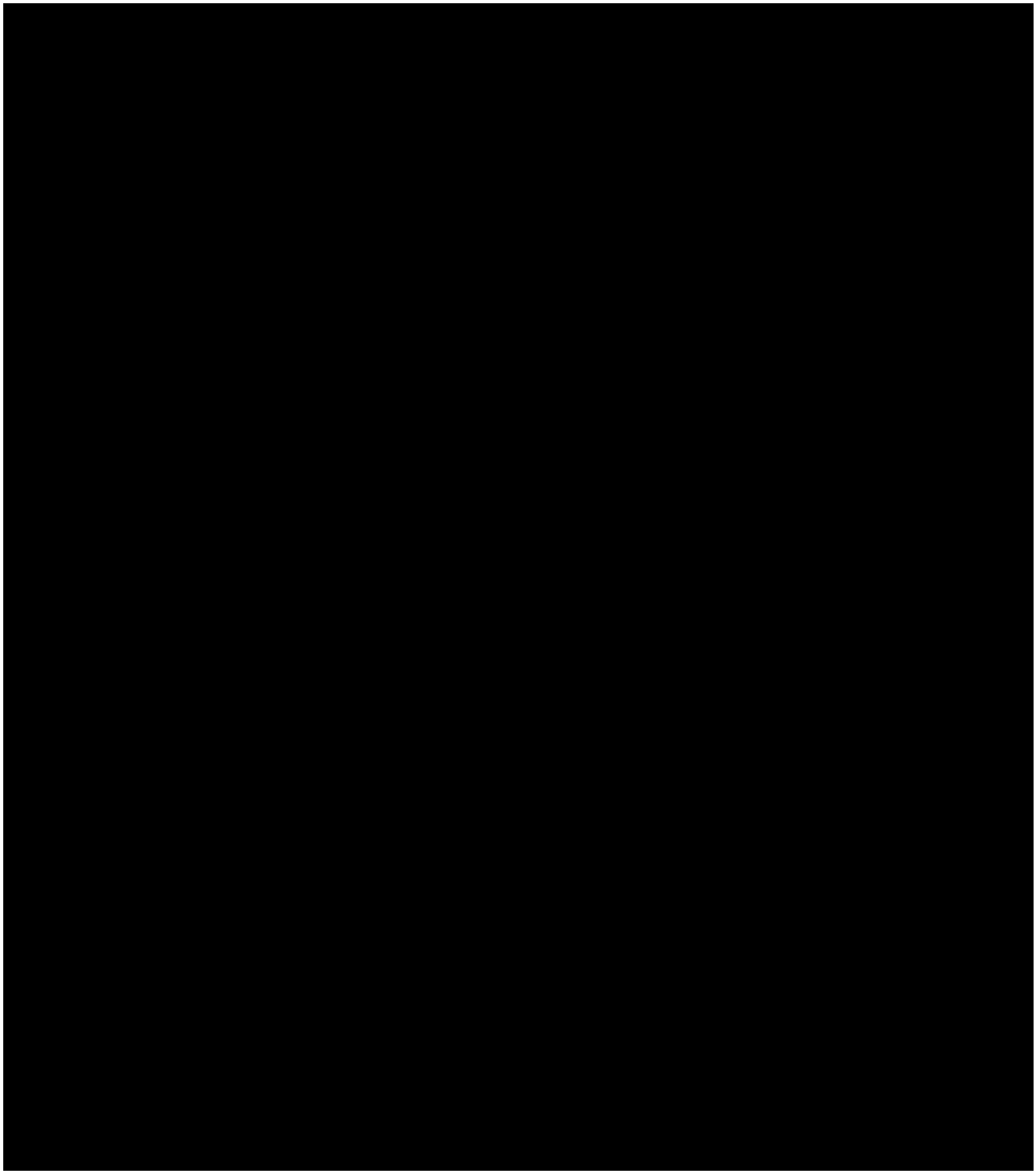

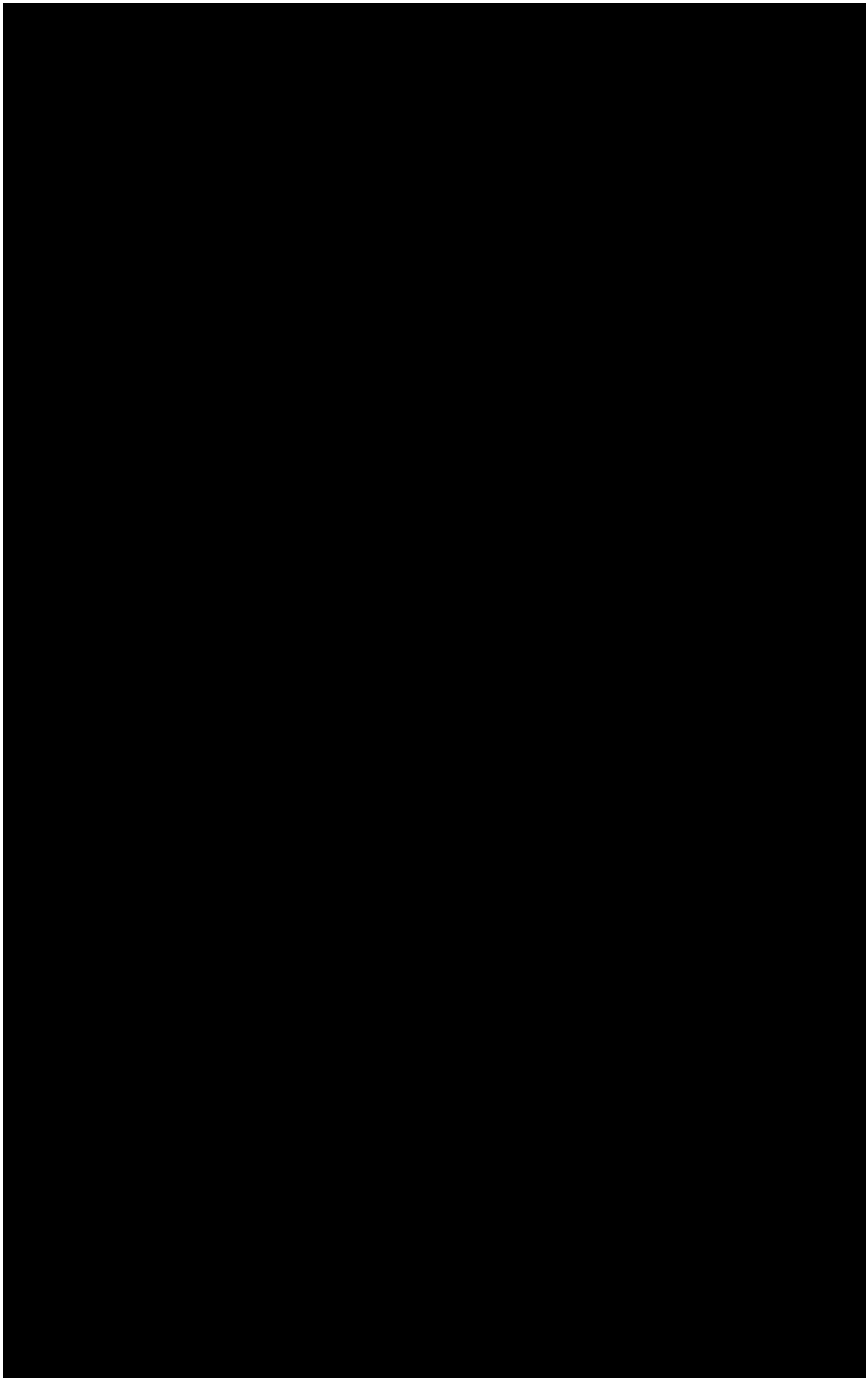

8.0.3 Models for Efficiency

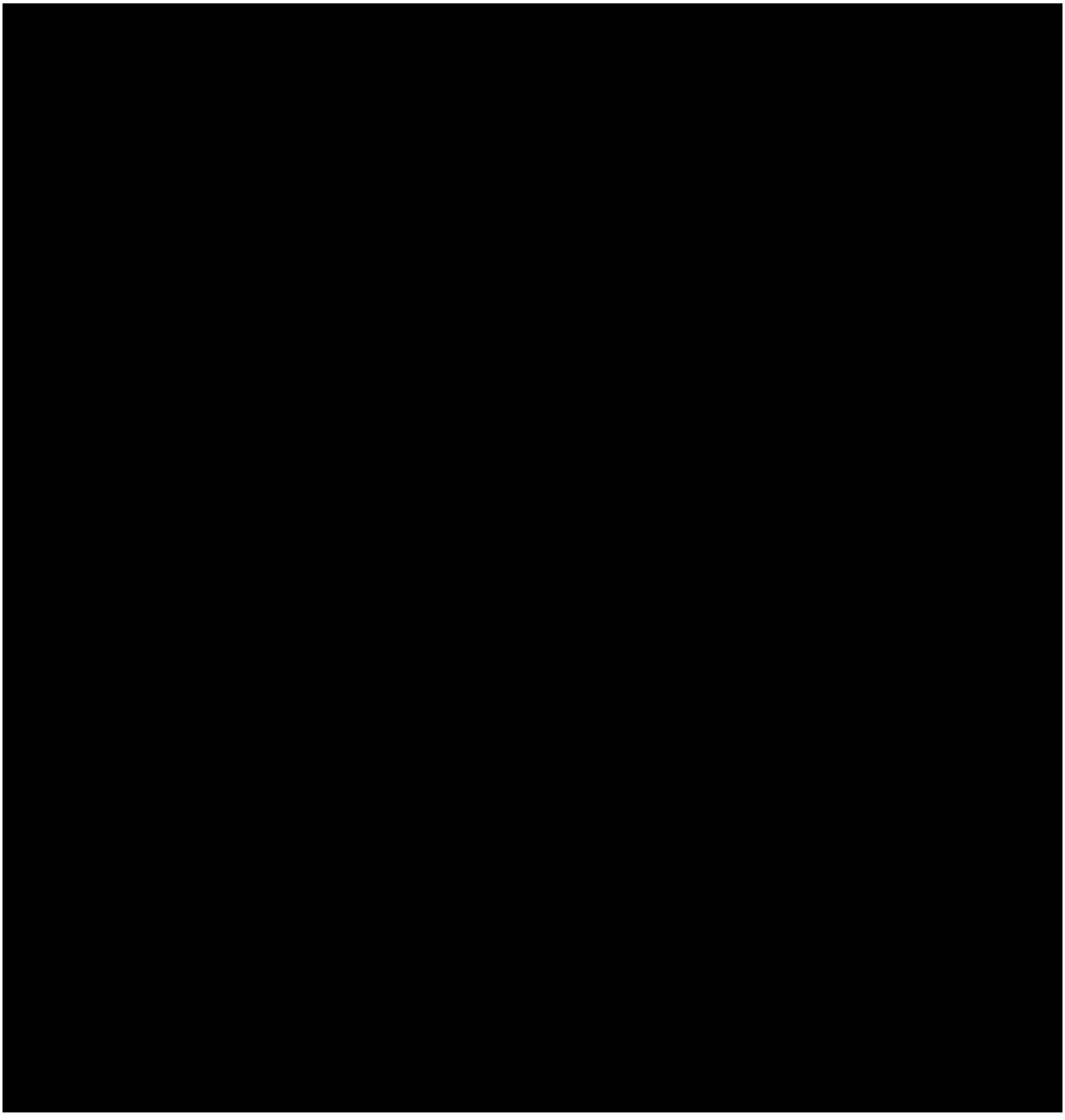

8.0.4 Method validation overview

8.0.5 Models for Air

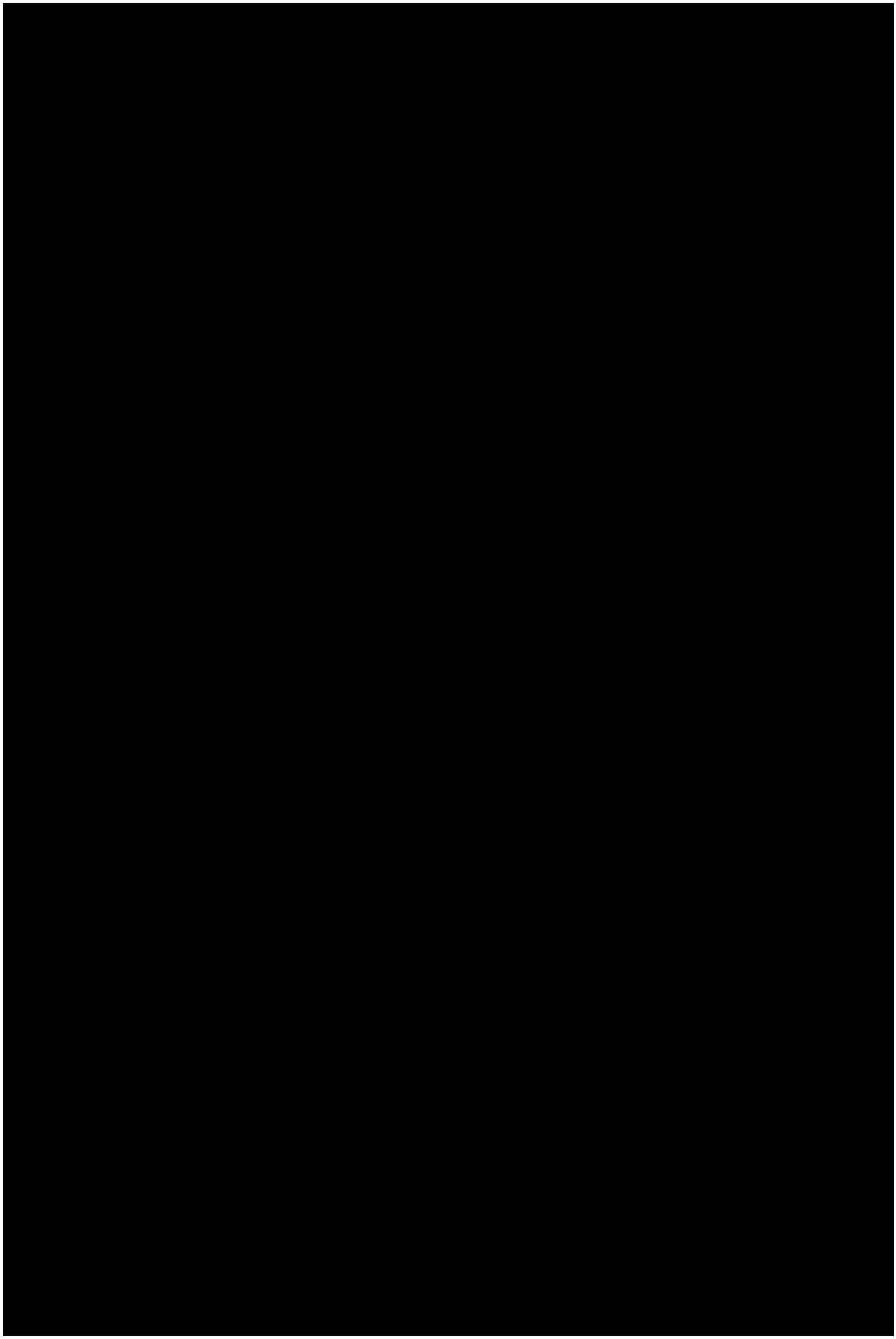

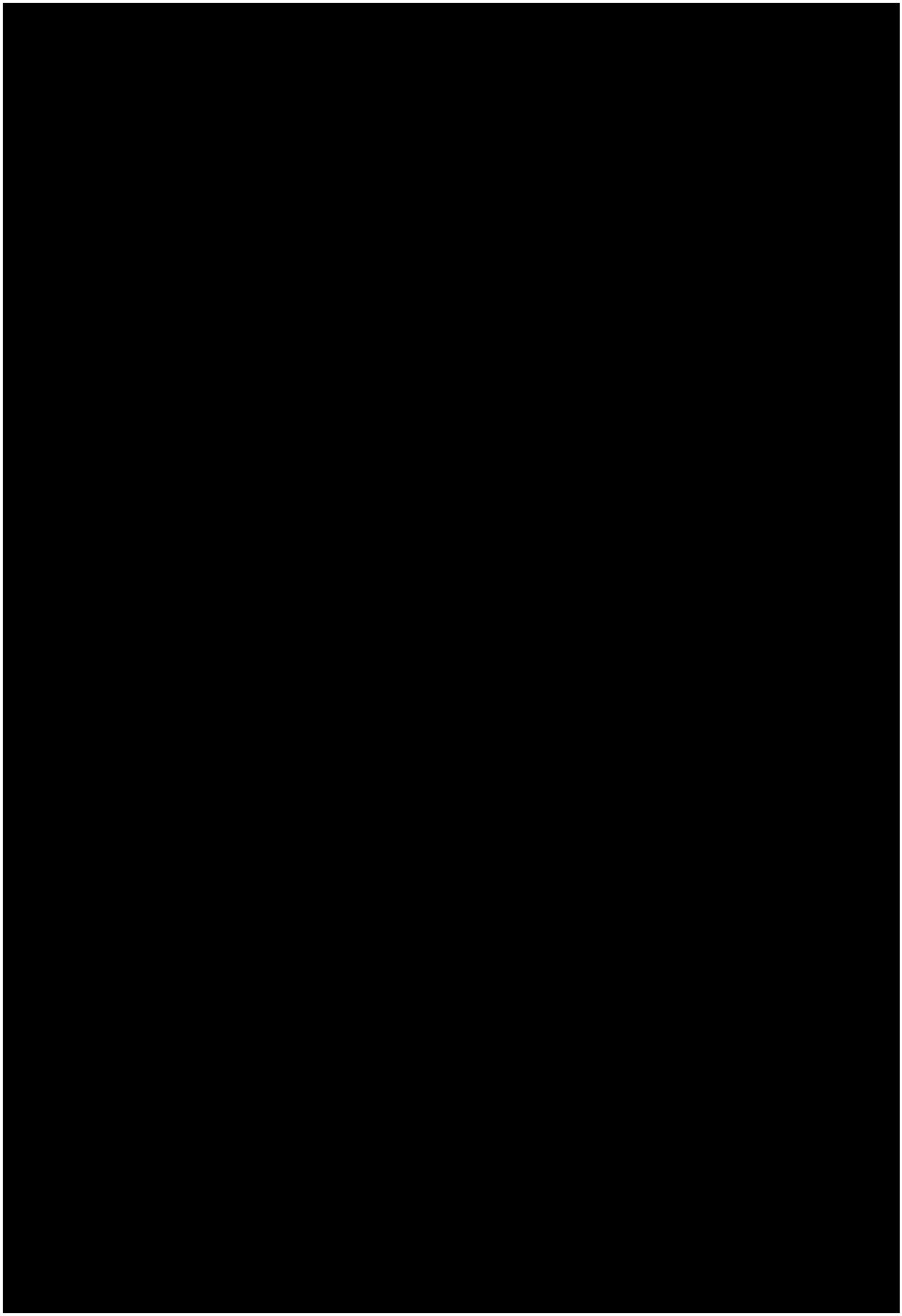

Chapter 9

Conclusions

9.1 Resume

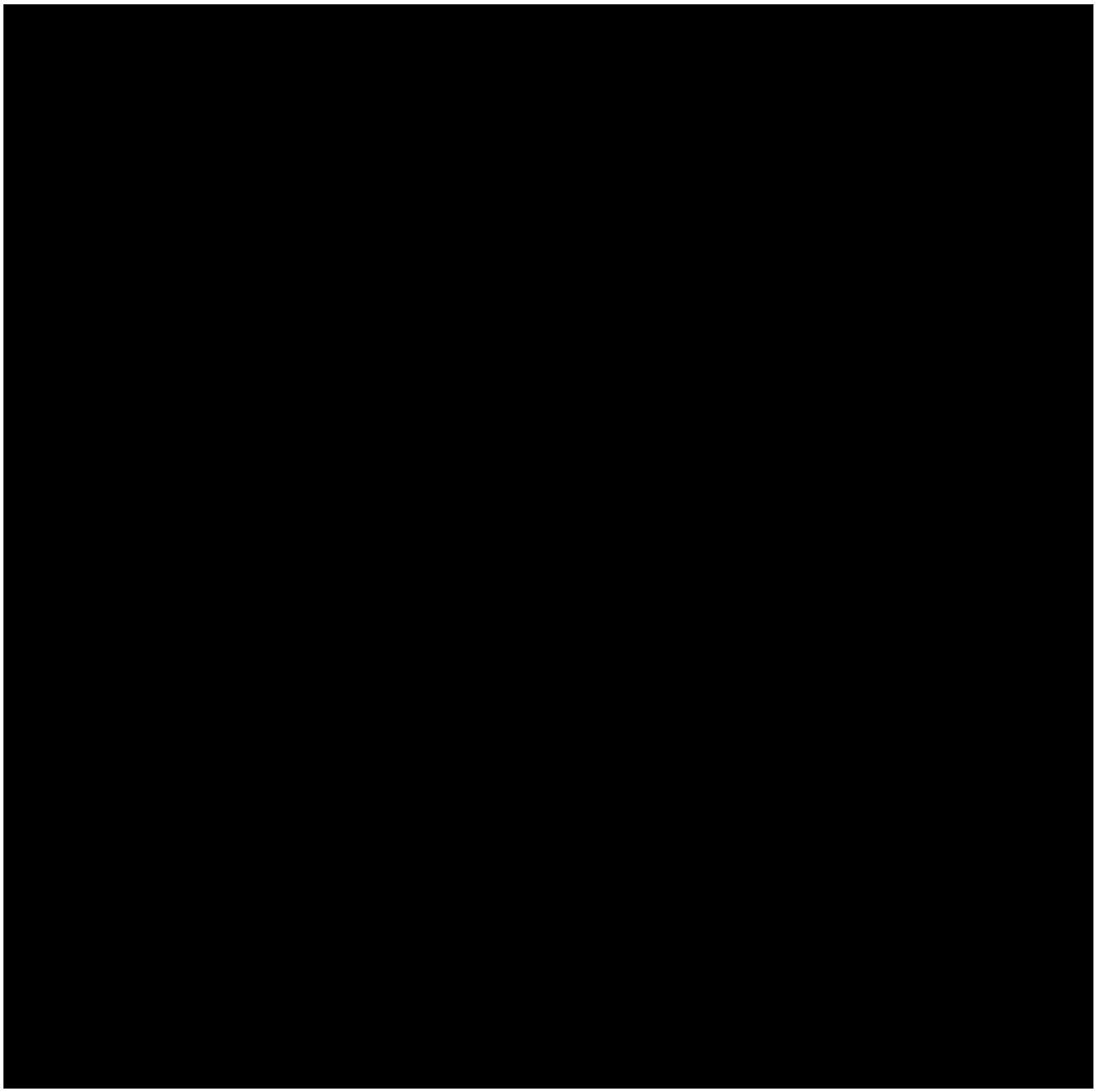

9.2 Conclusions

9.2.1 Influence of increased viscosity

9.2.2 Influence of dissolved gas

9.3 Recommendations

Bibliography

ANSI (2015). Hydraulic Institute Standard - ANSI/HI 9.6.7.

ANSI and Hydr (2004). Effect of liquid viscosity on pump performance. 9.6.7 [N12].

Bonnington, S. (1957). The effect of included solids on the characteristics of centrifugal pumps. *BHRA Fluid Engineering*.

Chhabra, R. P. and Richardson, J. F. (1999). Non-Newtonian flow in the process industries : fundamentals and engineering applications. pages xiii, 436.

Claeys, S., Van Hoestenberghe, T., Van Oyen, T., Roeyen, J., and Toorman, E. (2013). Sediment Related Nautical Research - Standard rheometer analyses of cohesive sediment for nautical and dredging applications. (May).

Duckham, C. (1971). Design of centrifugal pump installations for viscous and non-Newtonian fluids. *Chemical and Process Engineering*, 52(7):66–68.

Dullaert, K. and Mewis, J. (2005). Thixotropy : Build-up and breakdown curves during flow. *Journal of Rheology*, (Oktober).

EN12879 (2000). Characterization of sludges - Determination of the loss on ignition of dry mass.

E.T. (2017). Engineering Toolbox.

Florjancic, D. (1970). Einfluß von Gas- und Luftzuführung auf das Betriebsverhalten ein- und mehrstufiger Pumpen. *Techn Rundschau Sulzer*, pages 35–44.

Furlan, J., Visintainer, R., and Sellgren, A. (2016). Centrifugal pump performance when handling highly non-Newtonian clays and tailings slurries. *Canadian Journal of Chemical Engineering*, 94(6):1108–1115.

Graham, L., Pullum, L., Slatter, P., Sery, G., and Rudman, M. (2009). Centrifugal pump performance calculation for homogeneous suspensios. *The Canadian Journal of Chemical Engineering*, 87(4):526–533.

Guang, L. W. (2000). The sudden-rising head effect in centrifugal oil pumps. *World Pumps*, pages 34–36.

Guang, L. W. (2014). Mechanism for Onset of Sudden-Rising Head Effect in Centrifugal Pump When Handling Viscous Oils. *Journal of Fluids Engineering*, 136.

Gulich, J. F. (2008). *Centrifugal Pumps*. Springer, Berlin.

Hamkins, C. and al, E. (1987). Prediction of viscosity effects in centrifugal pumps by consideration of individual losses. *ImechE paper*.

Herbich, J. B. (1959). Characteristics of a model dredge pump, Project report no. 31. (31).

Hergt, P. and al, E. (1981). Verlustanalyse an einer Kreiselpumpe auf der Basis von Messungen bei hoher Viskosität des Fördermediums. *VDI Ber 424*.

Hydraulic Institute, H. (1983). Standards for centrifugal, rotary & reciprocating pumps. [N4]. Technical Report 14.

International Standard (2012). International Standard - Hydraulic performance acceptance tests - Grade 1, 2 and 3. (2).

Kabamba, B. (2006). *Evolution of centrifugal pump performance derating procedures for non-Newtonian slurries.* PhD thesis, Cape Peninsula University of Technology.

Kreiselpumpen KSB, A. (1989). KSB-Kreiselpumpen-Lexikon. 3. Aufl [B5].

Krieger, I. M. and Maron, S. H. (1952). Direct determination of the flow curves of non-Newtonian fluids. *Applied Physics*, pages 147–149.

Maris, T., Bruens, A., Van Duren, L., Vroom, J., Holzhauer, H., de Jonge, M., Van Damme, S., Nolte, A., Kuijper, K., Taal, M., Jeuken, C., Kromkamp, J., Van Wesebeeck, B. K., Van Ryckegem, G., Van den Berghe, E., Wijnhoven, S., and Meire, P. (2014). Evaluatiemethodiek Schelde-estuarium.

Matoušek, D. i. V. (2004). *Dredge Pumps And Slurry Transport (OE4625).* TU Delft, Delft, 1 edition.

Mollenkopf, G. (1978). Einfluß der Zähigkeit des Fördermediums auf das Betriebsverhalten von Kreiselpumpen unterschiedlicher spezifischer Schnelläufigkeit. *Pumpentagung Karlsruhe.*

Paterson, A. and Cooke, R. (1999). The design of slurry pupeline systems.

Pullum, L., Graham, L., and Wu, J. (2011). Centrifugal pump performance with non-Newtonian slurries. In *International conference on transport and sedimentation of solid particles.*, Wroclaw, Poland.

Rothman, P., Gysling, D., Loose, D., and Kravets, A. (2007). Method for calibrating a flowmeter having an array of sensors. (Patent).

S. Mikhail, Khalafallah, M., and M. El-Nady (2001). Disk Friction Loss In Centrifugal and Mixed Flow Pumps. *Seventh International Congress on Fluid Dynamics and Propulsion, Cairo, Egypt*, pages 1–6.

Sauer, M. (2002). *Einfluss der Zuströmung auf das Förderverhalten von Kreiselpumpen radialer Bauart bei Flüssigkeits-/Gasförderung.*

Saxena, S. and Et al, . (1996). Ermittlung von Korrekturfaktoren für Hochleistungs-Pipeline-Kreiselpumpen beim Fördern von Mineralölen mit erhöhter Viskosität. *Pumpentagung Karlsruhe*, (C7-3).

Scarlett, A. and Madsen, R. (2006). Quantification of phases with partial or no known crystal structure. *Powder Diffraction*, (4):278–285.

Sellgren, A., Addie, G., and Al, D. (2000). The effect of Sand-Clay slurries on the performance of centrifugal pumps. *The Canadian Journal of Chemical Engineering*, 78(4):764–769.

Sellgren, A., Addie, G., and Yu, W.-C. (1999). Effects of Non-Newtonian Mineral Suspensions on the Performance of Centrifugal Pumps. *Mineral Processing and Extractive Metallurgy Review*, 20:239–249.

Sellgren, A. and Furlan, J. (2017). A SelIgren Lulea University of Technology, Sweden. *Hydrotransport*, 20:401–414.

Sematech, N. (2017). Engineering Statistics handbook -Process Modeling - LOESS method.

Sery, G. and Slatter, P. (2002). Centrifugal pump derating for non-Newtonian slurries. In *Hydrotransport*, pages 679–692, Banff, Canada. BHR Group.

Slatter, P. (1986). The rheological characterisation of non-Newtonian slurries using a novel balanced beam tube viscometer. *University of Cape Town.*

Spek, A. M. V. D., Dopieralla, R., Viega, J., and Heude, N. (2016). New technology for dredging mixture velocity measurement. *WODCON XXI.*

Stoffel, B., Eikmeier, L., and Tamm, A. (2002). The influences of surface roughness on head, power input and efficiency of centrifugal pumps. In *Symp Hydraulic Machinery and Systems.*

Toorman, E. A. (1995). Controlled rate concentric cylinder rheometry of estuarine mud suspensios. (Report HYD148). Technical report, KU Leuven, Heverlee.

University of New South Wales - Australia (2017). Goodness-of-fit Statistics.

van den Berg, K. and Stam, N. (2013). *IHC Merwede Handbook for Centrifugal Pumps and Slurry Transportation*. MTI Holland, Kinderdijk, 31 edition.

Van Rhee, C. (2009). Centrifugal Pumps. In *Centrifugal Pumps - Lecture Notes*, page 11.

Vavra, M., Wiley, J., and Sons (1960). *Aero-thermodynamics and flow in turbomachines.*

Vlasbom, W. (2004). Dredge Pumps. In *Dredge Pumps*, page 66.

Walker, C. I. and Goulas, A. (1982). Performance characteristics of centrifugal pumps when handling non-Newtonian homogeneous slurries. *Proc. Inst Mech. Engrs.*, 198A:41–49.

Wikipedia (2017). Ammonia characteristics.

List of Figures

List of Tables

Chapter 10

Appendix

10.1 Rheological results

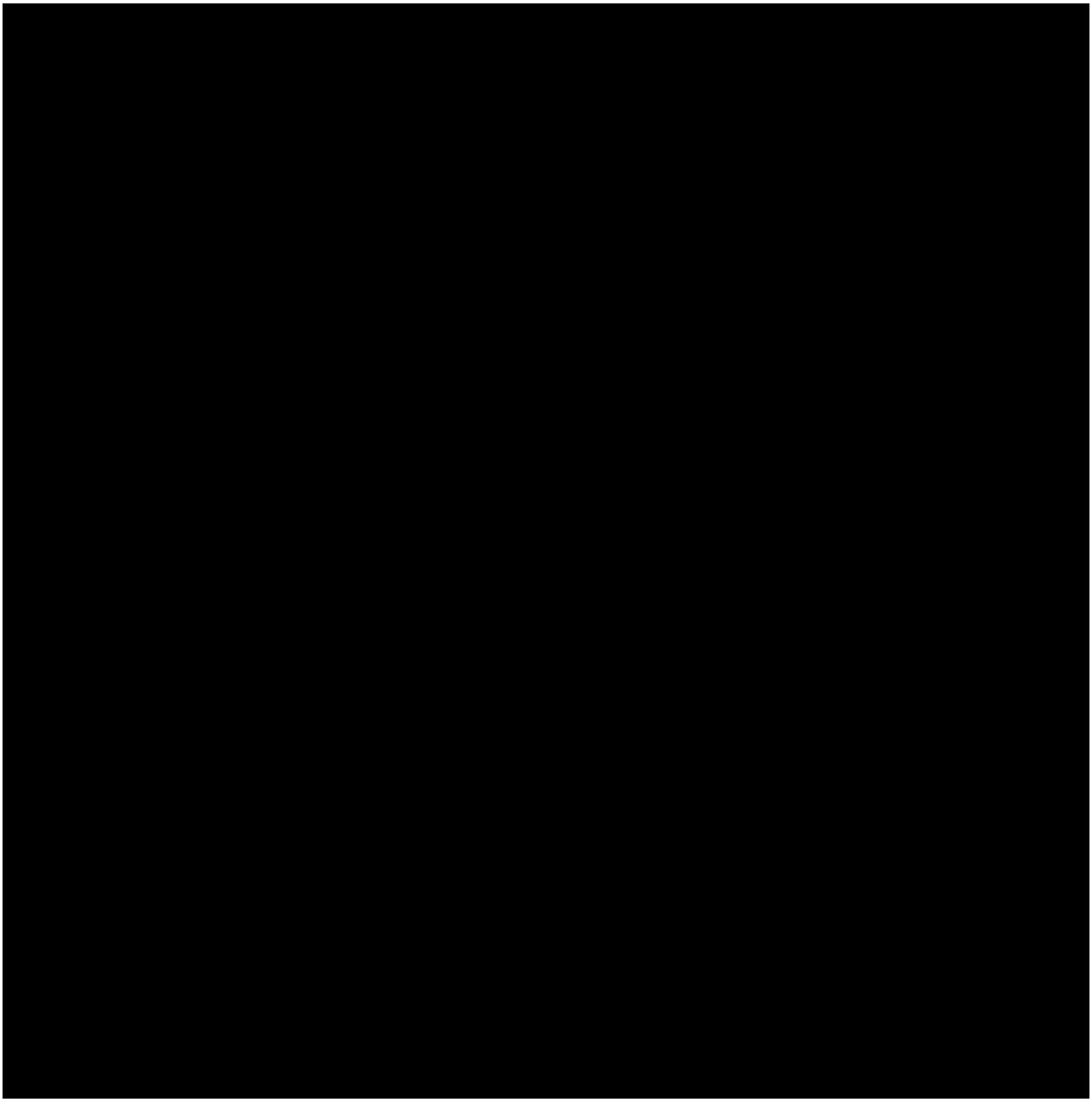

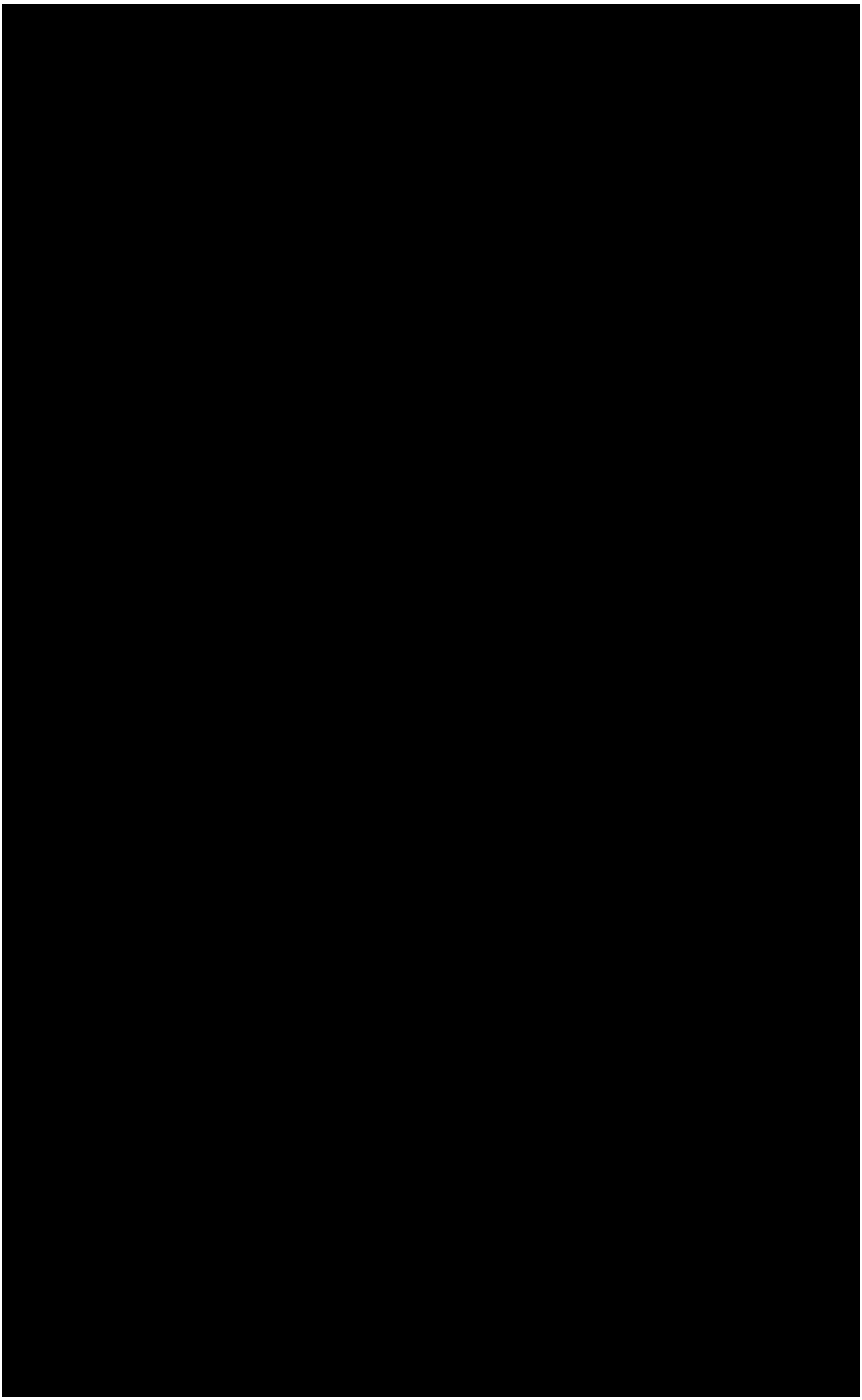

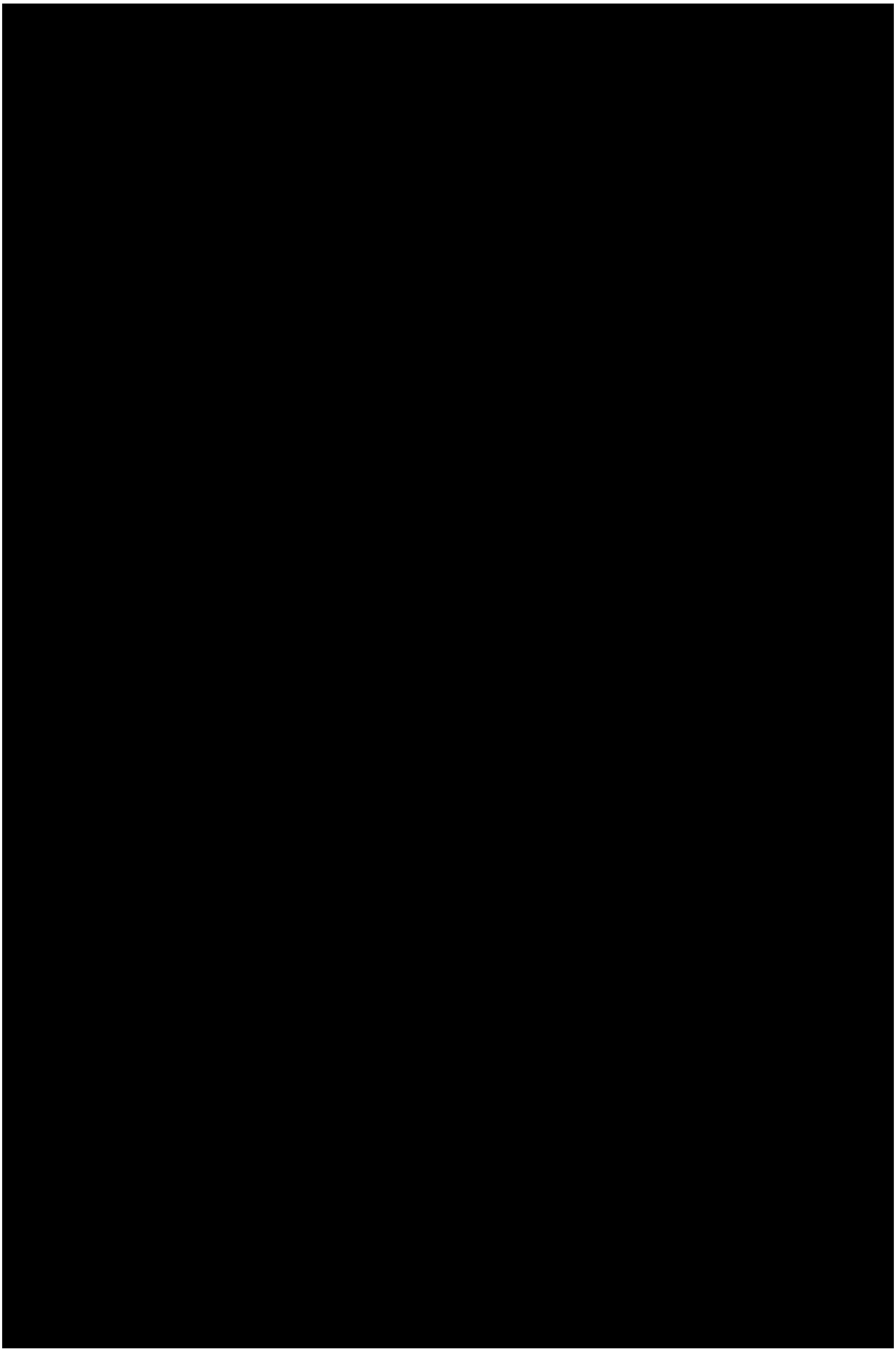

10.1.3 Location C

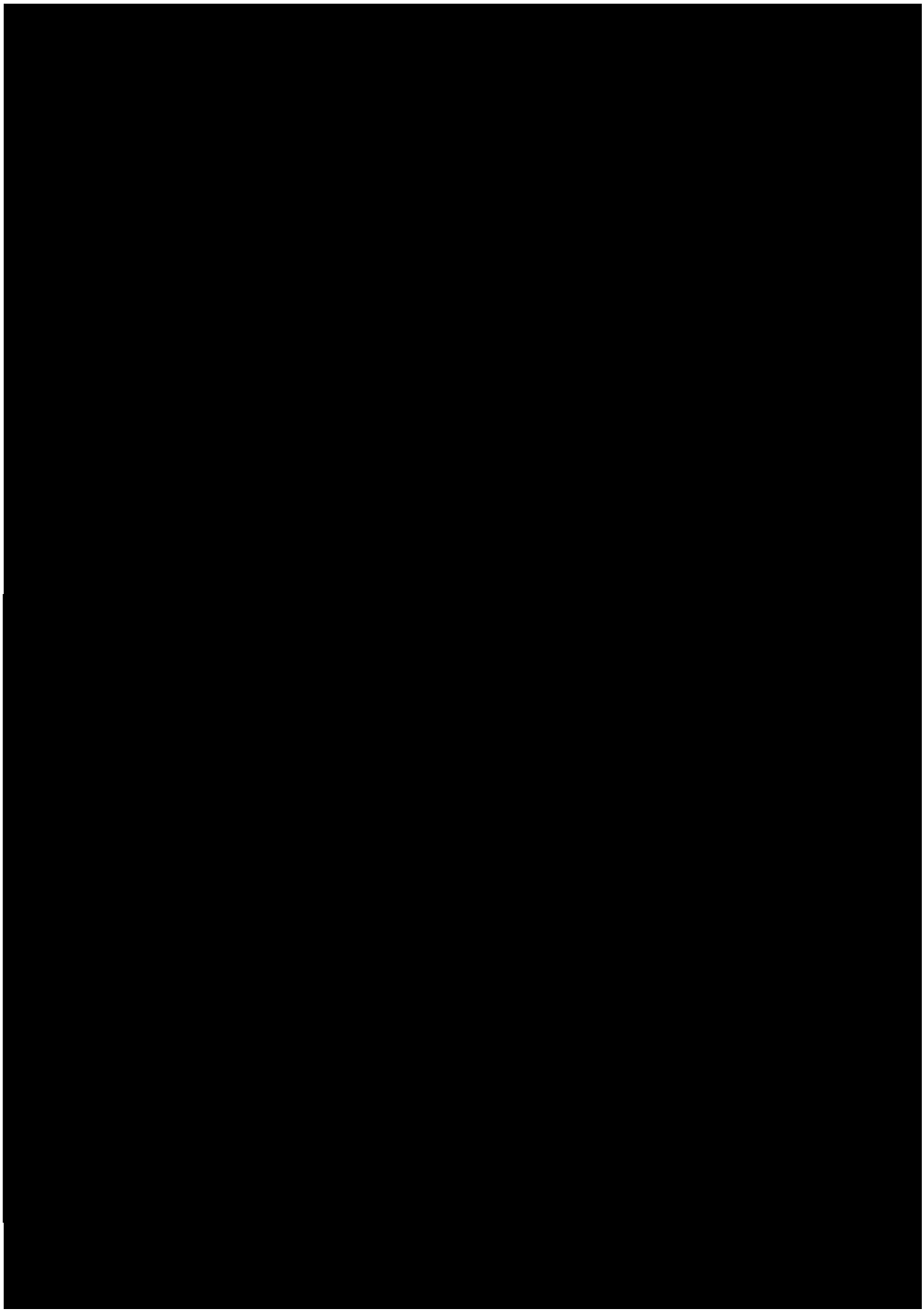

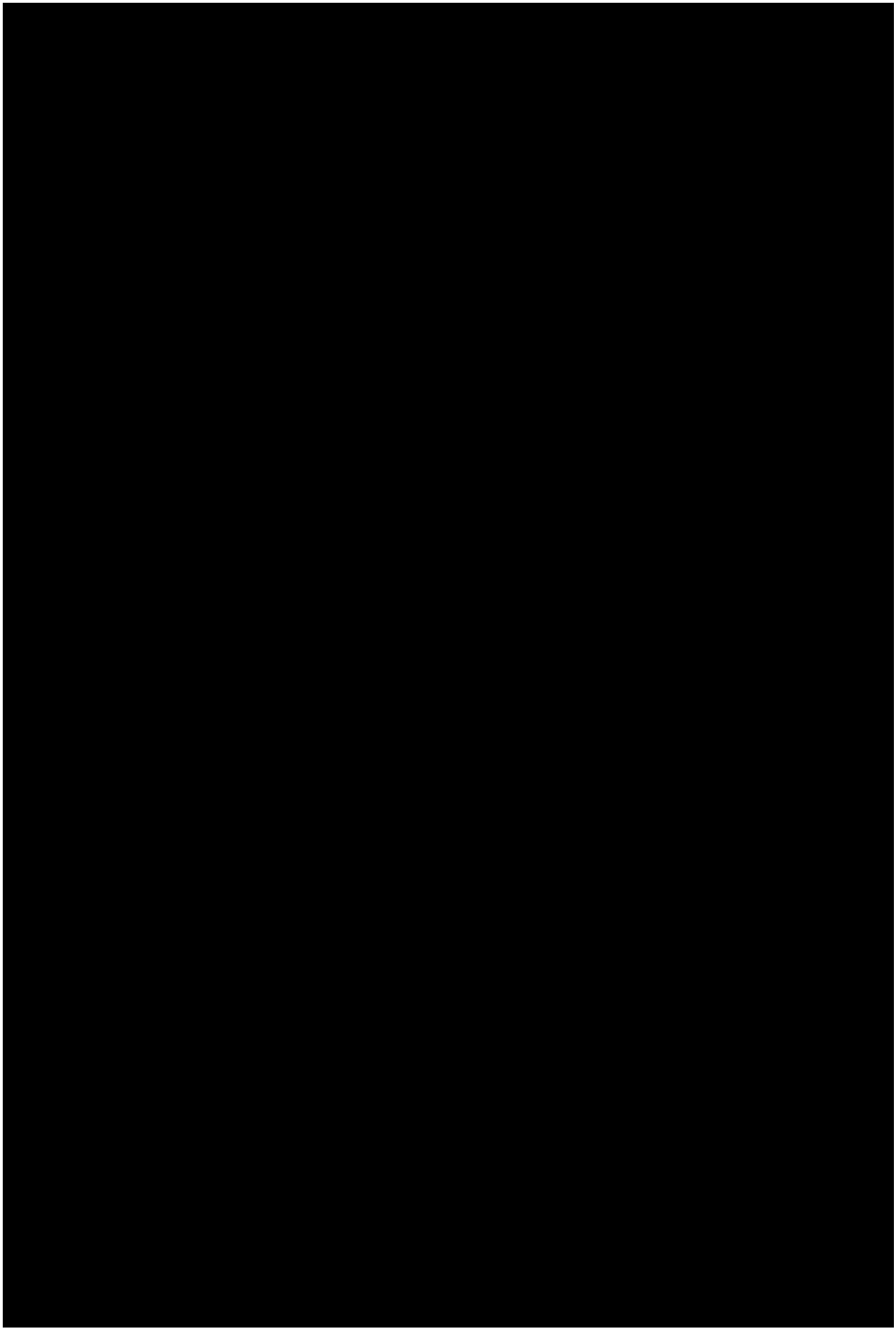

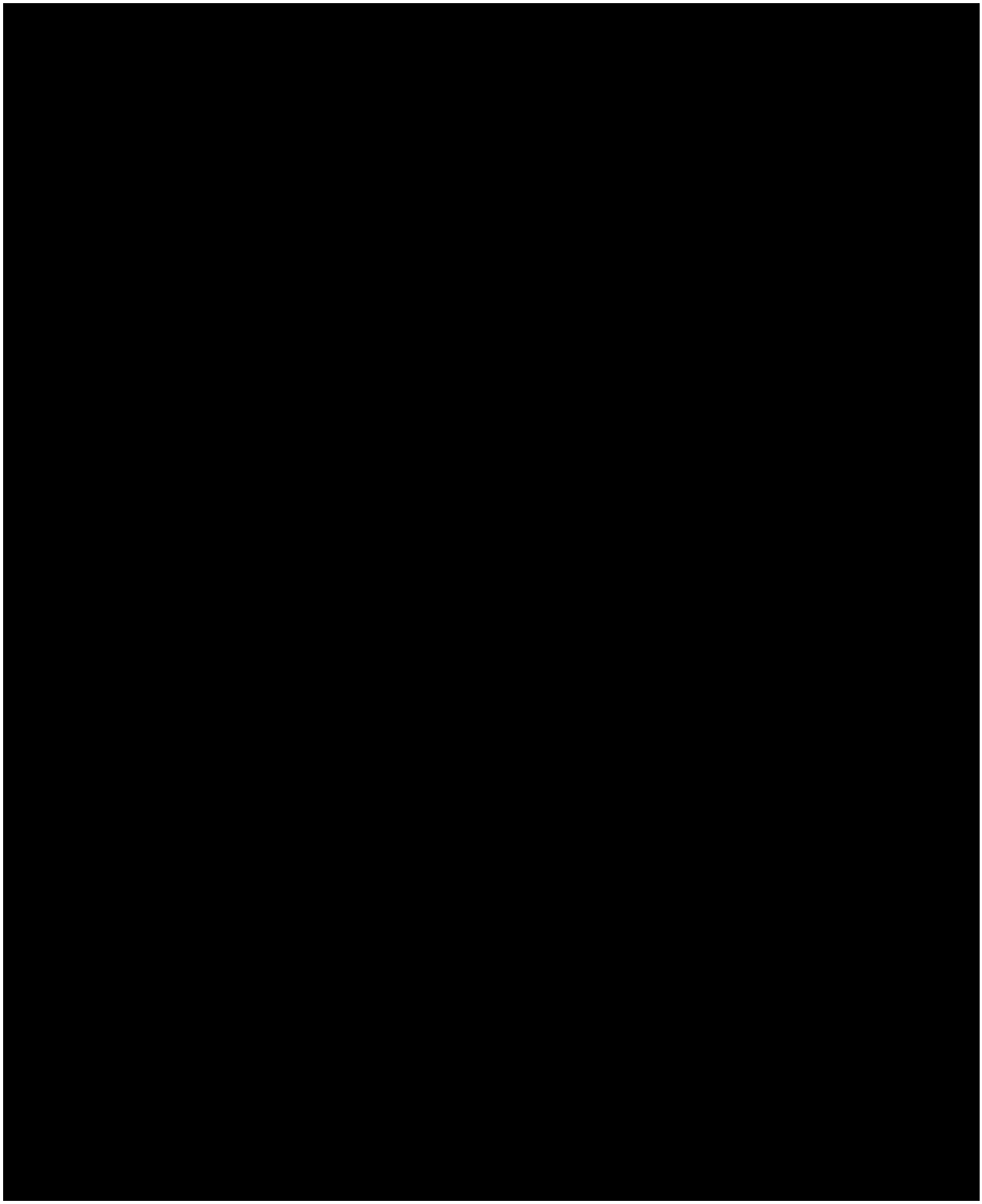

10.1.5 Rheological Overview

10.1.6 Rheological input parameters

For the case Newtonian de-rating models are used to research the influence of viscosity on pump performance, all rheological characterisation parameters of a non-Newtonian fluid need to be converted into one single value as used to represent the Newtonian characteristics. One way to approach this problem is by calculating the apparent viscosity at a predefined shear rate. In time various approaches are suggested at which shear rate the apparent viscosity yields the most accurate prediction. In Table 10.6 an overview can be found of suggested shear rates or input parameters which should be used in stead.

RHEOLOGICAL INPUT PARAMETERS	
Researcher	**Suggestion**
Duckham (1971)	Apparent viscosity at 100/s for psuedo-plastic, Bingham plastic and other shear thinning fluids. Apparent viscosity at 1000/s for dilatant materials.
Walker and Goulas (1982)	Plastic viscosity at a shear rate of 1500/s. (Equal to coefficient of rigidity for Bingham plastic fluids.)
Graham et al. (2009)	MODIFIED HYDRAULIC INSTITUTE Determine a equivalent 'pipe' for the pump based on main dimensions. Dependent on the flow regime: 1. Laminar flow: Determine equivalent pipe diameter, obtain shear rate from Rabinowitsch-Mooney diagram. Use this shear rate for apparent viscosity. 2. Turbulent flow: Use an apparent viscosity calculated at the shear rate of 4000/s. MODIFIED WALKER AND GOULAS Calculate the pump Reynolds number where the apparent viscosity is used as input. Good agreement was reached for shear rate of 4000/s.
Vavra et al. (1960)	Potential flow calculations in the blade passage of a rotating, radial-vaned impeller predict a shear rate of 2Ω .

Table 10.6: Overview of input parameters for Newtonian de-rating methods as used during previous research.

10.2 Mineralogy

10.3 Disk friction calculation

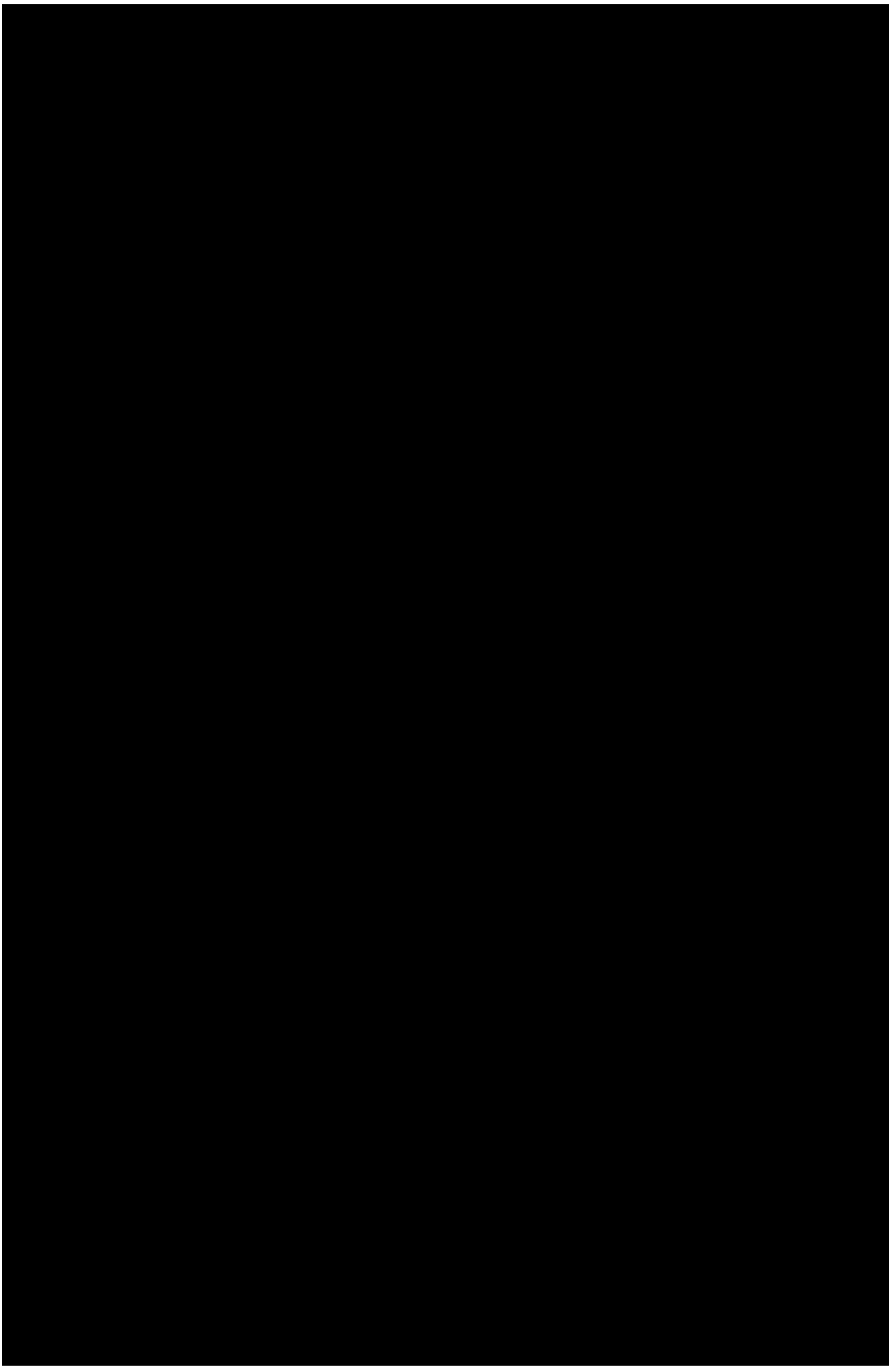

10.4 Surface roughness table

10.5 Measurement uncertainty

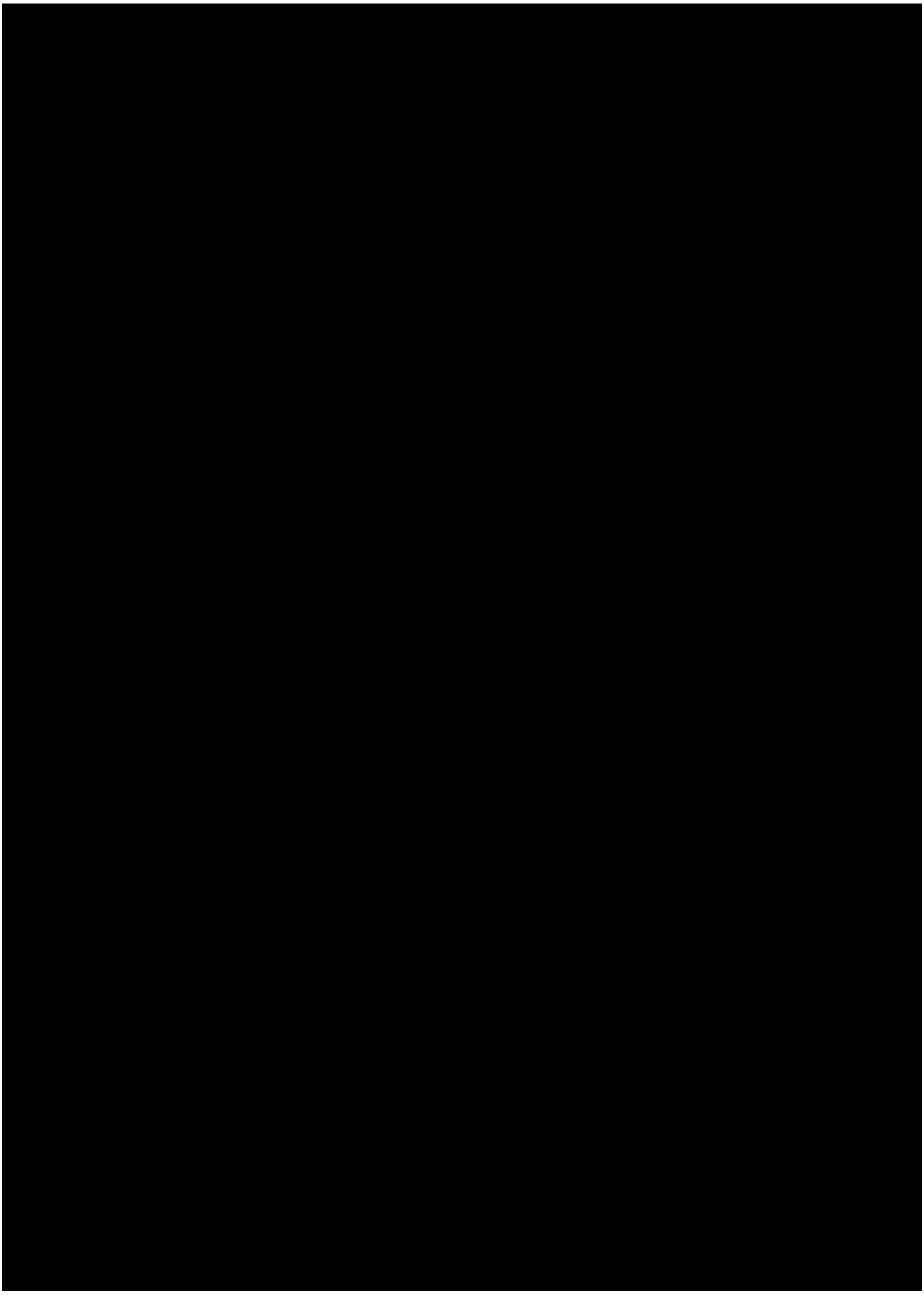

(a) Sonartrac.

(b) Pressure transducer.

Figure 10.7: Measurement apparatus on board Pallieter.

10.6 Torque Measurement Calculation

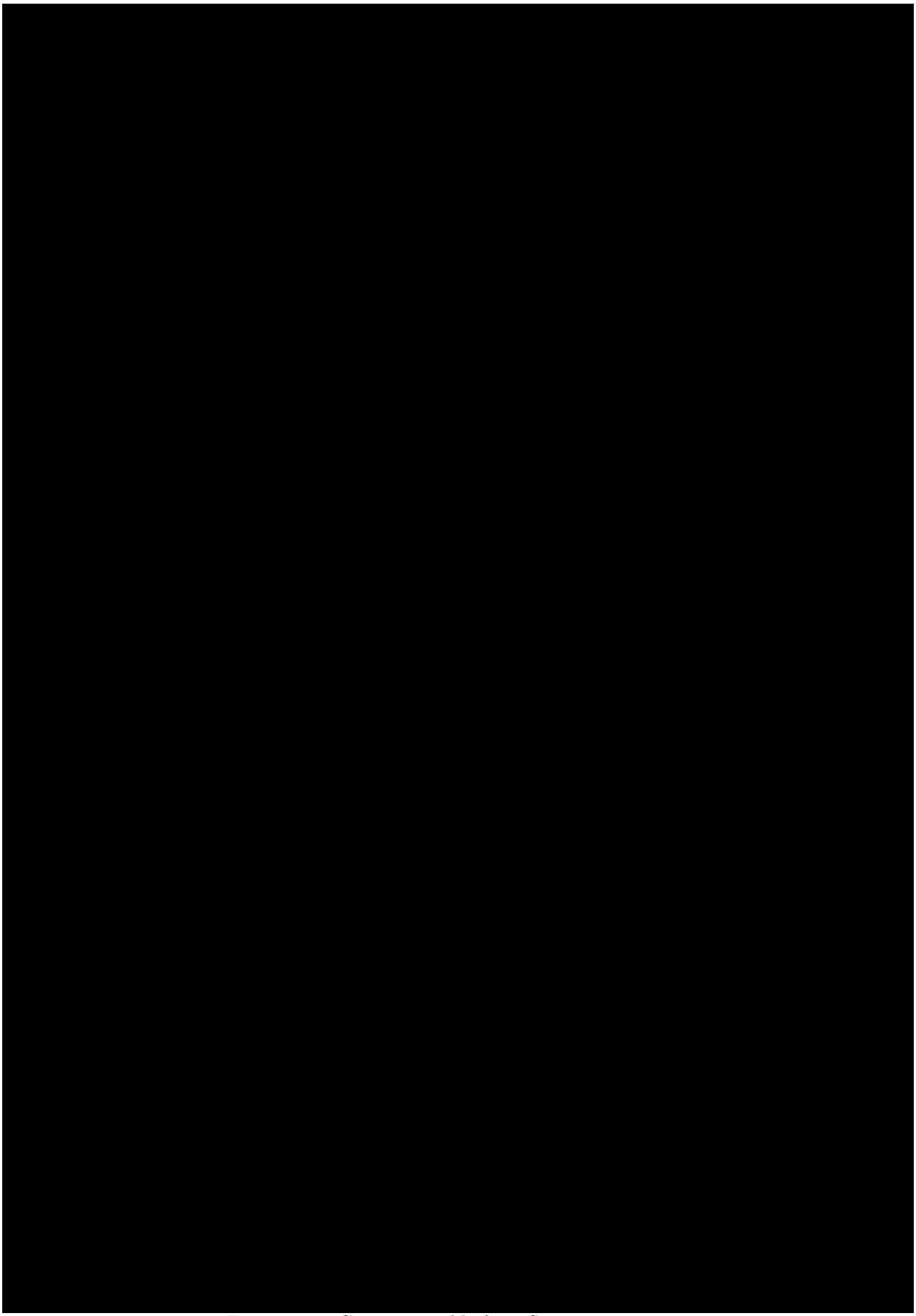

Figure 10.8: Coversion Table from Strain to Torque

10.7 Measurement device specifications

The measurement on board TSHD Pallieter encompassed a combination of signal processing and converting devices. An overview with device specifications will be presented below in the sequence of processing.

1. Strain Gauge: Micro Measurements - 250US - 350
   Resistance 350 ± 0.4 % Ohms.

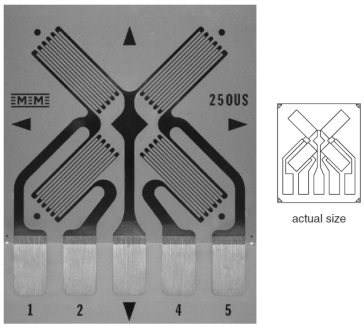

Figure 10.9: General Purpose Strain Gauge - 250US-350

2. Wireless transmitter: Mantracourt T24-ACMm
   In combination with 2x T24-BB1 battery pack to extend operational time.

Figure 10.10: Mantracourt T24 - ACMm Wireless transmitter

3. Wireless receiver: Mantracourt T24-Bsi (Basestation)
   Wireless signal can be processed, including zero reading and calibration. Output options are USB or further processing to RS232 or RS485. Due to practical limitations it was only possible to further process the signal when it was converted into RS232.

Figure 10.11: Mantracourt T24 - Bsi Wireless receiver (Basestation)

4. Signal converting: Mantracourt T24-SO (Serial - Output)
   To convert the digital measurement signal into a serial output, the T24-SO receives the signal wireless from the T24-BSi unit and generates a RS232 serial output message every 1000 ms.

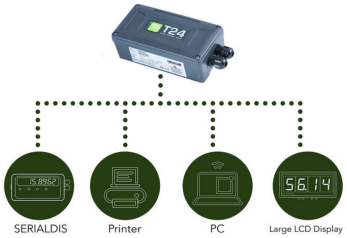

Figure 10.12: Mantracourt T24 - SO Serial Output

5. Signal converting: Mini Moxa NPort 6150 Series

The last step is to convert the serial RS232 message into a digital signal which is possible to transmit via UTP. From here the signal will be transmitted via VLAN-1 - UTP to the main Moxa switch on the bridge of the vessel.

Figure 10.13: Mini Moxa N PORT series 6150.

Figure 10.14: Mini Moxa N PORT series 6150 in combination with Mantracourt T24 series installed.

(a) Torque measurement system. (b) Torque measurement system covered.

Figure 10.15: Pump driving shaft with measurement system mounted.

10.8 Measurement results